

## Copyright Undertaking

This thesis is protected by copyright, with all rights reserved.

**By reading and using the thesis, the reader understands and agrees to the following terms:**

1. The reader will abide by the rules and legal ordinances governing copyright regarding the use of the thesis.
2. The reader will use the thesis for the purpose of research or private study only and not for distribution or further reproduction or any other purpose.
3. The reader agrees to indemnify and hold the University harmless from and against any loss, damage, cost, liability or expenses arising from copyright infringement or unauthorized usage.

If you have reasons to believe that any materials in this thesis are deemed not suitable to be distributed in this form, or a copyright owner having difficulty with the material being included in our database, please contact [lbsys@polyu.edu.hk](mailto:lbsys@polyu.edu.hk) providing details. The Library will look into your claim and consider taking remedial action upon receipt of the written requests.

The Hong Kong Polytechnic University  
Department of Applied Physics

A study of effective relative  
permittivity/permeability of a composite containing  
dielectric/magnetic inclusions by using analytic  
methods and numerical simulations

**CHAN Man**

A thesis submitted in partial fulfilment of the requirements  
for the degree of Master of Philosophy

**October 2008**

## **CERTIFICATE OF ORIGINALITY**

I hereby declare that this thesis is my own work and that, to the best of my knowledge and belief, it reproduces no material previously published or written, nor material that has been accepted for the award of any other degree or diploma, except where due acknowledgement has been made in the text.

\_\_\_\_\_  
(Signed)

\_\_\_\_\_  
CHAN Man

(Name of student)



## Abstract

We investigated the effective relative permittivity ( $\epsilon_{eff}$ ) (or permeability ( $\mu_{eff}$ )) composites containing dielectric (or magnetic) inclusions with various analytic and finite element (FE) methods. A FE model was made to contain a 4x4x4 or 6x6x6 inclusion arrays; and the result is assumed to be closer to real value compared with the analytic approaches. In addition, a method combining FE simulations and vibrating sample magnetometer (VSM) measurements is developed to determine the permeability ( $\mu$ ) of a soft magnet.

For 2-phase composites, all analytic results match with the FE data at low inclusion volume fraction ( $\phi_i \leq 0.1$ ), indicating that all these theories give rather correct estimates of  $\epsilon_{eff}$  (or  $\mu_{eff}$ ) at low  $\phi_i$ . However, at higher values of  $\phi_i$ , the analytic results are diversified. The data of the Maxwell-Garnett (M-G) and Landauer theories form the lower and upper bounds of the data. Results obtained from the Bruggeman, Rayleigh and Poon-Shin (P-S) theories rank in an ascending order. FE results are consistent with that of Rayleigh theory with deviation less than 0.2%, suggesting that the accuracy of FE simulations is high enough to determine the  $\epsilon_{eff}$  (or  $\mu_{eff}$ ) values of the models used in the study. For a model with a periodic inclusion array, the M-G



theory underestimates the  $\varepsilon_{eff}$  (or  $\mu_{eff}$ ) value, and other analytic theories overestimate the  $\varepsilon_{eff}$  (or  $\mu_{eff}$ ) value. Further modifications of these analytic approaches may be needed.

For 3-phase composites, a Maxwell-Garnett multiphase (MG-MP) theory and a Poon-Shin multiphase (PS-MP) theory were developed on the basis of 2-phase M-G and P-S theories. Three incremental-multiphase (I-MP) processes were proposed, in which inclusions are added in small incremental steps. The process in which the two types of inclusions are added in sequence is called as a sequential multiphase (SI-MP) process. The process in which the two types of inclusions are added randomly with fixed probabilities is called a randomly-accumulative multiphase (RA-MP) process. In the region of  $\phi_i \leq 0.3$ , all the analytic results are close to the FE results, indicating that all the analytic theories are valid in this region. For  $0.3 \leq \phi_i \leq 0.9$ , the analytic results deviate from FE data. The I-MP theory gives the highest  $\varepsilon_{eff}$  (or  $\mu_{eff}$ ) value and MG-MP theory gives the lowest one. The SI-MP process proceeded by adding the inclusions of a lower relative permittivity (or permeability) first gives a higher  $\varepsilon_{eff}$  (or  $\mu_{eff}$ ) among the three I-MP processes. The FE data lie between the SP-MP data and the MG-MP data. None of the analytic method is completely consistent with the FE method.



We verified the validity of the proposed method for estimating the dynamic permeability of a soft magnet. The VSM and calculated values of  $\mu$  for samples having different aspect ratios are compared. The experimental data are fitted to a group of theoretically predicted curves corresponding to a certain range of  $\mu$ . The mean value gives the best estimate of the real  $\mu$  value. The method was successful in predicting the permeabilities of iron and nickel, with an advantage of having no need to prepare a ring-shaped sample as required in a standard Rowland's ring test.



## Acknowledgements

Dr C. W. Ong, my chief supervisor and mentor, gave me lots of patience, support and guidance to meet the project goal with satisfactory results. He trained me up to have good problem solving and analytical skills in order to attain a high standard of experimental and simulation studies.

Dr. Y. W. Wong, my co-supervisor, gave his valuable comments and suggestions in my academic studies. His recommendations were useful to keep myself moving forward and to help me solving many technical problems.

Prof. F. G. Shin, my project advisor, was willing to share his viewpoints and insights pertaining to my study so that I could think out of box and produce more than I ever have before.

I also wish to express my appreciation to my group members Dr. Y. M. Poon, Dr. S. F. Wong, Mr. Y. M. Tang, Mr. Y. B. Chan, Mr. H. K. Chau and Mr. B. Guan for their valuable advice and discussion on my project. I am especially indebted to Mr. M. L. Yeung and Mr. K. H. Ho and Ms Y. Yeung for their technical support.



I also would like to be grateful to Dr. W. L. Sin, Dr. K. H. Lam, Mr. W. F. Cheng, Mr. Y. K. Chan, Mr. C. H. Chow, and Ms R. Xiang for their helpful suggestions.

I owe a great deal of my accomplishment to the immeasurable love and the never-ending support of my family and Wai. They are the ones who always believe that my efforts will be rewarded.



## Table of Contents

Abstract .....	I
Acknowledgements .....	IV
Table of Contents .....	VI
List of Figures .....	IX
List of Tables .....	XV
Chapter 1 Introduction	
1.1 Background .....	1
1.2 Scope of study and the structure of this thesis .....	6
Chapter 2 Analysis of 0-3 dielectric/magnetic composites with conventional analytical models and finite element simulations	
2.1 Introduction .....	9
2.2 Equivalency between the analyses of dielectric permittivity and magnetic permeability .....	12
2.3 Review of conventional analytic theories for the properties of a dielectric composite or a magnetic composite .....	19
2.3.1 Maxwell-Garnett (M-G) theory .....	19
2.3.2 Nonsymmetric-Bruggeman theory .....	23
2.3.3 Poon-Shin (P-S) model .....	27
2.3.4 Landauer model .....	29
2.3.5 Rayleigh model .....	31
2.3.6 Wiener bounds and Hashin-Shtrikman bounds .....	33
2.4 FE analysis for composites .....	35



2.4.1 Fundamentals of FE method .....	35
2.4.2 FE model used in the present study .....	38
2.4.3 Ranges of the parameters settings for 0-3 composite models.....	44
2.5 Results and Discussions .....	46
2.5.1 Convergence tests for FE analyses.....	46
2.5.2 Influence of the size of the inclusion array and $\mu_i$ .....	48
2.5.3 Influence of the volume fraction of inclusions .....	50
2.5.4 Influence of inclusion shape and alignment.....	55
Chapter 3 Analysis of 3-phase (0-0-3) composites containing dielectric or magnetic inclusions	
3.1 Introduction .....	58
3.2 Methods for analyzing 3-phase (0-0-3) composites.....	60
3.2.1 Maxwell-Garnett multiphase (MG-MP) theory .....	60
3.2.2 Poon-Shin multiphase (PS-MP) theory .....	63
3.2.3 Incremental multiphase (I-MP) method .....	64
3.2.3.1 Basic features .....	64
3.2.3.2 Effect of adding a small amount of inclusions.....	66
3.2.3.3 SI-MP methods .....	68
3.2.3.4 RA-MP method .....	71
3.2.4 FE method .....	73
3.3 Parameters and ranges of variations .....	76
3.4 Results and Discussions .....	79
3.4.1 Equivalency of using cubic and spherical inclusions in FE analyses .....	79



3.4.2 $\phi_i$ dependence of $\varepsilon_{eff}$ or $\mu_{eff}$ obtained from different methods .....	81
3.4.3 $\phi_l$ dependence of $\varepsilon_i$ and $\mu_{eff}$ obtained from different methods.....	91
3.4.4 Influence of the order of distribution of inclusions .....	96
Chapter 4 A method for determining the permeability of a material $\mu_{real}$ by combining vibrating sample magnetometer and FE method	
4.1 Conventional method and VSM for the determination of $\mu$ .....	99
4.2 Our method for the estimation of $\mu$ .....	104
4.2.1 VSM measurement.....	104
4.2.2 FEM simulations .....	105
4.2.3 Estimate $\mu_{real}$ by correlating the results of FE analyses and VSM measurements.....	112
4.3 Results and discussions of two application examples: Fe and Ni.....	114
Chapter 5 Conclusions	
5.1 Overall summary.....	119
5.2 Conclusions on the study of 2-phase composites .....	121
5.3 Conclusions on the study of 3-phase composites .....	123
5.4 Conclusions on the method for determining $\mu$ by combining VSM and FE simulations .....	126
References.....	127



## List of Figures

Fig. 2.1	Schematic diagram for magnetic simulations (Model 1) .....	17
Fig. 2.2	Schematic diagram for magnetic simulations (Model 2) .....	17
Fig. 2.3	Schematic diagram for dielectric simulations (Model 3) .....	17
Fig. 2.4	Deviation of the results of three different models which determine from 6x6x6 sphere inclusions at $\phi_i \sim 0.4$ .....	18
Fig. 2.5	M-G model in which a spherical inclusion is placed inside a matrix with boundary conditions as shown .....	20
Fig. 2.6a	The shaded region is an inclusion of phase 1, which is surrounded by a 2-phase medium .....	30
Fig. 2.6b	In the Laudauer model, the surrounding environment of an inclusion of phase 1 is imagined to be a single-phase uniform phase 3 having an effective relative permittivity $\epsilon_{eff}$ .....	30
Fig. 2.7	Rayleigh model in which spherical inclusions are arranged in a cubic array in an infinitely large matrix .....	32
Fig. 2.8	A sketch of a current source formed by element type “Source36” .....	40
Fig. 2.9	The structure of a composite model (A: Side view; B: 3-D) .....	40
Fig. 2.10a	Diagram showing “Solid96” element .....	41
Fig. 2.10b	Diagram showing “Solid122” element .....	42



Fig. 2.11	Effective relative permeability $\mu_{eff}$ versus element number for three models having the same inclusion volume fraction $\phi_i = 0.4$ and relative permeability of the matrix $\mu_m = 1$ . They are set to have: (i) a 1x1x1 inclusion matrix of $\mu_i = 10$ ; (ii) a 1x1x1 inclusion array of $\mu_i = 600$ , and (iii) a 4x4x4 inclusion array of $\mu_i = 10$ . ....	48
Fig. 2.12	Influence of $\phi_i$ on $\mu_{eff}$ obtained from various conventional effective medium theories (dotted curves) and numerical simulations (“○” : spherical inclusions and “□” : cubic inclusion ) for a model containing a 6x6x6 inclusion array having a $\mu_i = 10$ embedded in a matrix of $\mu_m = 1$ .....	50
Fig. 2.13	Distribution of H-field of 6x6x6 cubic array for $\phi_i = 0.96$ , where $t$ = gap between the cubic inclusions, and $a$ = inclusion cubic length .....	53
Fig. 2.14	Influence of $\phi_i$ on $\mu_{eff}$ obtained from various conventional effective medium theories (dotted curves) and numerical simulations (“○” : spherical inclusions and “□” : cubic inclusion ) for a model containing a 6x6x6 inclusion array having a $\mu_i = 1000$ embedded in a matrix of $\mu_m = 1$ .....	55
Fig. 2.15	Effective relative permeability $\mu_{eff}$ for a model with inclusions arranged in a 4x4x4 array, $\mu_i = 10$ and $\phi_i = 0.4$ and in various shapes. ....	56
Fig. 3.1	A simple model of a 3-phase mixture, two types of isotropic inclusions of dielectric constants ( $\varepsilon_1$ and $\varepsilon_2$ ) are embedded in an isotropic non-electroactive non-magnetic matrix material with a relative dielectric constant $\varepsilon_m$ .....	60



Fig. 3.2	Three paths for constructing 3-phase (0-0-3) composites containing two types of inclusions with respective volume fractions $\phi_{1,f}$ and $\phi_{2,f}$ .....	66
Fig. 3.3a	Flow chart of a program to implement a SI-MP <sub>12</sub> process. Inclusions of type 1 are added first, followed by inclusions of type 2 .....	70
Fig. 3.3b	Flow chart of a program to implement a SI-MP <sub>21</sub> process. Inclusions of type 2 are added first, followed by inclusions of type 1 .....	70
Fig. 3.3c	Flow chart used to calculate $\varepsilon_{eff}$ of a composite in a RA-MP process.....	72
Fig. 3.4a	FEA model of a 0-0-3 composite containing two types of 4x4x4 spherical inclusions .....	75
Fig. 3.4b	FEA model of a 0-0-3 composite containing two types of 4x4x4 cubic inclusions .....	75
Fig. 3.5	3-dimensional structure of the 4x4x4 array models containing two types of (a) spherical and (b) cubic inclusions randomly distributing at the sites. (c) The direction of $H_{applied}$ . ....	75
Fig. 3.6	Five schemes for varying $\phi_1$ and $\phi_2$ .....	78
Fig. 3.7	Comparison of FEA results of $\mu_{eff}$ deduced from various models containing spherical and cubic inclusions.....	80
Fig. 3.8	$\phi_i$ dependence of $\mu_{eff}$ obtained from PS-MP method (dotted curve); MG-MP method (dashed curve); SI-MP <sub>12</sub> method “□”; SI-MP <sub>21</sub> method “△”; RA-MP method “×” and FE simulations “○” for a model containing two types of inclusions arranged in a 4x4x4 array with $\mu_I=10$ and $\mu_2 = 2$ . The matrix has a $\mu_m$ of 1. $\phi_1:\phi_2 = 1:1$ . ....	84



- Fig. 3.9  $\phi_i$  dependence of  $\mu_{eff}$  obtained from PS-MP method (dotted curve); MG-MP method (dashed curve); SI-MP<sub>12</sub> method “□”; SI-MP<sub>21</sub> method “△”; RA-MP method “×” and FE simulations “○” for a model containing two types of inclusions arranged in a 4x4x4 array with  $\mu_1=10$  and  $\mu_2 = 2$ . The matrix has a  $\mu_m$  of 1.  $\phi_1:\phi_2 = 1:2$  .....85
- Fig. 3.10  $\phi_i$  dependence of  $\mu_{eff}$  obtained from PS-MP method (dotted curve); MG-MP method (dashed curve); SI-MP<sub>12</sub> method “□”; SI-MP<sub>21</sub> method “△”; RA-MP method “×” and FE simulations “○” for a model containing two types of inclusions arranged in a 4x4x4 array with  $\mu_1=10$  and  $\mu_2 = 2$ . The matrix has a  $\mu_m$  of 1.  $\phi_1:\phi_2 = 2:1$  ..... 86
- Fig. 3.11  $\phi_i$  dependence of  $\mu_{eff}$  obtained from PS-MP, MG-MP, SI-MP<sub>12</sub>, SI-MP<sub>21</sub> and RA-MP methods (dotted line) and FE simulations (“●”: spherical inclusions, “■”: cubic inclusions) for a model containing two types of inclusions arranged in a 6x6x6 array with  $\mu_1 = 100$  and  $\mu_2 = 10$ . The matrix has a  $\mu_m$  of 1.  $\phi_1:\phi_2 = 1:1$  .....88
- Fig. 3.12  $\phi_i$  dependence of  $\mu_{eff}$  obtained from PS-MP, MG-MP, SI-MP<sub>12</sub>, SI-MP<sub>21</sub> and RA-MP methods (dotted line) and FE simulations (“●”: spherical inclusions, “■”: cubic inclusions) for a model containing two types of inclusions arranged in a 6x6x6 array with  $\mu_1 = 100$  and  $\mu_2 = 10$ . The matrix has a  $\mu_m$  of 1.  $\phi_1:\phi_2 = 1:2$  .....89
- Fig. 3.13  $\phi_i$  dependence of  $\mu_{eff}$  obtained from PS-MP, MG-MP, SI-MP<sub>12</sub>, SI-MP<sub>21</sub> and RA-MP methods (dotted line) and FE simulations (“●”: spherical inclusions, “■”: cubic inclusions) for a model containing two types of



	inclusions arranged in a 6x6x6 array with $\mu_1 = 100$ and $\mu_2 = 10$ . The matrix has a $\mu_m$ of 1. $\phi_1:\phi_2 = 2:1$ .....90
Fig. 3.14	$\phi_I$ dependence of $\mu_{eff}$ under the condition of a fixed $\phi_i = 0.42$ , i.e. Scheme (iv) in Fig.3.6. $\mu_1 = 10$ and $\mu_2 = 2$ . PS-MP method (dotted curve); MG-MP method (dashed curve); RA-MP processes “×”; FEA simulations “○” associated with a 4x4x4 spherical inclusion array. ....92
Fig. 3.15	$\phi_I$ dependence of $\mu_{eff}$ under the condition of a fixed $\phi_i = 0.73$ , i.e. Scheme (v) in Fig.3.6. $\mu_1 = 10$ and $\mu_2 = 2$ . ....93
Fig. 3.16	$\phi_I$ dependence of $\mu_{eff}$ for $\mu_1$ and $\mu_2$ equal to 100 and 10; and 10 and 2 respectively. The overall inclusion volume fraction $\phi_i$ is fixed at 0.42....95
Fig. 3.17	Three FE models with inclusions located (i) randomly (random pattern); (ii) in two layers aligned in parallel to the applied field (parallel pattern) and (iii) in two layers perpendicular to the applied field (perpendicular pattern). In all cases, $\phi_1:\phi_2 = 1:1$ . ....97
Fig. 3.18	Estimated values of $\mu_{eff}$ obtained from distribution patterns of inclusions, with $\mu_1$ and $\mu_2$ set at 10 and 2, or 100 and 10; and $\phi_i$ set at 0.125 and 0.6. In all the calculations, $\phi_1:\phi_2$ is fixed at 1:1. ....98
Fig. 4.1	Configuration of a Rowland’s ring. .... 100
Fig. 4.2a	Schematic illustration of $\mu_{real} = B_{internal} / (H_{internal} \mu_0)$ , i.e. the slope of the true $M$ - $H_{internal}$ loop near $M = 0$ ..... 105
Fig. 4.2b	Schematic illustration of $\mu_{apparent} = B_{internal} / (H_{applied} \mu_0)$ , i.e. the slope of the $M$ - $H_{applied}$ loop near $M = 0$ ..... 105



Fig. 4.3	FEA model for the simulations of VSM processes. Samples are assigned to have square ( $x = y$ ), rectangular ( $x \neq y$ ), and circular (diameter = $d$ ) cross-sectional areas. Calculation for a spherical sample is preformed for reference .....	107
Fig.4.4	Predicted results of $\mu_{apparent}$ with VSM measurements versus aspect ratio $z/x$ or $z/d$ varying from 1 to 1000, for four $\mu_{real-i} = 10, 500, 3000$ and 10000 respectively. “ $\diamond$ ”: rectangular prism samples; “+”: rod samples.....	108
Fig. 4.5	Plots of $\mu_{apparent}$ versus aspect ratio ( $z/x$ ) with $\mu_{real}$ varying from 100 to 700.....	112
Fig. 4.6	Relationships of $M$ versus $H_{applied}$ of Fe and Ni wires with different aspect ratios recorded by using VSM. The slope of a curve at the low field region is labelled.....	115
Fig.4.7	Experimental $\mu_{measured}$ values of Fe and Ni wires bounded by corresponding curves of $\mu_{apparent}$ versus $z/x$ derived from Eq. (4-19) “ $\square$ ”: Fe wires; “ $\circ$ ”: Ni wires. ....	117
Fig. 4.8	Theoretically predicted apparent permeability $\mu_{apparent}$ obtained by using VSM measurements for rectangular prisms with $z/x = 100$ and $y/z$ from 0.01 to 1, showing increasing demagnetization effect with increasing width of the sample. ....	118



## List of Tables

Table 2.1	Parameters and their ranges of variations in the simulation processes .....	45
Table 3.1	Parameters, ranges of variations and the purposes of the related investigations in the FE analyses for 3-phases composites. $\mu_m$ of the matrix = 1 .....	77
Table 4.1	Optimized parameters in Eq. (4-10) to give the best fit to the curves shown in Fig. 4.4.....	110



# Chapter 1 Introduction

## 1.1 Background

In the past decades, electromagnetic composite materials, made by incorporating dielectric inclusions, or magnetic inclusions, or both in a non-electroactive matrix, have attracted wide attention, not only because of fundamental interest but also due to their tremendous application potential in many areas.

The increasing demands on soft magnetic composites mainly originate from their tailorable functional properties. For example, composites can be made to possess magnetostriction properties, and hence can be used in electro-mechanical transducers. Composite-based electronic materials, hard and soft polymer-bonded magnetic composites, iron-resin used in electrical motor to replace existing laminate materials [Shokrollahi and Jangorban, 2007] and electromagnetic shielding materials [Waki, et al., 2005a]. Another possible application is to make active storage material for data storage in an information system [Shokrollahi and Jangorban, 2007]. Composites containing microwire inclusions are used in producing high attenuation and shielding components for defense applications [Darius, 2008]. Other advantages are that they



have low density, low processing cost and relatively high toughness.

Dielectric and magnetic composites are also of academic interests. For these materials, the effective relative permittivity ( $\epsilon_{eff}$ ) and relative permeability ( $\mu_{eff}$ ) are important parameters, which should be estimated when designing materials for a specific application [Waki, et al., 2005b]. Many conventional analytic formulas have been developed for this purpose. Up to date, most of them are developed for 2-phase composite material systems. A 2-phase system, say 0-3 composite, is referred to a system containing dielectric or magnetic inclusions in a matrix. These theories include the Maxwell-Garnett formula (M-G) [Maxwell Garnett, 1904], nonsymmetric-Bruggeman, (in brief, Bruggeman) formula [Bruggeman, 1935], Poon-Shin formula (P-S) [Poon and Shin, 2004], Landauer formula [Landauer, 1952] and Rayleigh formula [Rayleigh, 1892] etc. In particular, the M-G theory, assumes that the composite contains only one spherical inclusion. In the Bruggeman and P-S theories, it is also assumed the inclusions are spheres, while the former incorporates the influence of the inclusions by continuously modifying the matrix properties with increasing volume fraction of the inclusions. The latter employs an alternative way to modify the matrix properties by taking account of the polarization effect of the



inclusions. Landauer employed a mechanism to introduce even stronger modification of the matrix, and hence the calculated results are in general larger than those deduced from other theories for a composite of the same inclusion fraction. The Rayleigh theory is particularly designed for a system containing infinite number of inclusions arranged in a periodic array. In principle, all these theories are expected to give the same results for a specific composite material. However, based on different assumptions, it is not unusual to find that the results derived by them are not identical. More reasons causing possible deviation of the predicted values from these theories are that: (i) the inclusion shape is mostly restricted to be spherical; (ii) the inclusion volume fraction is assumed to be low, such that the interaction between the inclusions is neglected while this is not the case in a real system, especially for those of high inclusion volume fractions. Finite element (FE) analysis is another approach which can be able to give accurate simulation of a real system. FE method is advantageous of having fewer restrictions from the shape, volume fraction and distribution of the inclusions, but the accuracy would depend on the capability of the computer, such as memory size. Though results from FE analysis can be as more reliable references for examining the correctness of those derived from analytic theories, to our knowledge, comparison analysis between the results obtained from these two groups of techniques has not been thoroughly



performed and reported in literature.

Further, all the theories mentioned above are mainly applied to 2-phase systems. It would also be interest to extend the study to 3-phase (or 0-0-3) systems, which is formed by incorporating two types of inclusions in a matrix. Some reports on this topic using both analytic and numerical approaches have been found in literature [Bregar, 2005; Bregar and Pavlin, 2004; Chevalier and Floc'h, 2001; Chew, et al., 2003; Daniel and Corcolle, 2007; Darius, 2008; Emets, 2005; Goncharenko, 2003; Hallouet and Pelster, 2007; Shamonin, et al., 2004; Waki, et al., 2005a; Waki, et al., 2005b; Waki, et al., 2006]. One way employed in analytics studies is to extend the 2-phase M-G theory by introducing additional terms related to the second types of inclusions in the same as the first one, and possibly some terms for additional modification of the matrix. However, the restrictions and problems in the 2-phase theories persist.

On the experimental side, determination of the  $\mu_{eff}$  value of a magnetic material is not a easy task [Cedillo, et al., 1980; Miles, et al., 1957]. The difficulty of using the conventional technique, Rowland's ring, is that the sample must be made in ring form. On the other hand, although vibrating sample magnetometer (VSM) is typical for



determining the magnetic dipole field created by a small sample of an arbitrary shape, demagnetization effect is inevitable, such that the magnetic field  $\vec{H}$  inside the sample is not directly measurable. Further complications for the measurement of  $\mu_{eff}$  of a magnetic composite are expectable because of possible variations of move factors such as the shape, orientation and distribution of the inclusions.



## 1.2 Scope of study and the structure of this thesis

Based on the above summary, this study is organized to consist of three major parts.

In the first part of this project, we calculate the  $\varepsilon_{eff}$  (or  $\mu_{eff}$ ) values of 2-phase composites with various conventional analytic theories and FE method. We re-examined the analytic theories by comparing their results with the simulated values. Details of this part of study are described in Chapter 2. It starts with an argument showing the mathematical equivalence between formulations used to analyze the permittivity of a dielectric composite and the permeability of a magnetic composite. A detailed review of various analytic theories is then performed to pinpoint their respective assumptions and limitations. We then presented the data of  $\varepsilon_{eff}$  (or  $\mu_{eff}$ ) of a composite derived from these theories and FE simulations. Attentions are paid on possible discrepancy and the causes. In FE analysis, we also investigated the influences of the shapes (i.e. spherical, cubic and wire) and volume fraction of the inclusions, and the randomness of their distribution. For the case of wire inclusions, the influence due to their orientation relative to the applied  $H$ -field was examined.



The second part of the study is presented in Chapter 3. We examined the  $\varepsilon_{eff}$  (or  $\mu_{eff}$ ) value of 3-phase (0-0-3) composite materials with three methods. The first method is modified from the M-G theory and P-S theory used for 2-phase systems by adding additional terms for the second type of inclusions and additional modification to the matrix. The effect is supposed to be equivalent to mixing the three constituents evenly in one single step. The second method is to introduce the inclusions with many infinitesimal incremental steps, where the properties of the mixture are modified successively after each step. This method was implemental with three approaches, depending on how the inclusions were added. In the first approach, one type of inclusions was added, which was followed by the other. In the second approach, this order was reversed. In the third approach, the two types of inclusions were incorporated stepwise with relative frequencies in the same ratio as that of the volume fractions of the two phases at the final state. The third method is FE analysis. We expect that all these results should be equal if they describe correctly the same system.

The third part of this study is presented in Chapter 4, which aims at determining the relative permeability  $\mu$  of a soft magnet by combining the VSM technique and FE simulations. This method can be applied to a sample with a shape not suitable for a



Rowland's ring test. Our method is to correlate the apparent relative permeability ( $\mu_{\text{apparent}}$ ) measured with VSM, which normally deviates from the real relative permeability due to demagnetization effect. The measured value is then converted to the real one with the results obtained from FE analysis. This method is expected to be useful for estimating the  $\mu_{\text{eff}}$  value of a magnetic specimen of a wire shape, which may be a pure metal, a composite wire, or a thin film.

Finally, we summarize the results in Chapter 5 to give conclusions of this study.



## **Chapter 2    Analysis of 0-3 dielectric/magnetic composites with conventional analytical models and finite element simulations**

### **2.1 Introduction**

A number of theories have been proposed to predict the performance of the effective relative dielectric permittivity ( $\epsilon_{eff}$ ) of a dielectric composite. Composites concerned mostly are those containing dielectric or magnetic inclusions spreading over in a non-electromagnetically active matrix. However, a review of theories shows that they have some constraints and may not be accurate enough.

First, the property of a real composite material system is normally difficult to be expressed accurately with analytic formula because of the complexity of the real situation. Therefore, the model used in an analytic analysis must be based on some assumptions to make it to be manageable with standard mathematical techniques. As such, the model is just an approximation of the real system. Different authors applied different assumptions to build up their own models, causing inconsistency among the



results derived from different theories [Drnovsek, 2008].

Second, when the volume fraction of the inclusions is high, the interaction between the inclusions is not negligible. Hence, the assumptions of most models would not be as effective as in the case of a dilute inclusion concentration. The accuracy of the results obtained from the models would have much larger errors, and the discrepancy among them is more pronounced.

In addition, some other factors, like the inclusion shape, preferential orientations of long inclusions and agglomeration of the inclusions etc, would further complicate the system. However, estimates of the influences due to these factors are difficult to be formulated analytically.

On the other hand, numerical simulation techniques, such as finite element (FE) analysis, can better emulate a real composite system. The drawback of FE method is that it cannot give an explicit functional expression to indicate the functional dependence of the result on the variables. However, once the fineness of the model is properly set and the convergence of a simulation process is detected, the FE result



would reflect more truly reflect the performance of a real system. Therefore, FE method is a good means to check the correctness of the analytic models. Up to date, a thorough comparison of the results obtained from these two approaches is little reported in literature.

In this chapter, we present the results of  $\varepsilon_{eff}$  (or  $\mu_{eff}$ ) of a composite derived from various analytic theories and FE analysis, and compare the two groups of data. Assuming that the FE analysis gives better results to represent the true values, we try to address the physical origin of the discrepancy between the analytic and numerical approaches.



## 2.2 Equivalency between the analyses of dielectric permittivity and magnetic permeability

We first prove that the electrostatic theory used for analyzing a dielectric has the same form as the magnetostatic theory for analyzing a magnetic material.

Maxwell's equations [Reitz, et al., 1962] describe the relationships among electric field ( $\vec{E}$ ), magnetic induction field ( $\vec{B}$ ), electric displacement ( $\vec{D}$ ), magnetic intensity ( $\vec{H}$ ), free charge density ( $\rho$ ) and free charge current densities ( $\vec{J}$ ). The equations, in a macroscopic point of view, are expressed as:

$$\nabla \cdot \vec{D} = \rho \quad (\text{Gauss' law for electricity}), \quad (2-1)$$

$$\nabla \cdot \vec{B} = 0 \quad (\text{Gauss' law for magnetism}), \quad (2-2)$$

$$\nabla \times \vec{E} = -\frac{\partial \vec{B}}{\partial t} \quad (\text{Faraday's law of induction}), \text{ and} \quad (2-3)$$

$$\nabla \times \vec{H} = \vec{J} + \frac{\partial \vec{D}}{\partial t} \quad (\text{Ampere's law}). \quad (2-4)$$

In a static case with no free charge density ( $\rho = 0$ ) and free charge current ( $\vec{J} = 0$ ),

Eqs. (2-1) to (2-4) become:

$$\nabla \cdot \vec{D} = 0, \quad (2-5)$$



$$\nabla \cdot \vec{B} = 0, \quad (2-6)$$

$$\nabla \times \vec{E} = 0, \quad \text{and} \quad (2-7)$$

$$\nabla \times \vec{H} = 0. \quad (2-8)$$

Furthermore, the constitutive equation for a linear dielectric is:

$$\vec{D} = \varepsilon_0 \vec{E} + \vec{P} = \varepsilon \varepsilon_0 \vec{E} \quad (2-9)$$

and that of a magnetic material is:

$$\vec{B} = \mu_0 (\vec{H} + \vec{M}) = \mu \mu_0 \vec{H}, \quad (2-10)$$

where  $\varepsilon$  and  $\mu$  are the relative permittivity and relative permeability of the substances.

For calculating the electric field inside the dielectric, or the magnetic field inside the magnet, we rewrite Eqs. (2-5) and (2-6) in the form of:

$$\nabla \cdot \vec{E} = 0 \quad \text{and} \quad (2-11)$$

$$\nabla \cdot \vec{H} = 0. \quad (2-12)$$

On the other hand, Eqs. (2-7) and (2-8) imply that  $\vec{E}$  and  $\vec{H}$  can be written as the gradients of respective scalar potentials  $\varphi_E$  and  $\varphi_H$ :

$$\vec{E} = -\nabla \varphi_E \quad \text{and} \quad (2-13)$$

$$\vec{H} = -\nabla \varphi_H. \quad (2-14)$$

After substituting Eqs. (2-13) and (2-14) to Eqs. (2-11) and (2-12), we get Laplace's



equations for the two cases:

$$\nabla^2 \varphi_E = 0 \quad \text{and} \quad (2-15)$$

$$\nabla^2 \varphi_H = 0. \quad (2-16)$$

The next is to refer to the boundary conditions of a specific problem to determine the solution. Applying the divergence theorem to Eq. (2-6), we have:

$$\bar{B}_1 \cdot \hat{n}_1 \Delta S + \bar{B}_2 \cdot \hat{n}_2 \Delta S = 0 \quad (2-17)$$

where  $\Delta S$  is a small surface element at the boundary between two media, and  $\hat{n}_1$  and  $\hat{n}_2 = -\hat{n}_1$  are the normal vectors of these two surfaces.

Therefore, the normal component of  $\bar{B}$  is continuous across the interface, i.e.

$$B_{1n} = B_{2n}. \quad (2-18)$$

Applying Stokes's theorem to Eq. (2-8), we have:

$$H_{1t} = H_{2t}. \quad (2-19)$$

Similarly, for the electrostatic case, we can write the boundary conditions at an interface between two media (i.e. the matrix and an inclusion):

$$D_{1n} = D_{2n} \quad \text{and} \quad (2-20)$$

$$E_{1t} = E_{2t}. \quad (2-21)$$



As a result, the formulations of the  $\vec{E}$  and  $\vec{D}$  for the case of a dielectric are the same as those of the  $\vec{H}$  and  $\vec{B}$  for a magnet. With the same forms of boundary conditions, the solution of  $\vec{E}$  would have the same function form as that of  $\vec{H}$ ; and the solution of  $\vec{D}$  would have the same function form of  $\vec{B}$ . As such, the quantity  $\frac{\vec{D}}{\vec{E}} = \varepsilon$  would also have the same function form as that of  $\frac{\vec{B}}{\vec{H}} = \mu$ .

In this work, we assume that the above arguments are applicable to a composite containing dielectric inclusions in a matrix having permittivities of  $\varepsilon_i$  and  $\varepsilon_m$  respectively; and a composite containing magnetic inclusions in a non-magnetic matrix having permeabilities of  $\mu_i$  and  $\mu_m$  respectively. The formulae derived for a dielectric composite reported in literature can thus be used for a magnetic composite by replacing  $\vec{E}$  with  $\vec{H}$ ,  $\vec{D}$  with  $\vec{B}$ , and the relative effective permittivity ( $\varepsilon_{eff}$ ) with the relative effective permeability ( $\mu_{eff}$ ). All the above vectors,  $\varepsilon_{eff}$  and  $\mu_{eff}$  are average quantities over the whole regions occupied by the sample, namely:

$$\bar{V} = \int \vec{V}(\vec{r}) d\vec{r}^3 \quad \text{with } \vec{V} \text{ being anyone of the field vector,} \quad (2-22)$$

$$\varepsilon_{eff} = \int D_z(\vec{r}) d\vec{r}^3 / \int E_z(\vec{r}) d\vec{r}^3, \quad \text{and} \quad (2-23)$$

$$\mu_{eff} = \int B_z(\vec{r}) d\vec{r}^3 / \int H_z(\vec{r}) d\vec{r}^3. \quad (2-24)$$

where  $D_z$ ,  $E_z$ ,  $B_z$ ,  $H_z$  are the components of the respective field vectors along the



direction of the applied  $\vec{E}$  or  $\vec{H}$ .

Based on the above reasoning, throughout this thesis, all the equations applied to dielectric cases will automatically assumed to be equally applicable to the magnetic cases with the above conversion rules.

This suggestion is further verified by the results of FE analyses for three models. The first model is illustrated in Fig. 2.1, where a sample is placed at the central point of a Helmholtz coil, and the magnetic field is applied by assigning a current to pass through the coils. The second model is shown in Fig. 2.2, where a constant magnetic scalar potential is applied across two opposite surfaces, meanwhile a periodic boundary condition (PBC) is applied on the rest four surfaces of the composite. The third model, as shown in Fig. 2.3, is similar to the Fig. 2.2, but a constant electric scalar potential difference is applied instead.

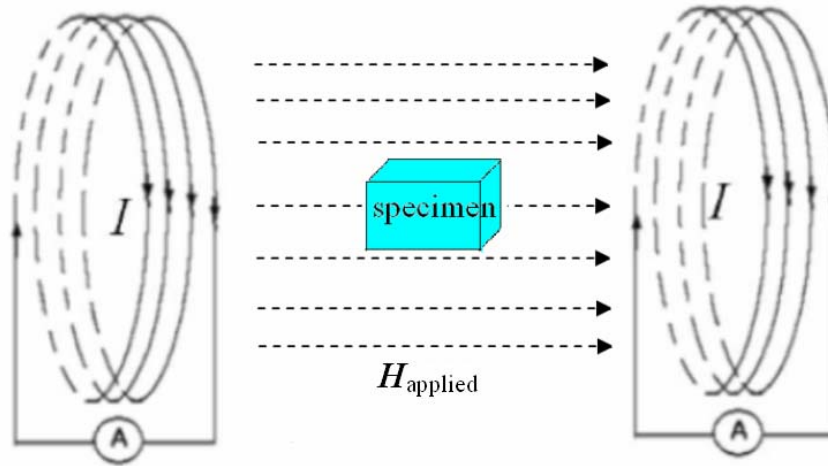


Fig. 2.1 Schematic diagram for magnetic simulations (Model 1).

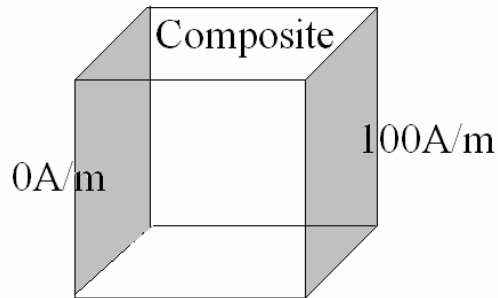


Fig. 2.2 Schematic diagram for magnetic simulations (Model 2).

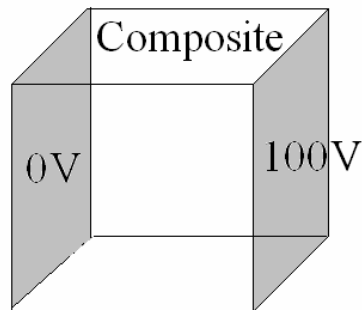


Fig. 2.3 Schematic diagram for dielectric simulations (Model 3).

Fig. 2.4 shows the comparison of the results determined by using three different models. Using the results of Rayleigh model of the same configuration as a common reference, the results of the above three models deviate from the reference value by 1.23, 0.11 and 0.26 % respectively, which are considered to be negligibly small.

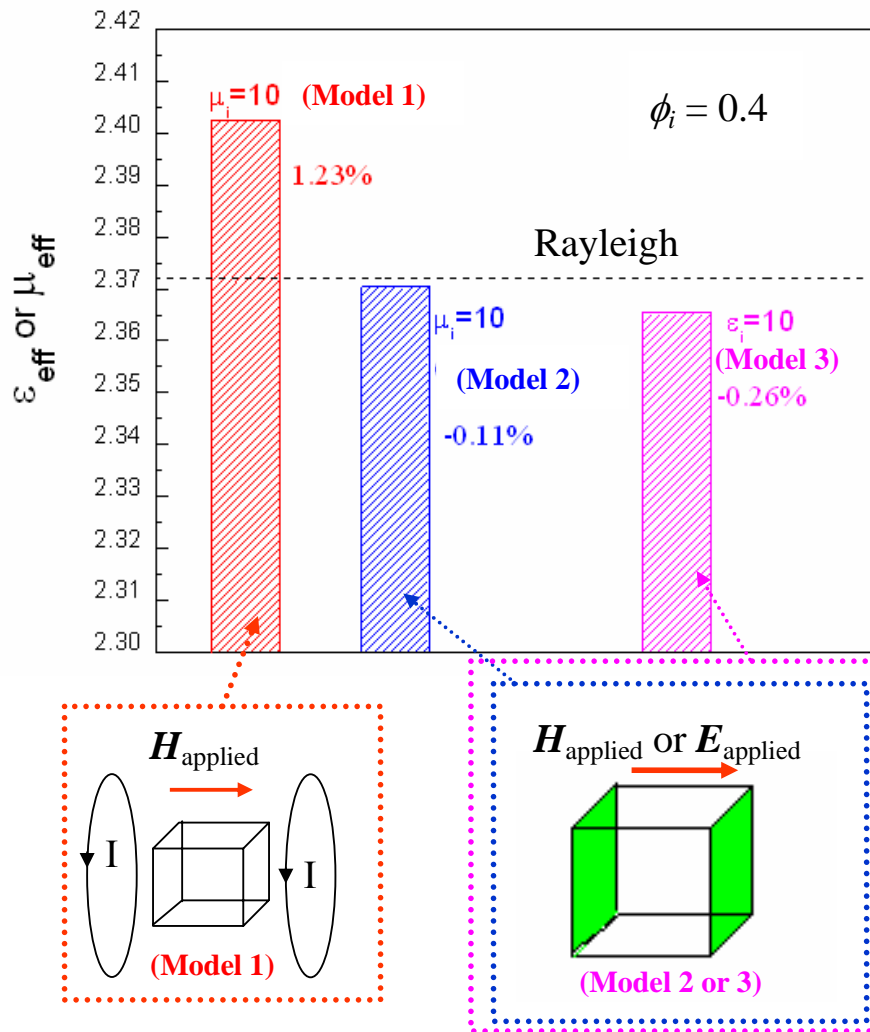


Fig. 2.4 Deviation of the results of three different models which determine from 6x6x6 sphere inclusions at  $\phi_i \sim 0.4$ .



## 2.3 Review of conventional analytic theories for the properties of a dielectric composite or a magnetic composite

In this section, we give a brief summary of many published analytic theories for describing the relative effective permittivity of a 2-phase (0-3) composite with dielectric or magnetic inclusions in a non-electromagnetically active matrix --- referred to as a 2-phase dielectric or magnetic composite afterwards in this thesis. These theories are the Maxwell-Garnett (M-G) theory, nonsymmetric-Bruggeman (or simply Bruggeman) theory, Poon-Shin (P-S) theory, Landauer theory and Rayleigh theory. The Rayleigh theory is unique for specifying the inclusions to be arranged in a periodic pattern.

### 2.3.1 Maxwell-Garnett (M-G) theory

The M-G theory [Maxwell Garnett, 1904] was proposed based on a model as depicted in Fig. 2.5. A dielectric sphere of radius ( $a$ ), having a linear and isotropic relative permittivity  $\varepsilon$ , is embedded in a matrix. The whole system is placed in an environment of a uniform external electric field  $\vec{E}_m$ . Assuming that there is no free charge in the boundary between the spherical inclusion and the matrix, the condition  $\rho = 0$  holds.

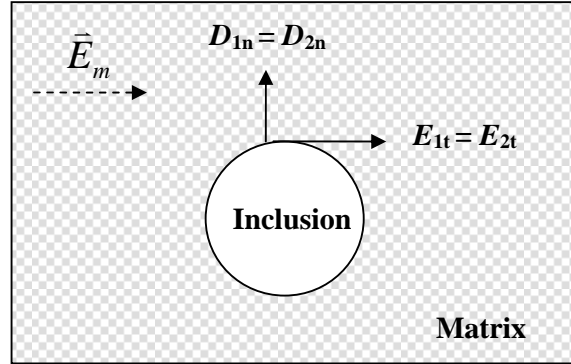


Fig. 2.5 M-G model in which a spherical inclusion is placed inside a matrix with boundary conditions as shown.

According to the boundary conditions stated in Eqs. (2-20) and (2-21), the electric scalar potentials in the inclusion ( $\varphi_i$ ) and matrix ( $\varphi_m$ ) can be determined as follows:

$$\varphi_i(r, \theta) = -\left(\frac{3\varepsilon_m}{\varepsilon_i + 2\varepsilon_m}\right)E_m r \cos \theta = -\left(\frac{3\varepsilon_m}{\varepsilon_i + 2\varepsilon_m}\right)E_m z, \quad \text{and} \quad (2-25)$$

$$\varphi_m(r, \theta) = -E_m r \cos \theta + \left(\frac{\varepsilon_i - \varepsilon_m}{\varepsilon_i + 2\varepsilon_m}\right)\left(\frac{a^3}{r^2}\right)E_m \cos \theta, \quad (2-26)$$

where  $E_m$  is the electric field in the matrix at a point far away from the sphere.

From Eq. (2-25), the electric field inside the dielectric sphere is:

$$\bar{E}_i = -\nabla \varphi_i = \left(\frac{3\varepsilon_m}{\varepsilon_i + 2\varepsilon_m}\right)E_m \hat{z}. \quad (2-27)$$

One can introduce two more equations according to the dielectric properties of the inclusion and matrix:



$$D_m = \varepsilon_m E_m, \quad \text{and} \quad (2-28)$$

$$D_i = \varepsilon_i E_i. \quad (2-29)$$

Combing Eqs. (2-27) to (2-29), one can prove that:

$$D_m = D_i + 2\varepsilon_m(E_i - E_m). \quad (2-30)$$

Two more equations are introduced to represent the average effective electric displacement  $D = \int D_z(\vec{r})dr^3$  and the average effective electric field  $E = \int E_z(\vec{r})dr^3$  of the composite. They are supposed to be related to the  $\bar{D}$  and  $\bar{E}$  fields in the inclusions and matrix, and the relative volume fractions of the two phases  $\phi_i$  and  $\phi_m$  in the form of:

$$D = \phi_i D_i + \phi_m D_m, \quad \text{and} \quad (2-31)$$

$$E = \phi_i E_i + \phi_m E_m. \quad (2-32)$$

We note that the Eqs. (2-31) and (2-32) are valid although  $\bar{D}$  and  $\bar{E}$  are 3-dimensional fields, each containing a dipole component due to the spherical inclusion. However, the spatial integration of a dipole field is zero, so that Eqs. (2-31) and (2-32) hold.



Expressions (2-28) to (2-32) form a set of five equations containing six unknowns. If  $D$  is solved in terms of  $E$ , the relative effective permittivity  $\varepsilon_{eff} = D/E$  can thus be deduced as:

$$\varepsilon_{eff} = \frac{D}{E} = \varepsilon_m + \phi_i \frac{3\varepsilon_m(\varepsilon_i - \varepsilon_m)}{\phi_m(\varepsilon_i + 2\varepsilon_m) + 3\phi_i\varepsilon_m}. \quad (2-33)$$

An alternative format of this solution is:

$$\frac{\varepsilon_{eff} - \varepsilon_m}{\varepsilon_{eff} + 2\varepsilon_m} = \phi_i \frac{\varepsilon_i - \varepsilon_m}{\varepsilon_i + 2\varepsilon_m}. \quad (2-34)$$

The M-G theory has some limitations because the model designed to have one sphere in an infinitely large matrix is over-simplified. In a real case (i) there are much more inclusions separated by finite distances such that the electrical field generated from individual inclusions would superimpose with each other, and (ii) the inclusion shape is unlikely to be spherical in reality, and (iii) the size of the matrix is finite such that edge effect would occur. Therefore, the M-G theory can only be a fairly good approximation when  $\phi_i$  is small enough (dilute case) and the inclusion shape is approximately spherical [Jylhä and Sihvola, 2007; Merrill, et al., 1999; Waki, et al., 2005a].



We further note that the M-G formula is valid for a composite containing dielectric microwires randomly oriented in an epoxy matrix, and if the permeability of the wire inclusions is high and  $\phi_i$  smaller than 0.13 [Darius, 2008]. It has also been proved that the model is valid when the spherical inclusions are randomly distributed in a homogeneous environment in the range of low  $\phi_i$  [Kärkkäinen, et al., 2001; Sihvola, 1999a].

### 2.3.2 Nonsymmetric-Bruggeman theory

Bruggeman [Bruggeman, 1935] modified the M-G formula by introducing a differentially mixing process, where infinitesimal spherical inclusions are added progressively and the permittivity of the matrix is modified cumulatively. At a particular moment, the composite containing inclusions with a volume fraction  $\phi_i'$  is regarded as a homogeneous substance, and is thus regarded as a “matrix”. The relative permittivity is denoted by  $\varepsilon_m$ , which should be a function of  $\phi_i'$ :

$$\varepsilon_m = \varepsilon(\phi_i'). \quad (2-35)$$

An infinitesimal volume  $\delta V$  is then added to the composite. The volume of the system is  $V$ . The increment in the inclusion volume fraction is thereby  $\delta\phi = \delta V/V$ . One can prove that the inclusion volume fraction (with  $V$  kept unchanged) is modified to



become:

$$\phi_i = \phi_i' + (1 - \phi_i')\delta\phi. \quad (2-36)$$

The corresponding change in the relative permittivity is  $\varepsilon(\phi_i) - \varepsilon(\phi_i')$ , which can be

derived with Taylor expansion as:

$$\varepsilon(\phi_i) - \varepsilon(\phi_i') = (1 - \phi_i')\delta\phi \frac{d\varepsilon(\phi_i)}{d\phi_i}. \quad (2-37)$$

The M-G formula Eq. (2-33),

$$\varepsilon_{eff} = \frac{D}{E} = \varepsilon_m + \phi_i \frac{3\varepsilon_m(\varepsilon_i - \varepsilon_m)}{\phi_m(\varepsilon_i + 2\varepsilon_m) + 3\phi_i\varepsilon_m}, \quad (2-33)$$

is applied, but,  $\varepsilon_{eff}$  is replaced by  $\varepsilon(\phi_i)$ , and  $\varepsilon_m$  by  $\varepsilon(\phi_i')$  which is the permittivity of

the composite before the infinitesimal spherical inclusion is added to modify the

composite. The small inclusion added is regarded to be completely “absorbed” by the

background matrix to form a homogenous new “matrix”. The increase in inclusion

fraction is assumed to be small, such that  $\phi_m$  is close to 1, and  $\phi_i$  is replaced by a small

$\delta\phi$ . As such, Eq. (2-33) becomes:

$$\varepsilon(\phi_i) - \varepsilon(\phi_i') \approx \delta\phi \frac{3\varepsilon(\phi_i')[\varepsilon_i - \varepsilon(\phi_i')]}{\varepsilon_i + 2\varepsilon(\phi_i')}. \quad (2-38)$$

Combining Eqs. (2-37) and (2-38), we have:

$$(1 - \phi_i') \frac{d\varepsilon(\phi_i)}{d\phi_i} = \frac{3\varepsilon(\phi_i')[\varepsilon_i - \varepsilon(\phi_i')]}{\varepsilon_i + 2\varepsilon(\phi_i')}. \quad (2-39)$$



Setting the dummy variables  $\phi_i$  and  $\phi_i'$  to be  $\phi$ , one obtains an integral formula:

$$\int_{\varepsilon_m}^{\varepsilon_{eff}} \frac{\varepsilon_i + 2\varepsilon}{3\varepsilon(\varepsilon_i - \varepsilon)} d\varepsilon = \int_0^{\phi_i} \frac{d\phi}{1-\phi}, \quad (2-40)$$

which gives:

$$\frac{\varepsilon_i - \varepsilon_{eff}}{\varepsilon_{eff}^{1/3}} = (1 - \phi_i) \left( \frac{\varepsilon_i - \varepsilon_m}{\varepsilon_m^{1/3}} \right). \quad (2-41)$$

This model is named as nonsymmetric-Bruggeman (or simply Bruggeman) model to be distinguished from the symmetric-Bruggeman model where the roles of inclusions and matrix are not differentiated (see 2.3.4).

The Bruggeman model is considered to be better than the M-G one. First, the employment of concurrent accumulative modification of the matrix properties with the addition of inclusions releases the geometrical constraint which limits the maximum inclusion volume fraction as in the case of the M-G model. Second, the approach attempts to include the influence of all the inclusions on the matrix (and hence the composite), such that the effect due to the interaction between the inclusions located closely is considered to some extent. As such, the predicted result of  $\varepsilon_{eff}$  is found to be



closer to the experimental one than that predicted by the M-G model. This is particularly true in the region of high inclusion volume fraction. Normally, the result of the Bruggeman theory is higher than that of the M-G theory.

On the other hand, in Bruggeman's approach, the inclusions are added in a way that as if they are "dissolved" in the matrix in successive differential steps, such that the substance constructed would be a continuous medium but cannot reproduce the real material structure [Chew, et al., 2003]. In particular, the boundaries between the inclusions and the matrix in the real system do not appear in the model. This is why the theory is also referred to as the "effective medium theory (EMT)". One would therefore expect that the  $\epsilon_{eff}$  value predicted with this theory would deviate more or less from the true one, especially when the inclusion volume fraction is large. In addition, the model does not reflect the influences due to some other factors, such as the inclusion shape and their distribution, which are the difficulties common to most analytic theories where exact formulation describing every detail of a real system is not easily established.



### 2.3.3 Poon-Shin (P-S) model

Poon and Shin [Poon and Shin, 2004] adapted another approach to introduce modification to the matrix. Different from Eq. (2-28) which states that  $D_m = \varepsilon_m E_m$ , it is assumed that the inclusions are polarized to introduce an addition term, such that the effective electric displacement in the matrix is modified to become:

$$D_m' = \varepsilon_m E_m + P = \varepsilon_m E_m + p_1 n/V, \quad (2-42)$$

where  $p_1$  is the dipole moment associated with one spherical inclusion, and  $n/V$  is the number concentration of the spheres.

Now, we derive the expression of  $p_1$ . If the potential field around a spherical inclusion in the matrix is still considered to have the form of Eq. (2-26):

$$\varphi_m(r, \theta) = -E_m r \cos \theta + \left( \frac{\varepsilon_i - \varepsilon_m}{\varepsilon_i + 2\varepsilon_m} \right) \left( \frac{a^3}{r^2} \right) E_m \cos \theta, \quad (2-26)$$

the second term should be equal to the potential associated with the dipole field of a spherical inclusion, which can also be expressed in a general form like:

$$\varphi_{p_1} = \frac{1}{4\pi\varepsilon_m} \frac{\vec{P} \cdot \vec{r}}{r^3} = \frac{1}{4\pi\varepsilon_m} \frac{p_1 \cos \theta}{r^2}. \quad (2-43)$$

Combing the second term on the right side of Eq. (2-26) and (2-43), one obtains:

$$p_1 = v (\varepsilon_i - \varepsilon_m) \frac{3\varepsilon_m E_m}{\varepsilon_i + 2\varepsilon_m} = v (\varepsilon_i - \varepsilon_m) E_i, \quad (2-44)$$



where  $v = 4\pi a^3/3$  is the volume of a spherical inclusion. Putting  $p_1$  into Eq. (2-42)

one obtains:

$$D_m' = \varepsilon_m E_m + v (\varepsilon_i - \varepsilon_m) E_i n/V = \varepsilon_m E_m + \phi_t (\varepsilon_i - \varepsilon_m) E_i. \quad (2-45)$$

If we modify Eq. (2-30) by replacing  $D_m$  with  $D_m'$  :

$$D_m' = D_i + 2\varepsilon_m (E_i - E_m), \quad (2-46)$$

then by combining this equation with Eq. (2-45), we obtain:

$$D_m + \phi_t (\varepsilon_i - \varepsilon_m) E_i = D_i + 2\varepsilon_m (E_i - E_m). \quad (2-47)$$

Further combining with

$$D = \phi_i D_i + \phi_m D_m, \quad (2-31)$$

$$E = \phi_i E_i + \phi_m E_m, \quad (2-32)$$

and the constitutive equations

$$D_m = \varepsilon_m E_m, \quad \text{and} \quad (2-28)$$

$$D_i = \varepsilon_i E_i, \quad (2-29)$$

we obtain the effective relative permittivity for the P-S theory as:

$$\varepsilon_{eff} = \varepsilon_m + \frac{\phi_i (\varepsilon_i - \varepsilon_m)}{\phi_i + (1 - \phi_i) \left[ \frac{\varepsilon_i + 2\varepsilon_m - \phi_i (\varepsilon_i - \varepsilon_m)}{3\varepsilon_m} \right]}. \quad (2-48)$$

This formula takes account of the interaction between the particulates by incorporating

the polarization field from a spherical inclusion [Wong, et al., 2002], such that it can



reflect better the modification of the matrix by the inclusions compared to the M-G model or possibly the Bruggeman model.

### 2.3.4 Landauer model

Landauer considered that the 2-phase background surrounding an inclusion in a real system (labeled by “1” and “2” in Fig. 2.6a) [Landauer, 1952], could be treated as if it is a uniform single-phase background (labeled by “3” in Fig. 2.6b). This phase 3 is regarded as a homogeneous matrix, which relative permittivity is set to be equal to the effective relative permittivity of the overall composite  $\varepsilon_{eff}$ . It is further assumed that the inclusion is in a spherical shape. No free charge exists in the system, particularly at the interface between the inclusion and the matrix, as assumed in the M-G model.

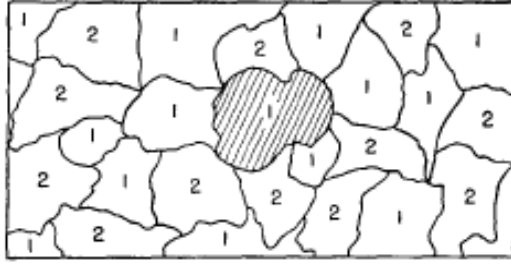


Fig. 2.6a

The shaded region is an inclusion of phase 1, which is surrounded by a 2-phase medium.

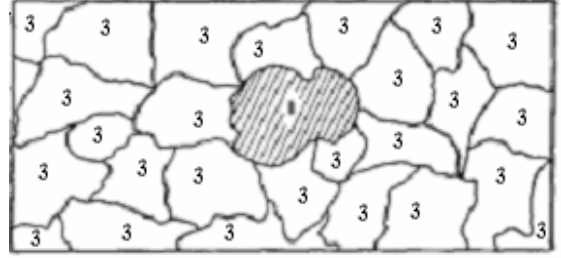


Fig. 2.6b

In the Laudauer model, the surrounding environment of an inclusion of phase 1 is imagined to be a single-phase uniform phase 3 having an effective relative permittivity  $\epsilon_{eff}$ .

These assumptions suggest to modify Eq. (2-30) by changing  $D_m$  to  $D$ ,  $\epsilon_m$  to  $\epsilon_{eff}$  and  $E_m$

to  $E$ , which becomes:

$$D = D_i + 2\epsilon_{eff}(E_i - E). \quad (2-49)$$

Combining this expression with:

$$D_m = \epsilon_m E_m, \quad (2-28)$$

$$D_i = \epsilon_i E_i, \quad (2-29)$$

$$D = \phi_i D_i + \phi_m D_m, \quad \text{and} \quad (2-31)$$

$$E = \phi_i E_i + \phi_m E_m, \quad (2-32)$$



one obtains the final result of  $\varepsilon_{eff}$  as:

$$\varepsilon_{eff} = \varepsilon_m + \phi_i \frac{3\varepsilon_{eff}(\varepsilon_i - \varepsilon_m)}{\varepsilon_i + 2\varepsilon_{eff}}. \quad (2-50)$$

An alternative expression of Eq. (2-50) is:

$$\phi_i \left( \frac{\varepsilon_i - \varepsilon_{eff}}{\varepsilon_i + 2\varepsilon_{eff}} \right) + \phi_m \left( \frac{\varepsilon_m - \varepsilon_{eff}}{\varepsilon_m + 2\varepsilon_{eff}} \right) = 0. \quad (2-51)$$

This formula is generally referred to as the symmetric-Bruggeman formula in literature

[Jylhä and Sihvola, 2007; Merrill, et al., 1999; Sihvola, 1999e; Stroud, 1979; Waki, et al., 2005a; Xue, 2003], because the roles of inclusion and matrix can be interchanged

by swapping  $\varepsilon_i$  and  $\varepsilon_m$ , and  $\phi_i$  and  $\phi_m$  respectively without affecting the value of  $\varepsilon_{eff}$ .

Landauer further proposed that the model can be used for arbitrary inclusion [Goncharenko, 2003; Landauer, 1952].

### 2.3.5 Rayleigh model

Rayleigh derived a set of formulae to estimate the relative effective permittivity of a dielectric composite based on the Lorentz-Lorentz theory [Rayleigh, 1892]. This model is distinctive as it is based on a model having spherical inclusions arranged in a cubic 3-D array (Fig. 2.7) or cylindrical inclusions arranged in a periodic 2-D array.

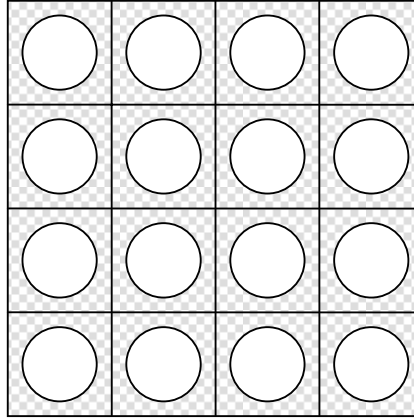


*Fig. 2.7 Rayleigh model in which spherical inclusions are arranged in a cubic array in an infinitely large matrix.*

In Rayleigh's original paper, he solved the model by expanding the potential function in a harmonic series. Different orders of approximation can be taken depending on how many terms in the expansion are used. For a lower level of approximation, a formula as follows was derived:

$$\frac{\varepsilon_{eff} - \varepsilon_m}{\varepsilon_{eff} + 2\varepsilon_m} \left( \frac{1}{\phi_i} \right) = \frac{\varepsilon_i - \varepsilon_m}{\varepsilon_i + 2\varepsilon_m}. \quad (2-52)$$

This formula is equivalent to the M-G formula [Sareni, et al., 1997; Sihvola, 1999b] describing the case of having one sphere embedded in an infinitely large matrix. By using more terms in the harmonic expansion of the potential function, a more accurate equation was achieved, which is expressed in the form of [Sihvola, 1999f]:



$$\varepsilon_{eff} = \varepsilon_m + \frac{3\phi_i \varepsilon_m}{\frac{\varepsilon_i + 2\varepsilon_m}{\varepsilon_i - \varepsilon_m} - \phi_i - 1.65 \frac{\varepsilon_i - \varepsilon_m}{\varepsilon_i + 4\varepsilon_m / 3} \phi_i^{10/3}}. \quad (2-53)$$

Rayleigh's approach is an accurate approach for a 2-phase mixture with a periodic array of spherical inclusions. The array is not necessary to be a cubic-one [Périn, 2004]. The problem of this model is that the value of the relative effective permittivity grows to infinity when the inclusions come to touch with each other. Hence it can only be applied to a composite of a relatively low inclusion volume fraction.

### 2.3.6 Wiener bounds and Hashin-Shtrikman bounds

The above models for a 0-3 composite are based on different assumptions and hence the results obtained may not be the same, and deviate from the real value to some extent. Thereby, bounds of the  $\varepsilon_{eff}$  values predicted by the theories are estimated. Two famous proposals of the bounds, namely the Wiener bounds [Kärkkäinen, et al., 2001] and the Hashin-Shtrikman bounds [Sihvola, 1999d], are described in this section.

The Wiener bounds are derived from the M-G equation for a composite containing aligned ellipsoidal inclusions. They are evaluated at two extreme conditions in which



the depolarization factor of the inclusions is assigned to be 0 and 1, respectively. The former corresponds to a case where the inclusions are long and narrow wires, aligned in parallel to the applied field. The latter is for the wires to be aligned perpendicular to the applied field. The values of  $\varepsilon_{eff}$  for these two special cases are:

$$\varepsilon_{eff, \max} = \phi_i \varepsilon_i + \phi_m \varepsilon_m, \quad \text{and} \quad (2-54)$$

$$\varepsilon_{eff, \min} = \frac{\varepsilon_i \varepsilon_m}{\phi_i \varepsilon_m + \phi_m \varepsilon_i}. \quad (2-55)$$

For deriving the Hashin-Shtrikman bounds, it is assumed that the mixture is macroscopically isotropic. The electrostatic energy can be expressed in terms of a volume integral of the dot product of the electric field and polarization in the system. The stationary property (e.g.  $\varepsilon_{eff}$ ) of the materials is estimated by applying various approximate trial fields. Results obtained are believed to be closer to the true value than those evaluated by the following two equations.

$$\varepsilon_{eff, \max} = \varepsilon_i + \frac{1 - \phi_i}{\frac{1}{\varepsilon_m - \varepsilon_i} + \frac{\phi_i}{3\varepsilon_i}}, \quad \text{and} \quad (2-56)$$

$$\varepsilon_{eff, \min} = \varepsilon_m + \frac{\phi_i}{\frac{1}{\varepsilon_i - \varepsilon_m} + \frac{1 - \phi_i}{3\varepsilon_m}}. \quad (2-57)$$

They are regarded as the upper and lower Hashin-Shtrikman bounds. We note that the lower bound Eq. (2-57) is the same as the M-G formula Eq. (2-33).



## 2.4 FE analysis for composites

### 2.4.1 Fundamentals of FE method

This section describes some general principles underlining FE. We refer to the scalar potential approach as described in the “Theoretical Reference for ANSYS and ANSYS Workbench” of the manual of the commercial code ANSYS 11.0. For analyzing the stationary properties of a medium, the constitution equation is written as [ANSYS, 2007a]:

$$\vec{B} = \mu \vec{H} + \mu_0 \vec{M}_0, \quad (2-58)$$

where  $\vec{B}$  and  $\vec{H}$  are magnetic induction and magnetic field vectors, and  $\vec{M}_0$  is the magnetization vector due to the presence of a magnetic phase.

To solve for  $\vec{H}$ , the program first sets:

$$\vec{H} = \vec{H}_g - \nabla \varphi_g, \quad (2-59)$$

with  $\vec{H}_g$  being a guessed  $\vec{H}$  and  $\varphi_g$  a generalized scalar potential. The next is to rewrite the constitutive equation by putting Eqs. (2-58) and (2-59) into  $\nabla \cdot \vec{B} = 0$ . One obtains the relationship that  $\varphi_g$  should obey, namely:

$$\nabla \cdot [\mu] \nabla \varphi_g - \nabla \cdot [\mu] \vec{H}_g - \nabla \cdot \mu_0 \vec{M}_0 = \bar{0}, \quad (2-60)$$

where  $[\mu]$  is the permeability matrix.



In Eq. (2-60),  $[\mu]$  and  $\bar{M}_0$  are given data.  $\bar{H}_g$  is primarily estimated from the excitation due to free charge current density ( $\bar{J} \neq 0$ ) through a volume integration:

$$\bar{H}_g = \frac{1}{4\pi} \int_{\text{volume}} \frac{\bar{J} \cdot \bar{r}}{|\bar{r}|^3} d(\text{volume}). \quad (2-61)$$

As such Eq. (2-60) can be solved numerically to give an approximation of  $\phi_g$ . It is then put into (2-59) to derive  $\bar{H}$ .

We further note that:

- (i) Other quantities, such as  $\bar{B}$  and  $\mu_{eff}$  concerned will be derived from  $\bar{H}$ .
- (ii) This is just one of employable approaches, and is used most of the time in this study. It is named as Reduced Scalar Potential (RSP) strategy in the manual.
- (iii) A treatment for magnetic substance is selected to describe here because we originally attempt to investigate the properties of magnetic composites due to the background of the project, but based on the argument in Section 2.2, there would have no distinction between the treatment for investigating the static properties of a magnetic composite and that for a dielectric composite.



A typical FE analysis process consists of five major parts as follows:

➤ Building up a model:

This is the most time consuming part in an analysis. It involves the construction of a structure according to the real system. In the present study, the model is made to contain inclusions of specific shape(s) distributed in a certain pattern. A mechanism is introduced to generate a magnetic field. In addition, the element types, meshing size, element real constants and material properties are specified.

➤ Meshing:

The model is then meshed by dividing it into a number of elements. The vertices of the elements are defined as nodes. The size of the elements should be appropriately selected, such that the nodes of two adjacent elements can properly match. If the elements are too coarse, the model would deviate significantly from the real system. Many details of the system cannot be reproduced. This induces some errors in the calculation. If the elements are too fine, the node number may be too large for the computer to handle.

➤ Applying loads:

In this step, loads such as forces, stresses, electric or magnetic field are applied to a system under investigation. In addition, the degree of freedom (DOF), constraints,



boundary conditions and symmetry are required to be specified.

➤ Obtaining solution:

Numerical calculation is then performed, say by sending the problem to a built-in processor of a software. A solution will be obtained if the problem is successfully solved.

➤ Reviewing results:

There are two types of calculated results, namely, the reckoned one and the derived one. The former refers to the data obtained directly from the calculations. In our case, they are the nodal magnetic field distribution. The derived data include induction field distribution, element averages of  $\vec{H}$  and  $\vec{B}$ , and element volumes etc. These results can be plotted as a vector diagram or a contour diagram. The numerical values can also be provided in a tabulated format. Further calculations can be performed by some built-in functions of the software.

### 2.4.2 FE model used in the present study

For performing FE analyses, the commercial source code ANSYS 11.0 was used. We calculate the values of  $\mu_{eff}$  of composites containing magnetic inclusions by using the model shown in Fig. 2.1, or that in Fig. 2.2 in which a constant magnetic scalar



potential drop is applied. For calculating  $\epsilon_{eff}$  of composite containing dielectric inclusions, the model shown in Fig. 2.3 is used where a constant electric scalar potential drop is applied. Based on the principle of equivalency as mentioned in Section 2.2, the value of  $\mu_{eff}$  derived is shown to be the same as that of  $\epsilon_{eff}$  of a composite with the same geometrical structure.

In particular, the current coil used in model 1 (Fig. 2.1) is assigned to be element type “Source36” as defined in ANSYS. The magnitude of current in the coils determines the magnetic field intensity. As shown in Fig. 2.8 [ANSYS, 2007c], three key points (I, J and K) are required to define the current coils. One also needs to set the length (DZ) and thickness (DY) of the coils, and the magnitude (CUR) and direction of the current flow. The applied field  $H_{applied}$  generated by a current source in a region embracing the whole system can thus be determined.

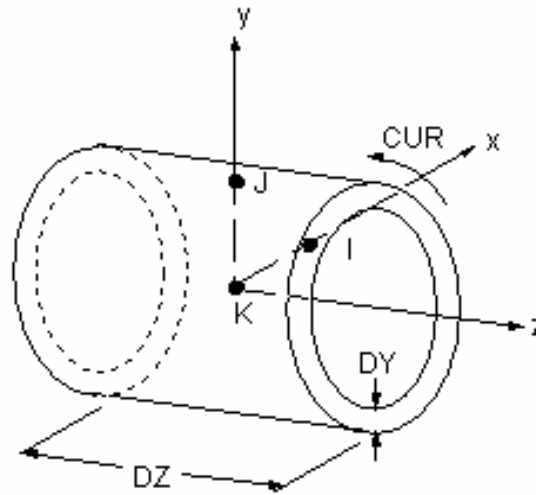
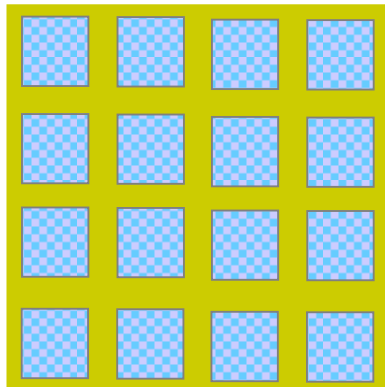


Fig. 2.8 A sketch of a current source formed by element type “Source36”.

The composite has a matrix containing dielectric or magnetic inclusions arranged in a 4x4x4 array (Fig. 2.9) or a 6x6x6 array. The inclusions are either in spherical or cubic shape. For example, the regions shown in gray represent the inclusions, and that in pale gray the non-dielectric (or non-magnetic) matrix.

(A)



(B)

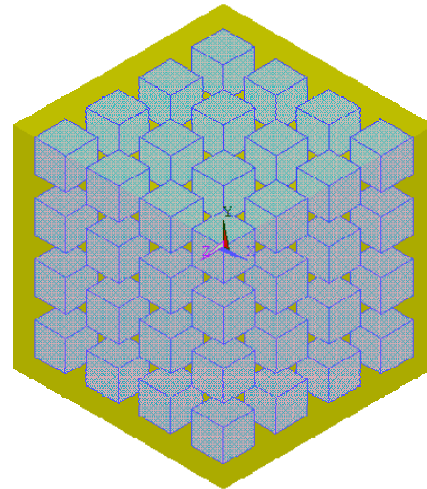


Fig. 2.9 The structure of a composite model (A: Side view; B: 3-D).



For magnetic models, element type “Solid96” defined in ANSYS is used to construct the magnetic inclusions, matrix and surrounding air, while “Solid122” is used for dielectric models. “Solid96” and “Solid122” elements are hexahedrons having 8-nodes at the corners, and 20-nodes at corners and the mid-edges, respectively. The geometries, node locations and the coordinate systems used to define a “Solid96” element and a “Solid122” element are shown in Figs. 2.10a and b [ANSYS, 2007d]. They can be degenerated in some circumstances to become a tetrahedron, a wedge, a pyramid and a prism. The output of both “Solid96” and “Solid122” can be the data evaluated at the nodes (nodal solution) or the averages of the elements (element solution).

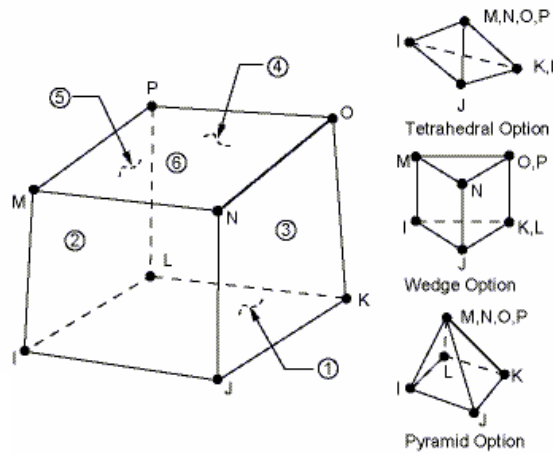


Fig. 2.10a Diagram showing “Solid96” element.

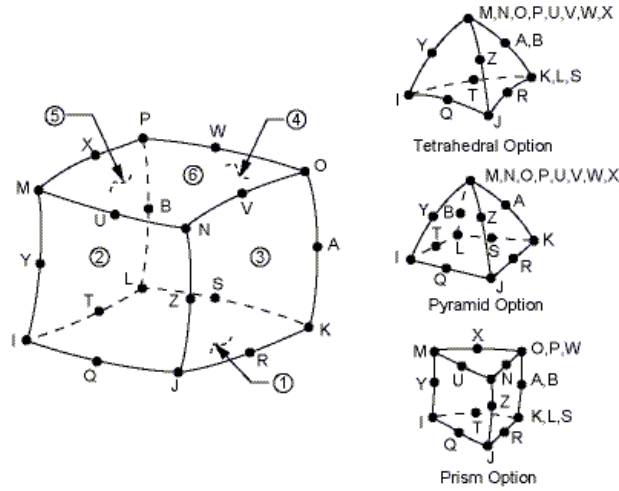


Fig. 2.10b Diagram showing “Solid122” element.

Before meshing the model, we need to specify the geometry and properties of the materials in all regions. They include:

- (i) the fineness of the meshes;
- (ii) the numbers of rows and columns (size) of the inclusion array;
- (iii) the values of the linear relative permeabilities of the inclusions ( $\mu_i$ ) and the matrix ( $\mu_m$ ), where  $\mu_m$  is constantly set to be 1 (air);
- (iv) the shape of the inclusions, which is set to be spherical, cubic and wires respectively;
- (v) the size of the inclusions which determines their volume fraction in the composite;
- (vi) the orientations for wire inclusions which can be set to be perpendicular to and in parallel with the applied field.



After fixing all these parameters, the model can be meshed with the “Smart Mesh” function, which helps to optimize the element sizes automatically. Alternatively, one can manually select the element size of each part. Also, the element size should be carefully selected. If it is set to be too small, the computation time would be very long, or the matrix size is too large for the computer to handle. However, if the elements are too coarse, the model would deviate from the real structure.

The problem is then sent to the solver to get a solution. Three possible strategies are available. They are [ANSYS, 2007b]:

- (i) reduced scalar potential (RSP)
- (ii) difference scalar potential (DSP) and
- (iii) general scalar potential (GSP)

RSP is applicable for the case when there is a free charge current distribution in the model; or there is no free charge current but has magnetic substance(s). DSP and GSP are for a system having free charge current as well as magnetic substance(s). We mostly applied RSP method, and the results were cross checked by using GSP. Mostly two approaches give the same result.



After getting the simulated results of  $\vec{H}$ , one can further calculate the  $\vec{B}$  and  $\mu_{eff}$  of the composite. In particular,  $\mu_{eff}$  is set to be equal to the ratio of average of the component of  $\vec{B}$  in parallel with the applied field ( $B_z$ ) to that of  $\vec{H}$  ( $H_z$ ):

$$\mu_{eff} = \frac{\int_v B_z dv}{\mu_0 \int_v H_z dv} \quad (2-62)$$

We believe that the results obtained by FE analysis reflects more accurately the real situation if the element sizes are properly selected. Hence, the FE results are more suitable to be referred to for examining the correctness of the results derived from conventional analytic theories. One restriction is that the size of the inclusion array cannot be too larger.

### 2.4.3 Ranges of the parameters settings for 0-3 composite models

The parameters in the FE analysis are varied in the ranges as shown in Table 2.1. The purposes for varying these parameters are also indicated in the table.



Table 2.1 Parameters and their ranges of variations in the simulation processes

Parameter	Range	Purpose of investigation
Number of elements	157603 – 538888	influences of the fineness of meshing
Size of the 3-D inclusion array	1x1x1 and 4x4x4	influences of the size of the inclusion array
$\mu_i$ for inclusions ( $\mu_m = 1$ )	10 and 600	influences of $\mu_i$ and its deviation for $\mu_m$
Inclusion volume fraction $\phi_i$	$\phi_i = 0 - 1$ $\mu_i = 10$ or 1000	trend of $\mu_{eff}$ with increasing inclusion volume fraction
Shape of inclusions	sphere, cube and wire	influences of demagnetization effect due to inclusion shape
Wire orientation	perpendicular to $H_{applied}$ parallel to $H_{applied}$	influences of demagnetization effect due to the orientation of long inclusions



## 2.5 Results and Discussions

### 2.5.1 Convergence tests for FE analyses

In a FE analysis, if the model is meshed coarsely, its structure would deviate more or less from the original one and leads to some error in the calculation. Though the accuracy can be improved by finer meshing, the element number cannot be increased infinitely, as the maximum manageable node number is limited by the capability of the computer, such as the size of the memory, and the speed of the CPUs which determines the time required for a single run. In order to maximize the accuracy, and to get a compromise between the accuracy and calculation time of an analysis, a series of pilot tests is performed first by systematically decreasing the element size (increasing the element number) in order to find out the condition for the results to approach asymptotically a certain limit. Until the calculated results become less sensitive to further increase in element number, fineness of the meshing is deemed to be appropriate. The process is referred to as the convergence test.

Fig. 2.11 shows the trend of  $\mu_{eff}$  increasing element number (N) for three systems. The first one contains only one single inclusion (specified as a 1x1x1 model), with a



permeability  $\mu_i = 10$ . When  $N$  increases from 760 to 6050, the simulated  $\mu_{eff}$  value drops by 5%. Further increase of  $N$  to 48300 further reduced  $\mu_{eff}$  by just 2%. Such a variation is considered to slow enough for the calculated  $\mu_{eff}$  value to be accepted as a reasonable estimate of the real value.

For the model containing 64 inclusions (specified as a 4x4x4 model) and  $\mu_i = 10$ , when  $N$  increases from 760 to 6050,  $\mu_{eff}$  merely drops by 3.5%, which is small enough for the result at  $N = 6050$  to be used to represent a good estimate of the true value, as further increase in the fineness will only give minor improvement.

At last, for a 1x1x1 model with  $\mu_i = 600$ , when  $N$  increases from 760 to 6050, and then to 48300, the calculated  $\mu_{eff}$  drops by 28% and 5% respectively. This demonstrates that results trend to approach some asymptotic value. We therefore infer that result evaluated at  $N = 48300$  or above close enough to the true  $\mu_{eff}$  value.

Based on the above observations, we decided to employ a 4x4x4 model meshed to include not less than 6050 elements to calculate  $\mu_{eff}$ . With  $\mu_i$  varying in the range of 1 to 600, true effective relative permeability is believed to be properly estimated.



We stuck to this guideline to construct the FE models.

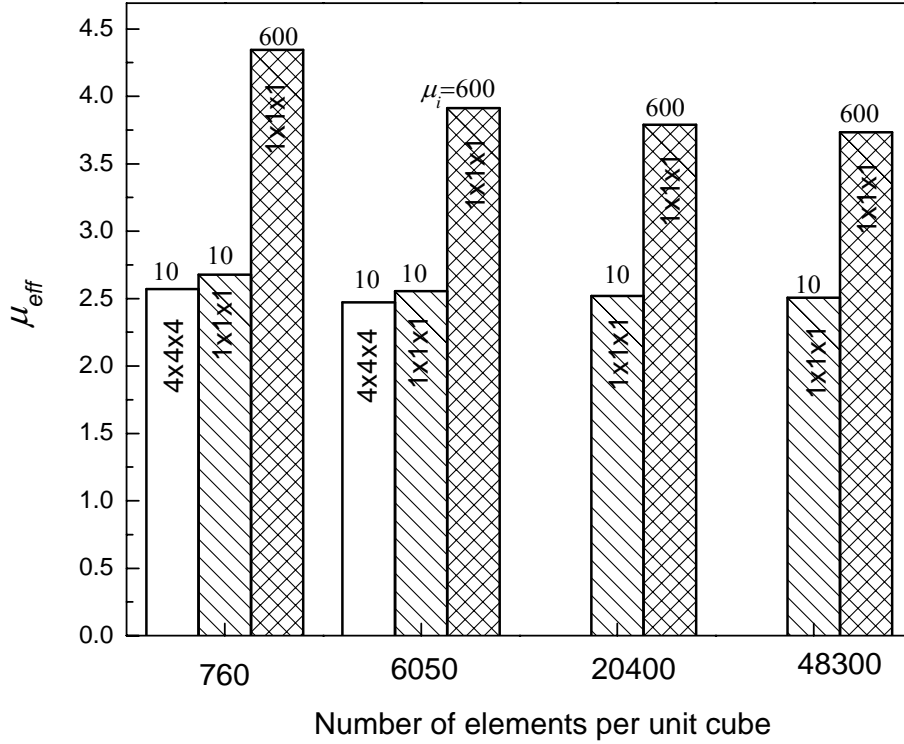


Fig. 2.11 Effective relative permeability  $\mu_{\text{eff}}$  versus element number for three models having the same inclusion volume fraction  $\phi_i = 0.4$  and relative permeability of the matrix  $\mu_m = 1$ . They are set to have: (i) a  $1 \times 1 \times 1$  inclusion matrix of  $\mu_i = 10$ ; (ii) a  $1 \times 1 \times 1$  inclusion array of  $\mu_i = 600$ , and (iii) a  $4 \times 4 \times 4$  inclusion array of  $\mu_i = 10$ .

## 2.5.2 Influence of the size of the inclusion array and $\mu_i$

All the analytic formulae described in section 2.3 are deemed to be applicable to composite containing a large number of inclusions. In principle, the result of a FE



analysis would be more accurate if a larger inclusion array is used. However, the maximum size of the array is limited by the capability of the computer. As such, a pilot test was preformed to determine the optimum of the inclusion array for calculating  $\mu_{eff}$ .

Fig. 2.11 shows the result of the test. Comparing the estimated  $\mu_{eff}$  for a model of a 1x1x1 cubic inclusion array and that of a model of a 4x4x4 cubic inclusion array, with both being meshed into more than 6050 elements, the latter gives a  $\mu_{eff}$  value of 3% lower than that of the former. If the number of inclusions exceeds 64, the simulation process cannot proceed. Therefore, we used a model containing a 4x4x4 inclusion array to perform FE analysis.

In addition, the  $\mu_{eff}$  value of the 4x4x4 model is smaller than that of the 1x1x1 model. It implies that addition of more inclusions in a matrix would reduce the value of  $\mu_{eff}$ , but the change is just within a few percents.

Also indicated in Fig.2.11, for a fixed inclusion volume fraction  $\phi_i = 0.4$ , as one can expect, the  $\mu_{eff}$  value of a system containing one single inclusion of  $\mu_i = 600$  is much higher than that having one single inclusion of  $\mu_i = 10$ .

### 2.5.3 Influence of the volume fraction of inclusions

Fig. 2.12 shows the results of  $\mu_{eff}$  as a function of the inclusion volume fraction  $\phi_i$  in the range from 0 to 1. The first group of data presented by dotted curves are derived from various conventional analytic theories, and the second group of data presented by symbols are obtained from numerical simulations.

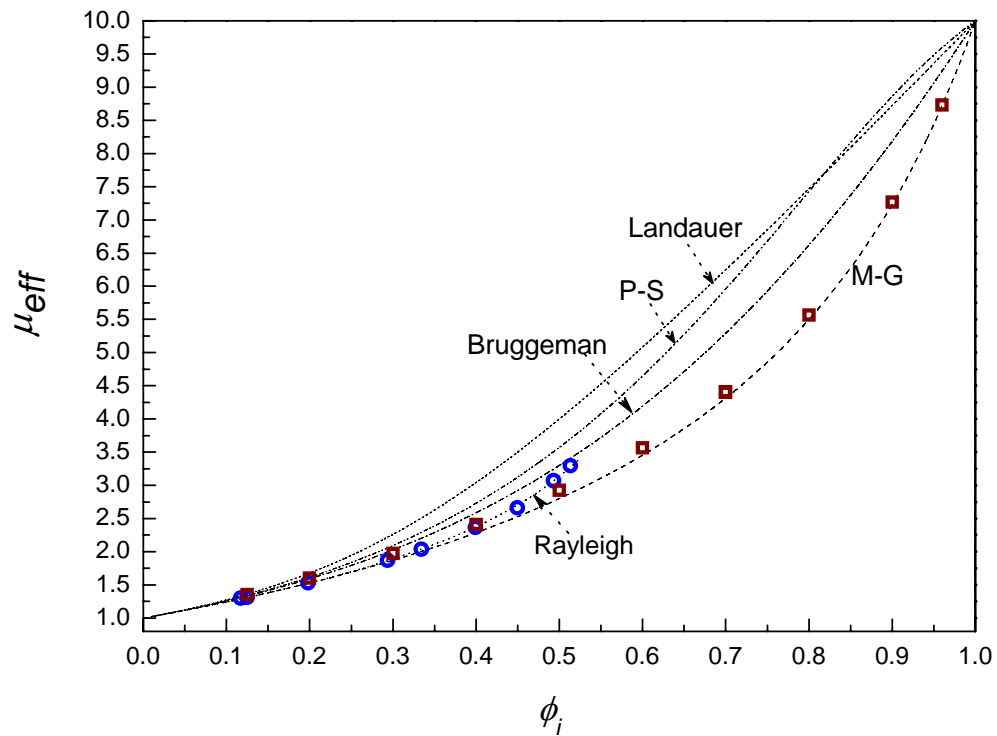


Fig. 2.12 Influence of  $\phi_i$  on  $\mu_{eff}$  obtained from various conventional effective medium theories (dotted curves) and numerical simulations (“ $\circ$ ” : spherical inclusions and “ $\square$ ” : cubic inclusion ) for a model containing a 6x6x6 inclusion array having a  $\mu_i = 10$  embedded in a matrix of  $\mu_m = 1$ .



Starting from looking at the results of the conventional analytic theories, one sees that in general the  $\mu_{eff}$  value increases when  $\phi_i$  increases. In the region of  $\phi_i \leq 0.12$ , the results of conventional analytic formulae are almost the same. With further increase in  $\phi_i$ , results of  $\mu_{eff}$  obtained from different theories deviate more prominently from each other. In fact, the M-G theory gives the lower bound of all the theoretical data in the whole range of  $\phi_i$  observed. This is because the M-G theory is based on the consideration of just one spherical inclusion with no modification of the matrix. The curve of the Bruggeman theory lies above the M-G one, because the matrix part undergoes accumulative modifications with successive increase in the inclusion volume fraction. The P-S model, based on another mechanism to modify the matrix, gives a  $\mu_{eff}$  values higher than those of the Bruggeman theory in the whole range of  $\phi_i$ . The Landauer theory results in the highest  $\mu_{eff}$  values as it imposes the greatest modification to the matrix material. Finally, we note that the Rayleigh theory, based on a structure of a periodic inclusion array, gives values in between those of the P-S model and Bruggeman model.

Next, let us look at the FE results for a model having a 6x6x6 inclusion array, with the inclusions arranged in the form of a cubic lattice. Their relative permeability is  $\mu_i = 10$ ,



and that of the matrix is  $\mu_m = 1$ . Meanwhile, the inclusion volume fraction  $\phi_i$  is varied by changing the inclusion size, by varying the radius of sphere or length of the cube edge. According to the experience gained from the convergence tests, error of the results thus produced would not be larger than around 2%.

At  $\phi_i$  roughly below 0.2, the simulated results match very well with those of all analytic theories indicating that all analytic approaches give accurate estimate of  $\mu_{eff}$  in the low  $\phi_i$  region. For  $\phi_i$  up to 0.52, the simulated results for spherical inclusion array agreed with the result of Rayleigh theory with error less than 0.2%. This is because the FE model used in this part of study has the same geometrical structure of the Rayleigh's model, and so should predict the same value of  $\mu_{eff}$ .

For higher  $\phi_i$  exceeding 0.52, the cubic inclusion array is used instead of spherical inclusion array. The simulated result increases slower than those derived from the Landauer, P-S and Bruggeman theories when  $\phi_i$  increases, suggesting that these theories give excessive modifications of the matrix. However, for even higher  $\phi_i$  above 0.9, the trend of the simulated results becomes closer to the M-G curve, because the two approaches are based on the same assumption that the inclusions are well



separated. More rigorous justification for this feature is given as follows. As an example, the  $H$ -field distribution in a composite containing a  $6 \times 6 \times 6$  cubic-inclusion array with  $\phi_i = 0.96$  obtained from FE analysis (Fig. 2.13) can be regarded as if the  $H$ -field distribution produced by a system of six parallel magnetic plates.

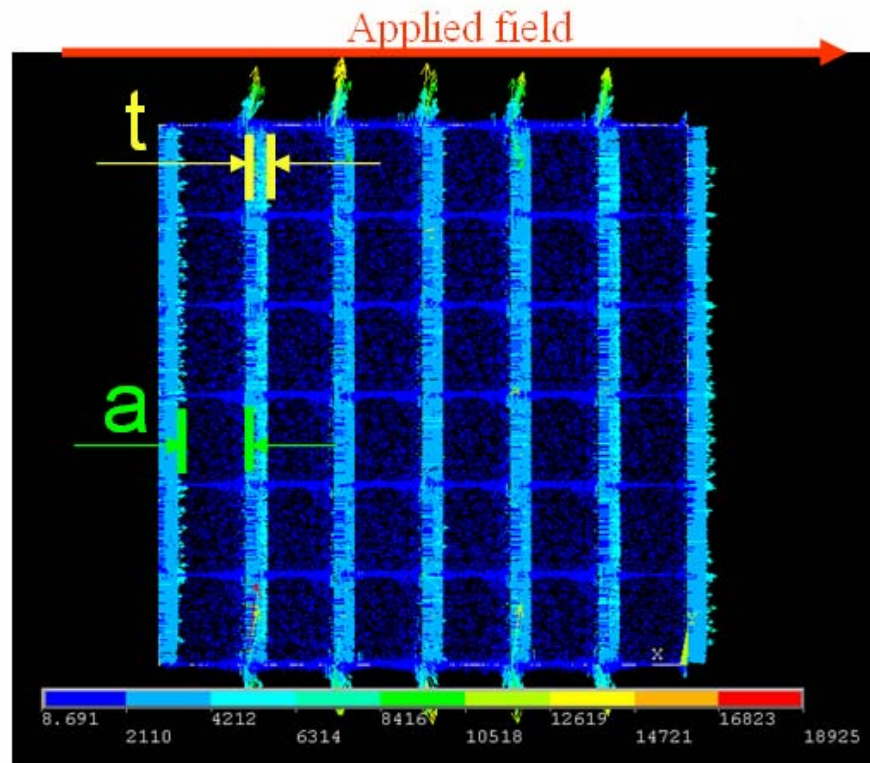


Fig. 2.13 Distribution of  $H$ -field of  $6 \times 6 \times 6$  cubic array for  $\phi_i = 0.96$ , where  $t = \text{gap}$  between the cubic inclusions, and  $a = \text{inclusion cubic length}$ .



Therefore, we get the following relationship:

$$\mu_i H_i = \mu_m H_m = H_m \quad (\text{for } \mu_m = 1) \quad (2-63)$$

Combine Eq. (2-63) and  $\langle B \rangle = \mu_{eff} \langle H \rangle$ , we have

$$\mu_i H_i (6a) + \mu_m H_m (6t) = \mu_{eff} [H_i (6a) + H_m (6t)] \quad (2-64)$$

By assuming  $\mu_i \gg \mu_m$  and  $\phi_i \rightarrow 1$ , the  $\mu_{eff}$  can be determined as

$$\mu_{eff} \cong \frac{3\mu_i}{\mu_i(1-\phi_i) + 3\phi_i} \quad (2-65)$$

According to M-G theory stated in Eq. (2-33),

$$\mu_{eff(M-G)} = \mu_m + \phi_i \frac{3\mu_m(\mu_i - \mu_m)}{\phi_m(\mu_i + 2\mu_m) + 3\phi_i\mu_m} \quad (2-33)$$

the same  $\mu_{eff}$  result as Eq. (2-56) can be determined

$$\mu_{eff(M-G)} \cong \frac{3\mu_i}{\mu_i(1-\phi_i) + 3\phi_i} \quad (2-65)$$

Fig. 2.14 shows the corresponding results with the inclusions in the model having a much higher  $\mu_i$  of 1000, which illustrate all the trends obtained in the case of a lower  $\mu_i$  of 10 as mentioned above. Differently, an abrupt rise in the Landauer curve at  $\phi_i \sim 1/3$  is observed, which is attributed to the onset of percolation and used by some authors to explain experimental results of similar trend.

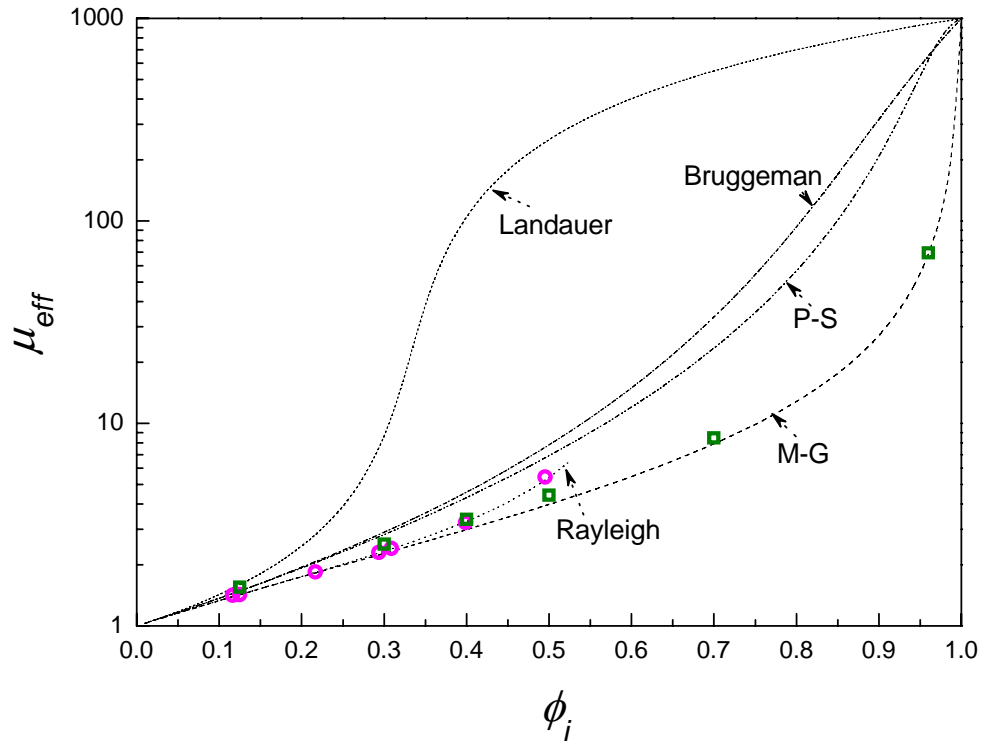


Fig. 2.14 Influence of  $\phi_i$  on  $\mu_{eff}$  obtained from various conventional effective medium theories (dotted curves) and numerical simulations (“○” : spherical inclusions and “□” : cubic inclusion ) for a model containing a 6x6x6 inclusion array having a  $\mu_i = 1000$  embedded in a matrix of  $\mu_m = 1$ .

## 2.5.4 Influence of inclusion shape and alignment

In this section, we examine how the shape of inclusions affects the value of  $\mu_{eff}$  of a composite. This study is less convenient to be carried out by employing an analytic method, because of the difficulty of the formulation.



Fig. 2.15 shows the results of  $\mu_{eff}$  of a model with a  $4 \times 4 \times 4$  array of inclusions of  $\mu_i = 10$  and a matrix of  $\mu_m = 1$ , where the inclusions are set to have spheres, cubes and wires respectively. In particular, wire inclusions are aligned to be in the parallel with or perpendicular to the applied field. The inclusion volume fraction  $\phi_i$  is fixed at 0.4.

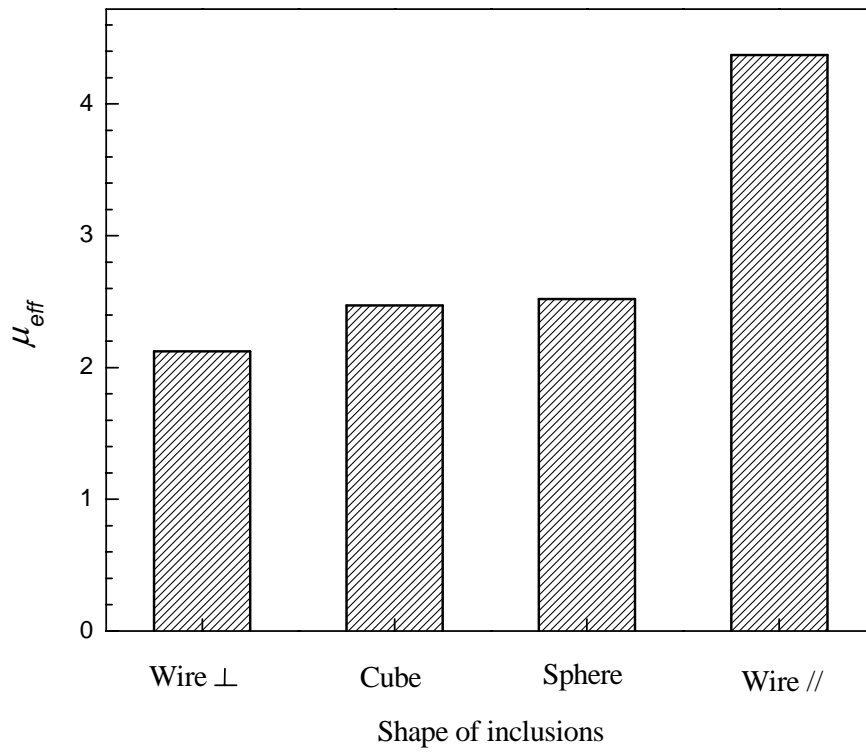


Fig. 2.15 Effective relative permeability  $\mu_{eff}$  for a model with inclusions arranged in a  $4 \times 4 \times 4$  array,  $\mu_i = 10$  and  $\phi_i = 0.4$  and in various shapes.

As shown in Fig. 2.15, wire inclusions with length aligned perpendicular to the applied  $H$ -field (labeled as wire  $\perp$ ) gives the lowest the  $\mu_{eff}$  value, because the demagnetization



effect in the wires is the largest. In this case, the demagnetization factor is closer to 1, corresponding to the Wiener lower bound of  $\mu_{eff}$ .

The  $\mu_{eff}$  values of the models containing a 4x4x4 cubic inclusion array and a 4x4x4 spherical inclusion array are almost the same, namely around 2.5. The demagnetization factors for these two cases are all close and are around 1/3. Due to a weak demagnetization effect, the  $\mu_{eff}$  values for these two cases are around 17% higher than that of the case of long wire inclusions aligned perpendicular to the applied  $H$ -field.

The last case is for a model with wire inclusions aligned in parallel with the applied  $H$ -field. Its  $\mu_{eff}$  value is twice of that of the case with wire inclusions aligned perpendicular to the applied  $H$ -field, and is 76% higher than that of the case with spherical and cubic inclusions. These results are again attributed to the weaker demagnetization effect in the wires. In an extreme case when the length-to-width ratio is very large, the demagnetization factor approaches 0, corresponding to the Wiener upper bound of  $\mu_{eff}$ .



## **Chapter 3    Analysis of 3-phase (0-0-3) composites**

### **containing dielectric or magnetic**

### **inclusions**

#### **3.1 Introduction**

Up to date, most analytic formulae for determining  $\varepsilon_{eff}$  value are mainly developed for 2-phase composites, while studies on multiphase mixtures are rare. Though the properties of multiphase composites containing more than one type of inclusions are of both fundamental and practical interests, the related studies are relatively rare. Some examples are as follows.

Sihvola et al. developed a formula [Sihvola, 1999c] based on the M-G theory, which is referred to as the Maxwell-Garnett formula for multiphase composites (MG-MP) in the following discussion.

Chen et al. [Chen, et al., 1998] calculated the  $\varepsilon_{eff}$  value of a 3-phase mixture with a two-steps process. The first step is to combine the contribution of layers of dielectric



spheres to give an overall effect equivalent to that caused by a homogeneous sphere of a relative dielectric constant of  $\varepsilon_a$  and a radius of  $a_l$ . The estimated value of  $\varepsilon_{eff}$  of the whole system is produced by applying a 2-phase formula. The authors found that the results were the same as that derived by using the MG-MP method.

Whites [Whites, 1999] proposed another approach by calculating the  $\varepsilon_{eff}$  value of a 3-phase system based on a model constructed of four unit cells, having a total of eight spherical inclusions. The dipole moment of each sphere in a unit cell is determined first. The scattering of the scalar potential due to the presence of surrounding inclusions is then computed. The  $\varepsilon_{eff}$  value is thus deduced according to the polarization and the computed scattering of the scalar potential.

In this Chapter, we reported a more detailed study of the values of  $\varepsilon_{eff}$  of 3-phase (0-0-3) composites by using several analytic methods and FE method, and the results are compared with the FE data as references. The methods used in this study are described in more detail in Section 3.2, and the results and analyses are presented in Section 3.3.

## 3.2 Methods for analyzing 3-phase (0-0-3) composites

### 3.2.1 Maxwell-Garnett multiphase (MG-MP) theory

This is an analytic method obtained from modifying the 2-phase M-G method [Sihvola, 1999c; Whites, 1999]. It does not include feature to reflect the sequence for adding the two types of inclusions. The model used in this method is depicted schematically in Fig. 3.1. It contains two kinds of isotropic spherical inclusions with different linear dielectric permittivities  $\epsilon_1$  and  $\epsilon_2$ . They are embedded in an isotropic non-electroactive non-magnetic matrix. The composite is placed in a uniform external electric field  $\vec{E}_m$ . It is further assumed that there is no free surface charge density at the inclusion-matrix interface, i.e.  $\rho = 0$ .

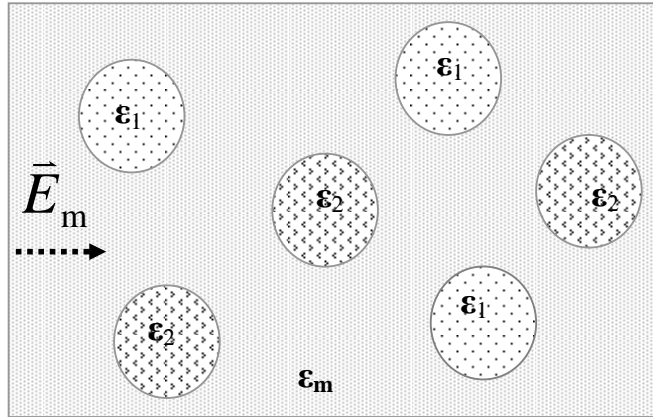


*Fig. 3.1 A simple model of a 3-phase mixture, two types of isotropic inclusions of dielectric constants ( $\epsilon_1$  and  $\epsilon_2$ ) are embedded in an isotropic non-electroactive non-magnetic matrix material with a relative dielectric constant  $\epsilon_m$ .*



Let us start from the 2-phase M-G theory described in Section 2.3.1. It involves five equations and six unknowns. The unknowns include the electric displacements in the inclusions and matrix, denoted as  $D_i$  and  $D_m$ , and the corresponding electric fields  $E_i$  and  $E_m$ :

$$D_m = \varepsilon_m E_m, \quad (2-28)$$

$$D_i = \varepsilon_i E_i, \quad (2-29)$$

$$D_m = D_i + 2\varepsilon_m (E_i - E_m), \quad (2-30)$$

$$D = \phi_i D_i + \phi_m D_m, \quad \text{and} \quad (2-31)$$

$$E = \phi_i E_i + \phi_m E_m. \quad (2-32)$$

The volume fraction of the inclusions  $\phi_i$  is regarded as a parameter, while that of the matrix is denoted as  $\phi_m = 1 - \phi_i$ . The ratio  $D/E$  can be solved to give the predicted effective relative permeability of the 2-phase composite.

This equation set is modified for the use of analyzing a 3-phase (0-0-3) composite containing two types of spherical inclusions with dielectric coefficients  $\varepsilon_1$  and  $\varepsilon_2$ , and volume fractions  $\phi_1$  and  $\phi_2$ . The electric displacements and electric fields inside them are denoted as  $D_1$  and  $D_2$ , and  $E_1$  and  $E_2$ , respectively. The modified equations become:

$$D_m = \varepsilon_m E_m, \quad (2-28)$$



$$D_1 = \varepsilon_1 E_1, \quad (3-1)$$

$$D_2 = \varepsilon_2 E_2, \quad (3-2)$$

$$D_m = D_1 + 2\varepsilon_m(E_1 - E_m), \quad (3-3)$$

$$D_m = D_2 + 2\varepsilon_m(E_2 - E_m), \quad (3-4)$$

$$D = \phi_1 D_1 + \phi_2 D_2 + \phi_m D_m, \quad \text{and} \quad (3-5)$$

$$E = \phi_1 E_1 + \phi_2 E_2 + \phi_m E_m. \quad (3-6)$$

Eqs. (2-28), (3-1) to (3-6) are solved to obtain an expressive of effective relative permittivity:

$$\varepsilon_{eff} = \varepsilon_m + 3\varepsilon_m \frac{\phi_1 \frac{\varepsilon_1 - \varepsilon_m}{\varepsilon_1 + 2\varepsilon_m} + \phi_2 \frac{\varepsilon_2 - \varepsilon_m}{\varepsilon_2 + 2\varepsilon_m}}{1 - \phi_1 \frac{\varepsilon_1 - \varepsilon_m}{\varepsilon_1 + 2\varepsilon_m} - \phi_2 \frac{\varepsilon_2 - \varepsilon_m}{\varepsilon_2 + 2\varepsilon_m}}. \quad (3-7)$$

An alternative format of this solution is:

$$\frac{\varepsilon_{eff} - \varepsilon_m}{\varepsilon_{eff} + 2\varepsilon_m} = \phi_1 \frac{\varepsilon_1 - \varepsilon_m}{\varepsilon_1 + 2\varepsilon_m} + \phi_2 \frac{\varepsilon_2 - \varepsilon_m}{\varepsilon_2 + 2\varepsilon_m}. \quad (3-8)$$

This approach is named as the MG-MP model, because Eqs. (3-7) and (3-8) are developed on the basis of the M-G theory for 2-phase systems.



### 3.2.2 Poon-Shin multiphase (PS-MP) theory

Another analytic approach is named as the PS-MP method, which is modified from the 2-phase P-S method. Not unlike the MG-MP method, it does not include any feature to indicate the sequence of adding the two types of inclusions, but it is supposed to be superior to the MG-MP method according to the comparison between the M-G and P-S theories for 2-phase composites.

The equations of the P-S theory for a 2-phase composite are (Section 2.3.3):

$$D = \phi_i D_i + \phi_m D_m, \quad (2-31)$$

$$E = \phi_i E_i + \phi_m E_m, \quad (2-32)$$

$$D_m' = \varepsilon_m E_m + \phi_i (\varepsilon_i - \varepsilon_m) E_i, \quad \text{and} \quad (2-45)$$

$$D_m' = D_i + 2\varepsilon_m (E_i - E_m), \quad (2-46)$$

They are modified for the use of analyzing a 3-phase composite as follows. First,

Eqs. (2-31) and (2-32) are revised as:

$$D = \phi_1 D_1 + \phi_2 D_2 + \phi_m D_m, \quad \text{and} \quad (3-9)$$

$$E = \phi_1 E_1 + \phi_2 E_2 + \phi_m E_m. \quad (3-10)$$

Analogous to Eq. (2-45), the electric displacement in the matrix is modified to become:

$$D_m' = D_1 + 2\varepsilon_m (E_1 - E_m) \quad \text{or} \quad D_m' = D_2 + 2\varepsilon_m (E_2 - E_m).$$



Using them to modify Eq. (2-46) for the two types of inclusions respectively, one obtains two new equations as follows:

$$D_m + \phi_1 (\varepsilon_1 - \varepsilon_m) E_1 + \phi_2 (\varepsilon_2 - \varepsilon_m) E_2 = D_1 + 2\varepsilon_m (E_1 - E_m) \quad \text{and} \quad (3-11)$$

$$D_m + \phi_1 (\varepsilon_1 - \varepsilon_m) E_1 + \phi_2 (\varepsilon_2 - \varepsilon_m) E_2 = D_2 + 2\varepsilon_m (E_2 - E_m) \quad (3-12)$$

Finally, Eqs. (2-28), (3-1), (3-2), (3-9) to (3-12) form a complete equation set for a 3-phase composite, which lead to an expression for  $\varepsilon_{eff}$ :

$$\frac{\frac{\varepsilon_{eff} - \varepsilon_m}{\varepsilon_{eff} + 2\varepsilon_m}}{1 + \phi_m \frac{\varepsilon_{eff} - \varepsilon_m}{\varepsilon_{eff} + 2\varepsilon_m}} = \phi_1 \frac{\varepsilon_1 - \varepsilon_m}{\varepsilon_1 + 2\varepsilon_m} + \phi_2 \frac{\varepsilon_2 - \varepsilon_m}{\varepsilon_2 + 2\varepsilon_m}. \quad (3-13)$$

Compared with Eq. (3-8) for the MG-MP theory, Eq. (3-13) has an additional factor

$$1 + \phi_m \frac{\varepsilon_{eff} - \varepsilon_m}{\varepsilon_{eff} + 2\varepsilon_m} \quad \text{in the denomination of the left side.}$$

### 3.2.3 Incremental multiphase (I-MP) method

#### 3.2.3.1 Basic features

In this method, inclusions are added into a matrix with differential steps. After each step, the properties of the composite are modified accordingly. These features make



this method to be greatly different from the M-G and P-S methods, and also allow the inclusions to be added in different sequences which we call them to be “paths” in the following discussions.

Fig.3.2 shows three typical paths, all leading to the same final state having the volume fractions of the two types of inclusions equal to  $\phi_1$  and  $\phi_2$  respectively. In particular:

- (i) The first path, named as sequential-incremental multiphase (SI-MP<sub>12</sub>) process, is presented by dotted lines in which inclusions of type 1 are added first, followed by the addition of the other.
- (ii) The second path is also a sequential incremental multiphase process and denoted symbolically as a SI-MP<sub>21</sub> process. It is presented by dashed lines, where inclusions of types 2 are added first.
- (iii) The third path is named as a randomly-accumulative multiphase (RA-MP) process in which small increments of the two types of inclusions are randomly with respective probabilities in a ratio equal to the ratio of  $\phi_1$  to  $\phi_2$ .

One expects that the results of  $\varepsilon_{eff}$  obtained from all the above three paths should be the same. Otherwise, the theory may have some defects and are needed to be modified somehow.

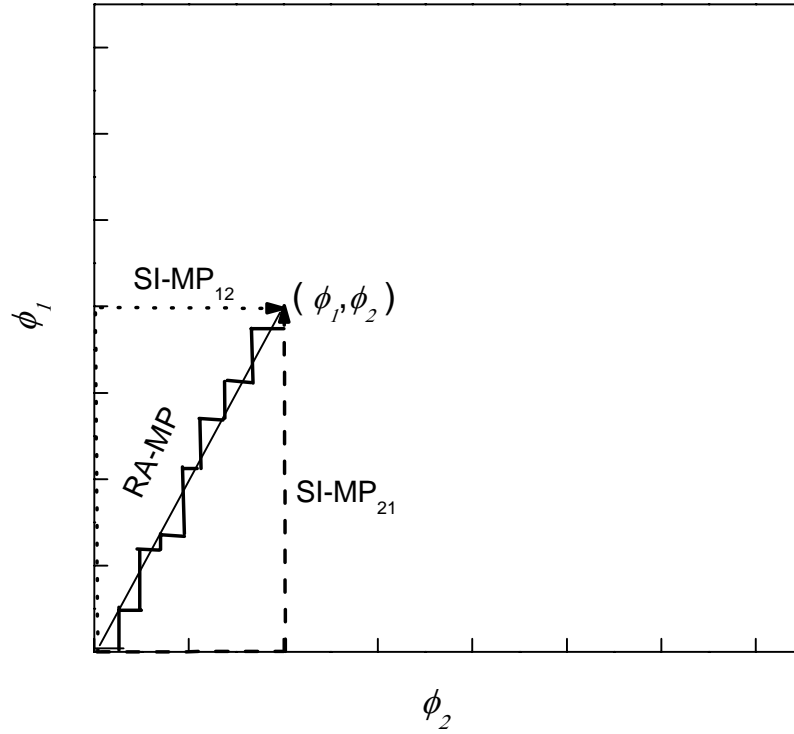


Fig. 3.2 Three paths for constructing 3-phase (0-0-3) composites containing two types of inclusions with respective volume fractions  $\phi_{1,f}$  and  $\phi_{2,f}$ .

### 3.2.3.2 Effect of adding a small amount of inclusions

We apply Eq. (2-34) of the M-G theory for a 2-phase composite to investigate the effect of adding a small amount of inclusions in the matrix. It is rewritten as:

$$\frac{\varepsilon_{eff}' - \varepsilon_{eff}}{\varepsilon_{eff}' + 2\varepsilon_{eff}} = \delta \xi \frac{\varepsilon_i - \varepsilon_{eff}}{\varepsilon_i + 2\varepsilon_{eff}}, \quad (3-14)$$

$\varepsilon_{eff}$  and  $\varepsilon_{eff}'$  are the effective relative permittivities of the overall composite before and after adding a small amount of one type of inclusions. The index “ $i$ ” can be “1” or “2”,



which is used to label the type of the inclusions added.  $\delta\xi = \delta V/V$  is the related change in the volume fraction.

Assuming that a small increment of type 1 inclusions is introduced, the volume fractions of the two types of inclusions are changed from  $\phi_1$  and  $\phi_2$  to  $\phi_1'$  and  $\phi_2'$ , which are related with the expressions of:

$$\phi_1' = \phi_1 + (1 - \phi_1)\delta\xi_1, \quad \text{and} \quad (3-15)$$

$$\phi_2' = \phi_2 - \phi_2\delta\xi_1. \quad (3-16)$$

By introducing a parameter:

$$X_1 = \delta\xi_1 \frac{\varepsilon_1 - \varepsilon_{eff}}{\varepsilon_1 + 2\varepsilon_{eff}}, \quad (3-17)$$

Eq. (3-14) is simplified to become:

$$\varepsilon_{eff}' = \varepsilon_{eff} \left( \frac{1 + 2X_1}{1 - X_1} \right). \quad (3-18)$$

On the other hand, if a smaller increment of type 2 inclusions is introduced, the above derivation is still value after replacing the index “1” by “2”. Eqs. (3-15) to (3-17) become:

$$\phi_1' = \phi_1 - \phi_1\delta\xi_2, \quad (3-19)$$



$$\phi_2' = \phi_2 + (1 - \phi_2)\delta\xi_2, \quad \text{and} \quad (3-20)$$

$$X_2 = \delta\xi_2 \frac{\varepsilon_2 - \varepsilon_{eff}}{\varepsilon_2 + 2\varepsilon_{eff}}. \quad (3-21)$$

The effective relative permittivity is modified as:

$$\varepsilon_{eff}' = \varepsilon_{eff} \left( \frac{1 + 2X_2}{1 - X_2} \right). \quad (3-22)$$

### 3.2.3.3 SI-MP methods

In a SI-MP<sub>12</sub> process, after inclusions of type 1 are completely added, the volume fraction of this inclusion type is  $\phi_{1,midway}$ . At this moment, there is no any type 2 inclusion yet. At this moment, if a small increment of type 2 inclusions is introduced, the volume fraction of this inclusion type is increased to  $\delta\xi_2$ . Eqs. (3-19) and (3-20) show that the changes of  $\phi_1$  and  $\phi_2$  are:

$$\delta\phi_1 = \phi_1' - \phi_1 = -\phi_1\delta\xi_2, \quad \text{and} \quad (3-23)$$

$$\delta\phi_2 = \phi_2' - \phi_2 = (1 - \phi_2)\delta\xi_2. \quad (3-24)$$

Inclusions of type 2 are continuously added until the volume fractions of the inclusions reach their final values of  $\phi_{1,final}$  and  $\phi_{2,final}$ . Eqs. (3-23) and (3-24) are then integrated to give:



$$\int_{\phi_{1,midway}}^{\phi_{1,final}} \frac{1}{\phi_1} d\phi_1 = - \int_0^{\xi} d\xi \quad (3-25)$$

$$\int_0^{\phi_{2,final}} \frac{1}{1-\phi_2} d\phi_2 = \int_0^{\xi} d\xi \quad (3-26)$$

By eliminating  $\xi$  from Eqs. (3-25) and (3-26), we obtain the expression of  $\phi_{1,midway}$ :

$$\phi_{1,midway} = \frac{\phi_{1,final}}{1 - \phi_{2,final}} \quad (3-27)$$

The value of  $\phi_{1,midway}$  is needed in the program for calculating the  $\varepsilon_{eff}$  value of a 0-0-3 composite constructed with a SI-MP process. Fig. 3.3a shows the flow chart of the program used to calculate  $\varepsilon_{eff}$ .

The same argument is applied to a SI-MP<sub>21</sub> process where type 2 inclusions are added first. For this process, the intermediate volume fraction of type 2 inclusions ( $\phi_{2,midway}$ ) is obtained by swapping the indices “1” and “2” in Eq. (3-27):

$$\phi_{2,midway} = \frac{\phi_{2,final}}{1 - \phi_{1,final}} \quad (3-28)$$

The flow chart of the corresponding program is shown in Fig. 3.3b.

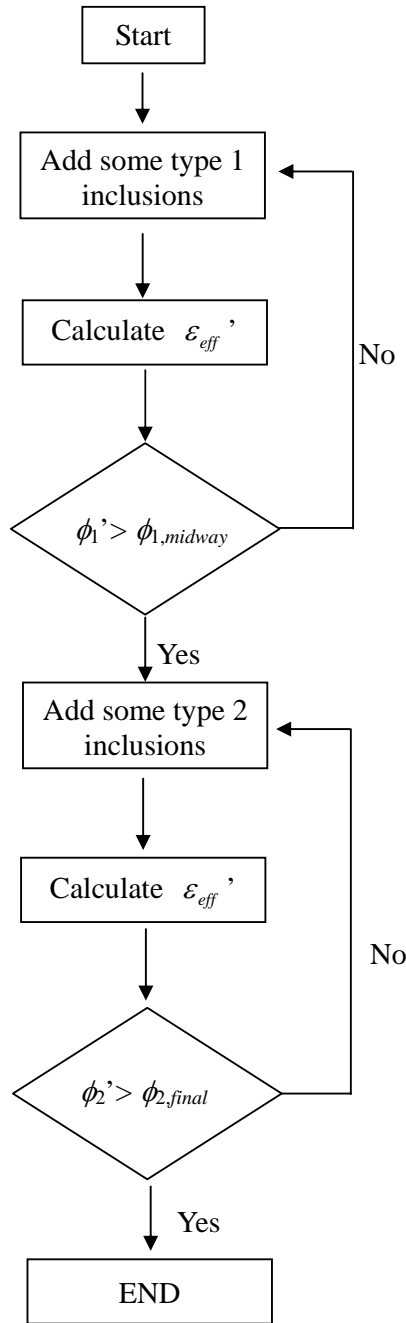


Fig. 3.3a

Flow chart of a program to implement a SI-MP<sub>12</sub> process. Inclusions of type 1 are added first, followed by inclusions of type 2.

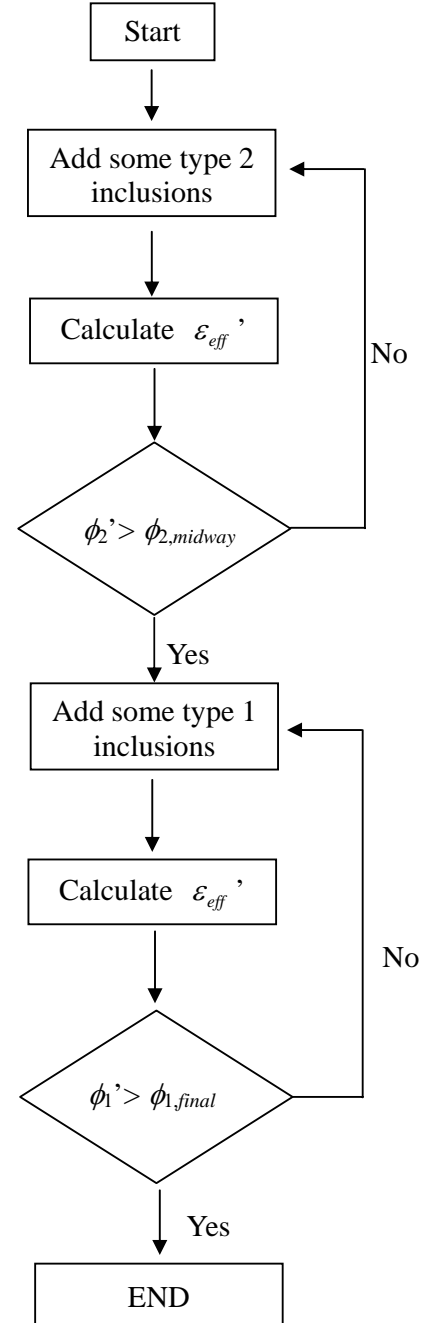


Fig. 3.3b

Flow chart of a program to implement a SI-MP<sub>21</sub> process. Inclusions of type 2 are added first, followed by inclusions of type 1.



#### 3.2.3.4 RA-MP method

In a RA-MP process, a 0-0-3 composite is built up by introducing small amounts of the two types of inclusions in a random pattern with respective probabilities in a ratio equal to the ratio of their volume fractions in the final state. Eqs. (3-15) to (3-18) are still used to describe the modification of  $\varepsilon_{eff}$  after a small amount of type 1 inclusions is added, and Eqs. (3-19) to (3-22) are for the same purpose after adding a small amount of type 2 inclusions. The flow chart of the program used to calculate  $\varepsilon_{eff}$  is shown in Fig. 3.3c.

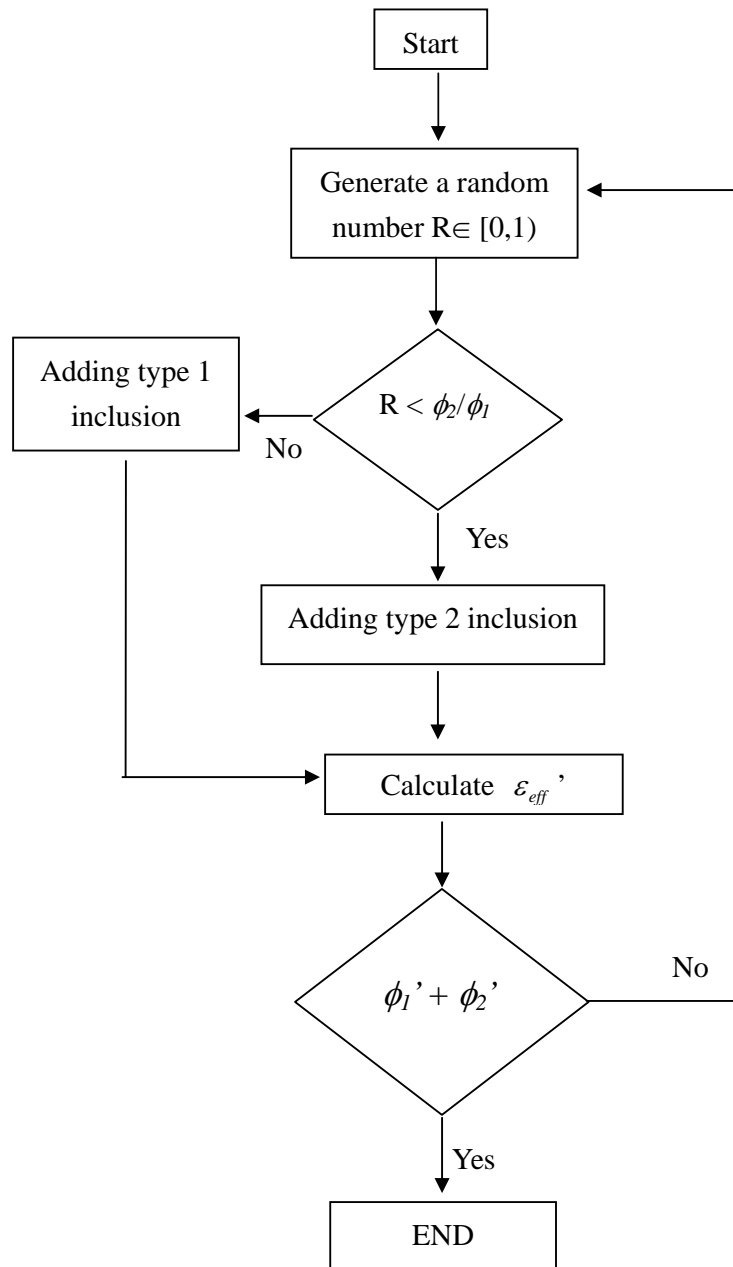


Fig. 3.3c Flow chart used to calculate  $\epsilon_{eff}$  of a composite in a RA-MP process.



### 3.2.4 FE method

FE method is supposed to be able to reproduce more detailed features of a real system, and hence the  $\epsilon_{eff}$  deduced is believed to be closer to the real value and be useable as a better reference for judging the effectiveness of other analytic methods.

The simulation processes employed are for analyzing composites of magnetic inclusions due to the original objectives of the project, but the results of  $\epsilon_{eff}$  are believed to be comparable with the effective relative permeability of a composition containing dielectric inclusions due to the mathematical equivalence of these two problems.

The model employed is similar to that used for analyzing a 2-phase composite (Section 2.4.2), except that two kinds of inclusions of different magnetic properties in terms of respective permeabilities  $\mu_1$  and  $\mu_2$ , are involved in the present case, which are interweaved at the sites of a 4x4x4 array. Two inclusions shapes, namely the cubic and spherical geometries, were used. Fig. 3.4a shows the cross section of a model containing spherical inclusions; and Fig. 3.4b shows that of a model containing cubic inclusions. Figs. 3.5a and 3.5b are the corresponding 3-dimensional sketches. In each



figure, inclusions of different magnetic properties are presented by using different patterns or colors. The configuration including the sample, surrounding non-magnetic environment (air) and the Helmholtz coils, is placed in a uniform applied  $H$ -field ( $H_{\text{applied}}$ ) generated by a pair of Helmholtz coils in the  $z$ -direction (Fig. 3.5c). The use of cubic inclusion shape allows the model to contain a higher inclusion volume fraction, but that of spherical inclusions with a single size is capped at around 0.4. Results of  $\mu_{\text{eff}}$  evaluated at inclusion volume fractions exceeding this limit is of great interest, because it can be referred to for examining the effectiveness of many conventional analytic models which are based on the condition of lower inclusion content and may be not accurate enough in the range of high inclusion content. Though for 2-phase composites discussed in Chapter 2, the calculated  $\varepsilon_{\text{eff}}$  values for models containing cubic and spherical inclusions at volume fractions up to around 0.4 are basically consistent, some preliminary calculations are needed to be performed for 3-phase cases in this part of study.

We also apply the condition of convergence obtained from Chapter 2 for 2-phase composites, which shows that when the number of elements exceeds 6050 per unit cube, the estimated value of  $\varepsilon_{\text{eff}}$  would be fairly close to the real one. An inclusion

array with a size of 4x4x4 or 6x6x6 is thought to be appropriate to give a reasonably good result.

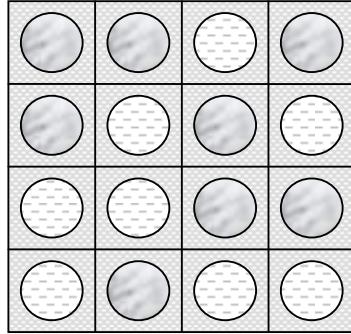


Fig. 3.4a

FEA model of a 0-0-3 composite containing two types of 4x4x4 spherical inclusions.

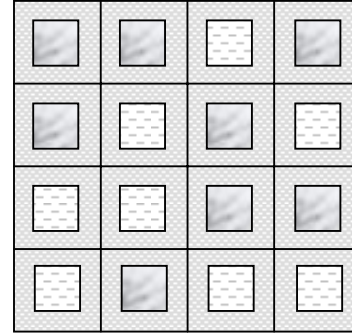


Fig. 3.4b

FEA model of a 0-0-3 composite containing two types of 4x4x4 cubic inclusions.

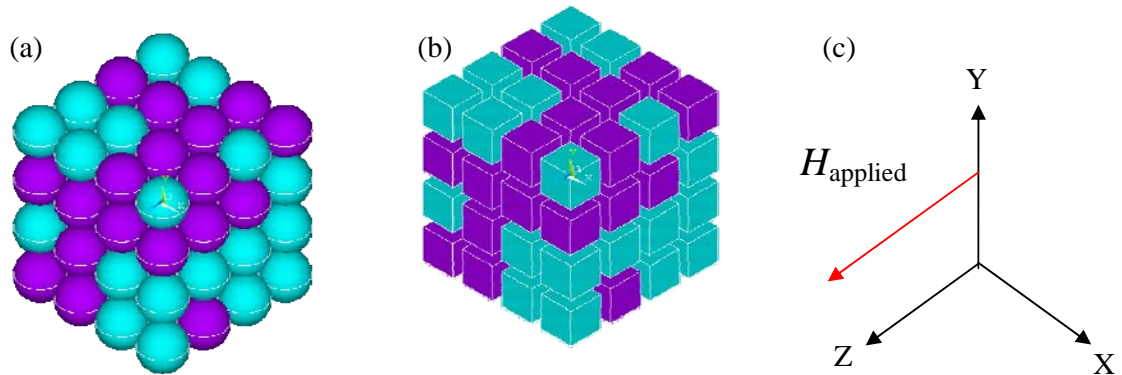


Fig. 3.5 3-dimensional structure of the 4x4x4 array models containing two types of (a) spherical and (b) cubic inclusions randomly distributing at the sites. (c) The direction of  $H_{\text{applied}}$ .



### 3.3 Parameters and ranges of variations

The parameters and ranges of their variations are shown in Table 3.1 and Fig. 3.6. Two combinations of  $\mu_1$  and  $\mu_2$  were used, namely 10 and 2; and 100 and 10 respectively. For each of these settings, five different schemes were used to vary  $\phi_1$  and  $\phi_2$ . For Scheme (i), (ii) and (iii) as shown in Fig. 3.6, the total inclusion volume fraction  $\phi_i = \phi_1 + \phi_2$  is varied from 0 to 0.6 (or from 0 to 1) with the ratio  $\phi_1:\phi_2$  fixed at 1:1, 1:2 and 2:1 respectively. In Scheme (iv), the total inclusion volume fraction  $\phi_i = \phi_1 + \phi_2$  is fixed at 0.42, and  $\phi_1$  is varied from 0 to 0.42 (or  $\phi_2$  from 0.4 to 0). In Scheme (v),  $\phi_i$  is fixed at 0.73, whereas  $\phi_1$  is varied from 0 to 0.73 (or  $\phi_2$  from 0.73 to 0). For FE analyses, two inclusion shapes, namely spherical and cubic geometries, were applied.

*Table 3.1 Parameters, ranges of variations and the purposes of the related**investigations in the FE analyses for 3-phases composites.  $\mu_m$  of the matrix = 1*

Parameters	Scheme	Values	Purposes of investigations
$\mu_1$ and $\mu_2$ :	---	10 and 2	Influence of the magnetic properties of the inclusions
	---	100 and 10	
$\phi_i (= \phi_1 + \phi_2)$	(i)	0 to 0.6 (or 0 to 1) with $\phi_1/\phi_2 = 1:1$	Dependence on the volume fractions of inclusions
	(ii)	0 to 0.6 (or 0 to 1) with $\phi_1/\phi_2 = 1:2$	
	(iii)	0 to 0.6 (or 0 to 1) with $\phi_1/\phi_2 = 2:1$	
$\phi_1$ (or $\phi_2$ )	(iv)	0 to 0.4 with $\phi_i = 0.42$	Dependence on the volume fractions of inclusions
	(v)	0 to 0.73 with $\phi_i = 0.73$	
Inclusion shape (for FE analysis)	---	Spherical	Influence of the shape of inclusions
	---	Cubic	

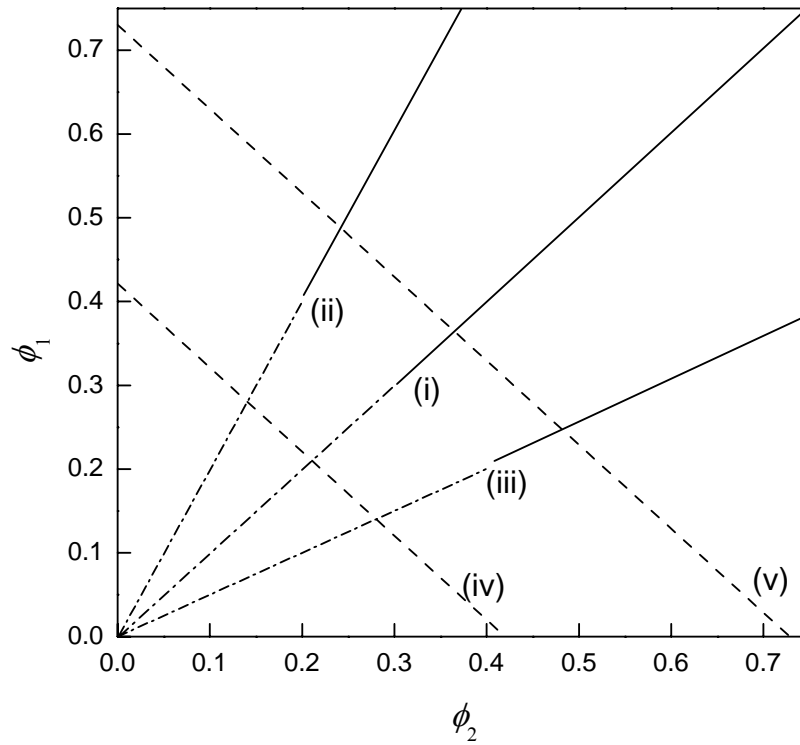


Fig. 3.6 Five schemes for varying  $\phi_1$  and  $\phi_2$ :

- (i)  $\phi_1:\phi_2 = 1:1$  [ $\phi_i$  from 0 to 0.6 ( $\mu_1$  and  $\mu_2 = 10$  and 2);  
and  $\phi_i$  from 0 to 1 ( $\mu_1$  and  $\mu_2 = 100$  and 10)]
- (ii)  $\phi_1:\phi_2 = 1:2$  [ $\phi_i$  from 0 to 0.6 ( $\mu_1$  and  $\mu_2 = 10$  and 2);  
and  $\phi_i$  from 0 to 1 ( $\mu_1$  and  $\mu_2 = 100$  and 10)]
- (iii)  $\phi_1:\phi_2 = 2:1$  [ $\phi_i$  from 0 to 0.6 ( $\mu_1$  and  $\mu_2 = 10$  and 2);  
and  $\phi_i$  from 0 to 1 ( $\mu_1$  and  $\mu_2 = 100$  and 10)]
- (iv)  $\phi_i = 0.42$  [ $\phi_i$  from 0 to 0.42 ( $\mu_1$  and  $\mu_2 = 10$  and 2; and 100 and 10)]
- (v)  $\phi_i = 0.73$  [ $\phi_i$  from 0 to 0.73 ( $\mu_1$  and  $\mu_2 = 10$  and 2; and 100 and 10)]



## 3.4 Results and Discussions

### 3.4.1 Equivalency of using cubic and spherical inclusions in FE

#### analyses

The volume fraction of spherical inclusions  $\phi_i$  in a matrix is capped at around 0.4, hindering the attempt of comparing the results of  $\mu_{eff}$  (or  $\varepsilon_{eff}$ ) of composites obtained from FE and analytic methods in the region of high inclusion volume fractions. This restriction can be eliminated if cubic inclusions are used in FE simulations, whereas calculations can be proceeded at with a high inclusion occupancy.

Fig. 3.7 shows the results of  $\mu_{eff}$  obtained from various FE models containing spherical and cubic inclusions, respectively, in order to reflect the influence of the inclusion geometry. In all the calculations,  $\mu_m = 1$ , the total inclusion volume fraction  $\phi_i = \phi_1 + \phi_2$  is fixed at 0.4, and the inclusions are arranged in a pattern of a 4x4x4 array. Comparison are made between the  $\mu_{eff}$  values of the models associated with the two inclusions shapes, under the conditions of  $\phi_1:\phi_2 = 1:1$ , 1:2 and 2:1 respectively, with each case having  $\mu_1$  and  $\mu_2 = 10$  and 2; and 100 and 10, respectively.



Results of all these comparisons show that the variation of the calculated  $\mu_{eff}$  caused by the replacement of spherical inclusions by cubic inclusions or vice versa would not exceed 3%. We thus assert that the use of cubic inclusions in calculating the  $\mu_{eff}$  value of a composite is acceptable for the purpose of the present study. The error is even smaller at the region of low inclusion volume fractions. We further postulate that this guideline is still valid at the region of higher inclusion volume, say up to a level of 0.6 as adopted in this study.

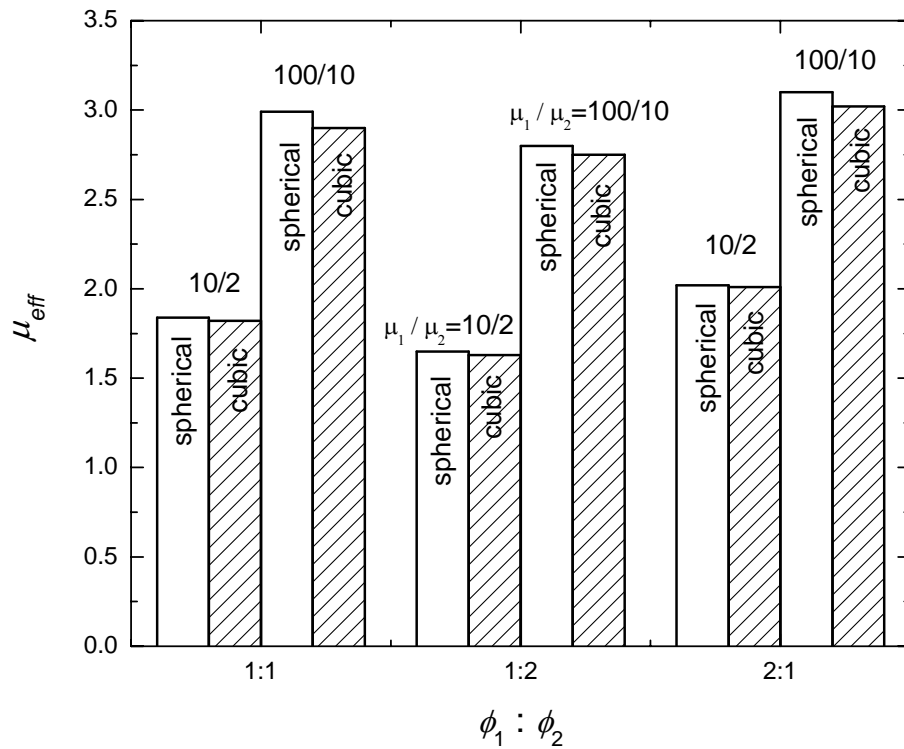


Fig. 3.7 Comparison of FEA results of  $\mu_{eff}$  deduced from various models containing spherical and cubic inclusions.



### 3.4.2 $\phi_i$ dependence of $\varepsilon_{eff}$ or $\mu_{eff}$ obtained from different methods

Figs. 3.8 to 3.10 show  $\phi_i$  dependence of  $\varepsilon_{eff}$  or  $\mu_{eff}$  with  $\phi_i$  varying according to Scheme (i), (ii) and (iii) as shown in Fig. 3.6, where  $\phi_i$  is varied from 0 to 0.6, and  $\mu_1$  and  $\mu_2$  are fixed at 10 and 2. It should be emphasized at this point that we would not distinguish permittivity and permeability in the following discussion.

The dotted curves and dashed curves are used to represent the results obtained from the PS-MP and MG-MP methods. Symbols “□”, “△” and “×” are used to indicate the results obtained from the SI-MP<sub>12</sub>, SI-MP<sub>21</sub> and RA-MP methods. Data expressed with the symbol “○” represent the results obtained from FE analysis simulations based on models containing 4x4x4 inclusion arrays, where the two types of inclusions are randomly interweaved.

Some common features are seen in these figures. At first, in the low inclusion region of  $\phi_i \leq 0.1$ , results obtained from all the above methods are close. In the region of higher  $\phi_i$ , the results of the PS-MP and MG-MP theories start to deviate from each other and form the upper and lower bounds of the data pointed derived from other approaches.



This is understood because the PS-MP model introduces the higher degree of modification to the matrix properties among the methods under consideration. On the contrary, the MG-MP model is based on the introduction of a spherical inclusion and basically does not consider any modification to the matrix. Hence the permeability derived is the lowest among those of other methods.

Furthermore, results obtained from the three I-MP processes are closer to the PS-MP curve. The deviations observed are less than 2%. This implies that the I-MP processes give similar modification to the matrix as that of the PS-MP method. More detailed inspection to the figures show that the results of the three I-MP processes are not the same, though they are expected to be identical. In general, the result obtained from the SI-MP<sub>21</sub> is larger than that of SI-MP<sub>12</sub>. Their differentiations are more readily seen at  $\phi_i = 0.6$ . We suggest that addition of inclusions having a smaller permeability followed by the other kind of inclusions of a higher permeability would lead to successive enhancements of the effective permeability of the matrix and thus the whole composite system. If the order is reversed, the modification caused by adding the first kind of inclusions with a higher permeability could be watered down by the addition of the second type of inclusions with a lower permeability.



The FE data are found to lie around the midway between the PS-MP and MG-MP curves. They are lower than the results of the three I-MP processes at a specific  $\phi_i$ . One sees that the data evaluated at  $\phi_i = 0.6$  in the three figures are 6%, 3% and 8% lower than the corresponding I-MP data. If the FE data are really closer to the true value due to having a higher emulation of the real system, one would then suggest that the PS-MP method and the three I-MP processes overestimates the  $\mu_{eff}$  value due to excessive modification of the matrix. On the other hand, the MG-SP method oversimplifies the real system by just introducing one spherical inclusion in the model, such that it underestimates  $\mu_{eff}$  of the real system. The same feature was detected and explained for 2-phase systems as seen in Chapter 2.

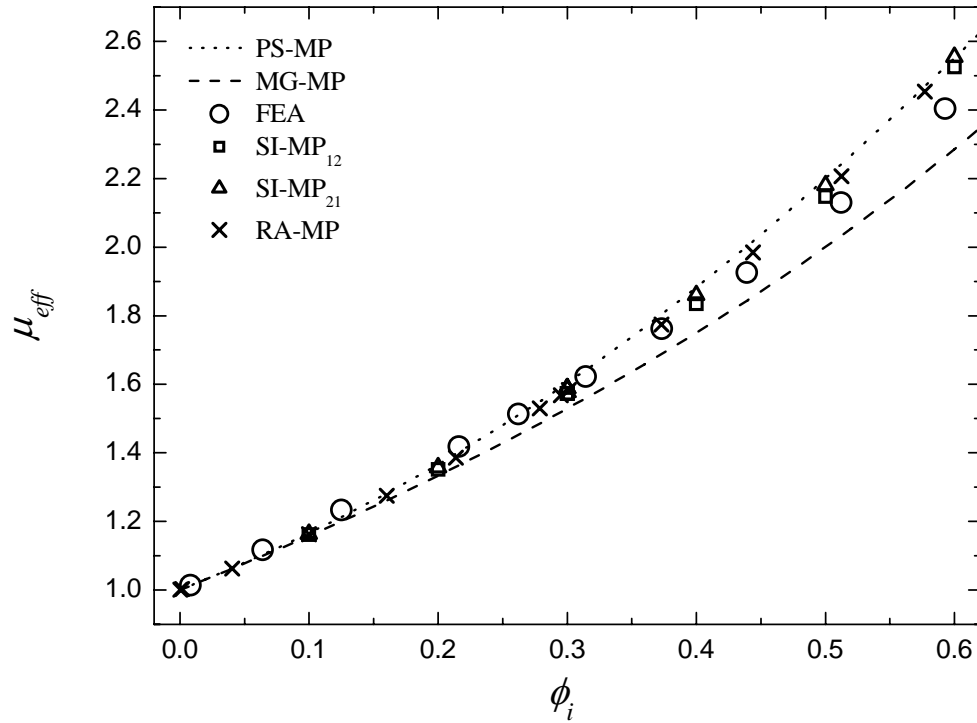


Fig. 3.8  $\phi_i$  dependence of  $\mu_{eff}$  obtained from PS-MP method (dotted curve); MG-MP method (dashed curve); SI-MP<sub>12</sub> method “□”; SI-MP<sub>21</sub> method “△”; RA-MP method “×” and FE simulations “○” for a model containing two types of inclusions arranged in a 4x4x4 array with  $\mu_1 = 10$  and  $\mu_2 = 2$ . The matrix has a  $\mu_m$  of 1.  $\phi_1:\phi_2 = 1:1$ , i.e. Scheme (i) in Fig.3.6.

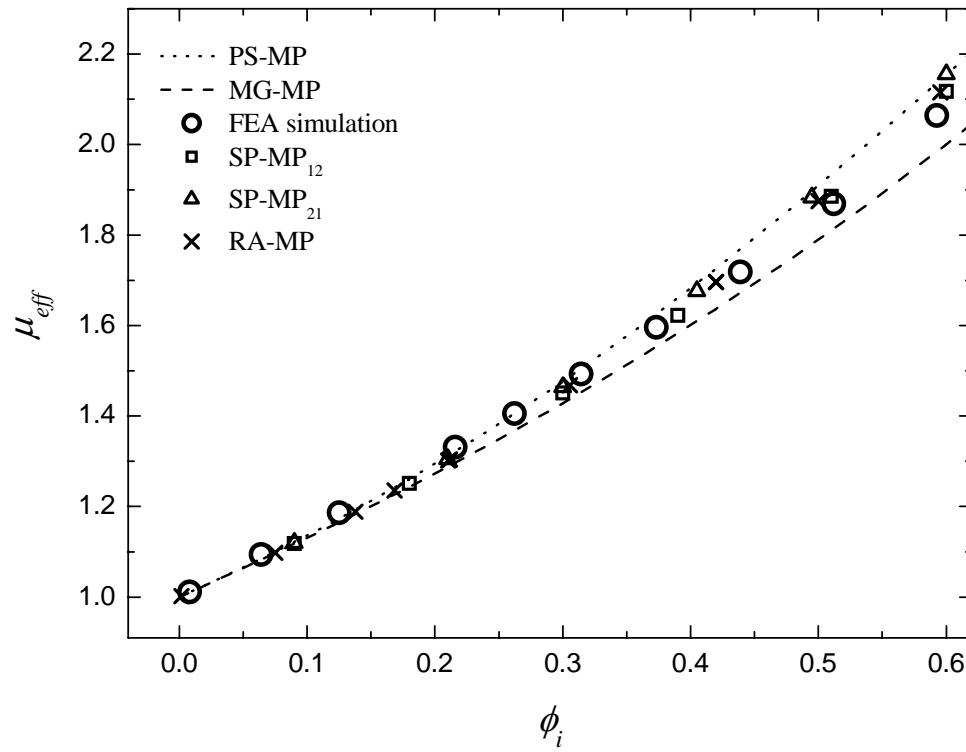


Fig. 3.9  $\phi_i$  dependence of  $\mu_{eff}$  obtained from PS-MP method (dotted curve); MG-MP method (dashed curve); SI-MP<sub>12</sub> method “□”; SI-MP<sub>21</sub> method “△”; RA-MP method “×” and FE simulations “○” for a model containing two types of inclusions arranged in a 4x4x4 array with  $\mu_1 = 10$  and  $\mu_2 = 2$ . The matrix has a  $\mu_m$  of 1.  $\phi_1:\phi_2 = 1:2$ , i.e. Scheme (ii) in Fig.3.6.

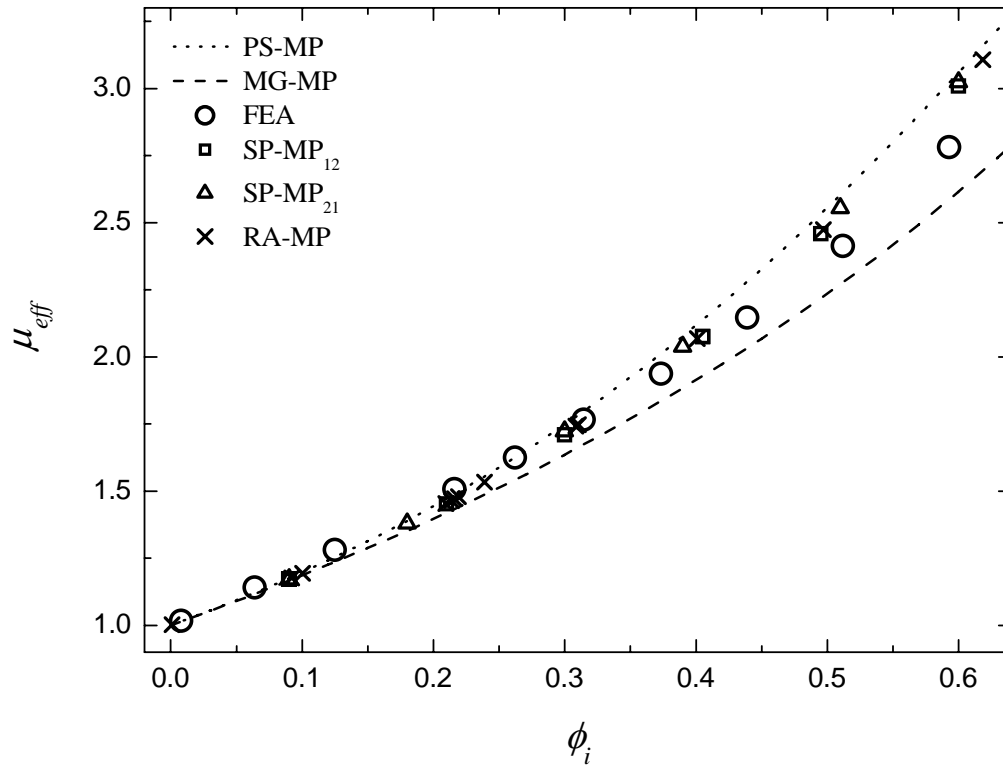


Fig. 3.10  $\phi_i$  dependence of  $\mu_{eff}$  obtained from PS-MP method (dotted curve); MG-MP method (dashed curve); SI-MP<sub>12</sub> method “□”; SI-MP<sub>21</sub> method “△”; RA-MP method “×” and FE simulations “○” for a model containing two types of inclusions arranged in a 4x4x4 array with  $\mu_1 = 10$  and  $\mu_2 = 2$ . The matrix has a  $\mu_m$  of 1.  $\phi_1:\phi_2 = 2:1$ , i.e. Scheme (iii) in Fig.3.6.



Figs. 3.11 – 3.13 show the  $\phi_i$  dependence of  $\mu_{eff}$  for a model containing a 6x6x6 spherical or cubic inclusion array with  $\mu_1$  and  $\mu_2 = 100$  and 10 respectively, and  $\phi_i$  varying from 0 to 1 according to Scheme (i), (ii) and (iii) shown in Fig. 3.6. The features observed in Figs. 3.8 to 3.10 are basically retained and highlighted in the following.

- (i) In the region of  $\phi_i$  below 0.2, data produced by various methods match quite well.
- (ii) The MG-MP values form the lower bound of other data points.
- (iii) The data points obtained from the three I-MP methods, i.e. the SI-MP<sub>21</sub>, SI-MP<sub>12</sub> and RA-MP processes, are found to distribute in a range broader than that in the previous case with lower  $\mu_1$  and  $\mu_2$ . In particular, the I-MP values are higher than most of those of the FE data. The  $\mu_{eff}$  value of the SI-MP<sub>21</sub> process is higher than that of a SI-MP<sub>12</sub> process at the region of  $\phi_i < 0.9$ , while SI-MP<sub>12</sub> process gives the highest when  $\phi_i > 0.9$ .
- (iv) The RA-MP data at a certain  $\phi_i$  is roughly equal to the mean of the SI-MP<sub>21</sub> and SI-MP<sub>12</sub> data, and is close to the PS-MP value when  $\phi_i < 0.8$ . Therefore, RA-MP results can be regarded as a representative of the three I-MP approaches.
- (v) The FE results for the cases of  $\phi_1/\phi_2 = 1:1$ , 1:2 and 2:1 do not lie in the midway between the PS-MP curve and MG-MP curve as in the case of using lower  $\mu_1$  and



$\mu_2$  of 10 and 2. Instead, they tend to be closer to the MG-MP in the region of  $0.3 \leq \phi_i \leq 0.9$ . Provided that the FE results reflect better the true value of  $\mu_{eff}$ , one may conclude that the PS-MP and I-MP methods give more serious overestimations of the  $\mu_{eff}$  when the inclusions have higher permeabilities.

The MG-MP method still underestimates the value of  $\mu_{eff}$ .

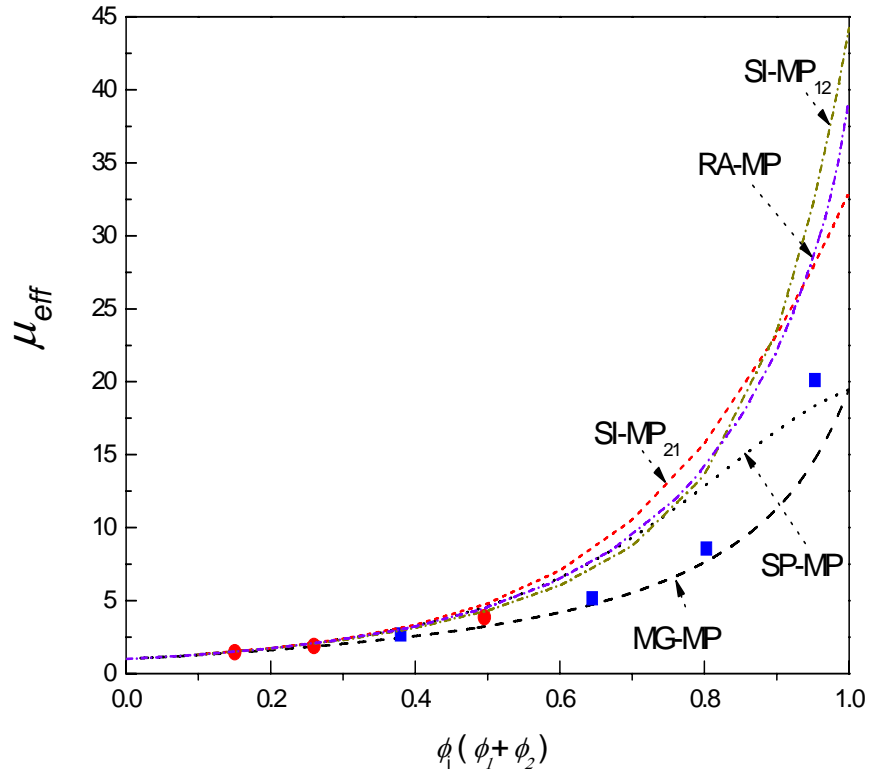


Fig. 3.11  $\phi_i$  dependence of  $\mu_{eff}$  obtained from PS-MP, MG-MP, SI-MP<sub>12</sub>, SI-MP<sub>21</sub> and RA-MP methods (dotted line) and FE simulations (“●”: spherical inclusions, “■”: cubic inclusions) for a model containing two types of inclusions arranged in a 6x6x6 array with  $\mu_1 = 100$  and  $\mu_2 = 10$ . The matrix has a  $\mu_m$  of 1.  $\phi_1:\phi_2 = 1:1$ , i.e. Scheme (i) in Fig.3.6.

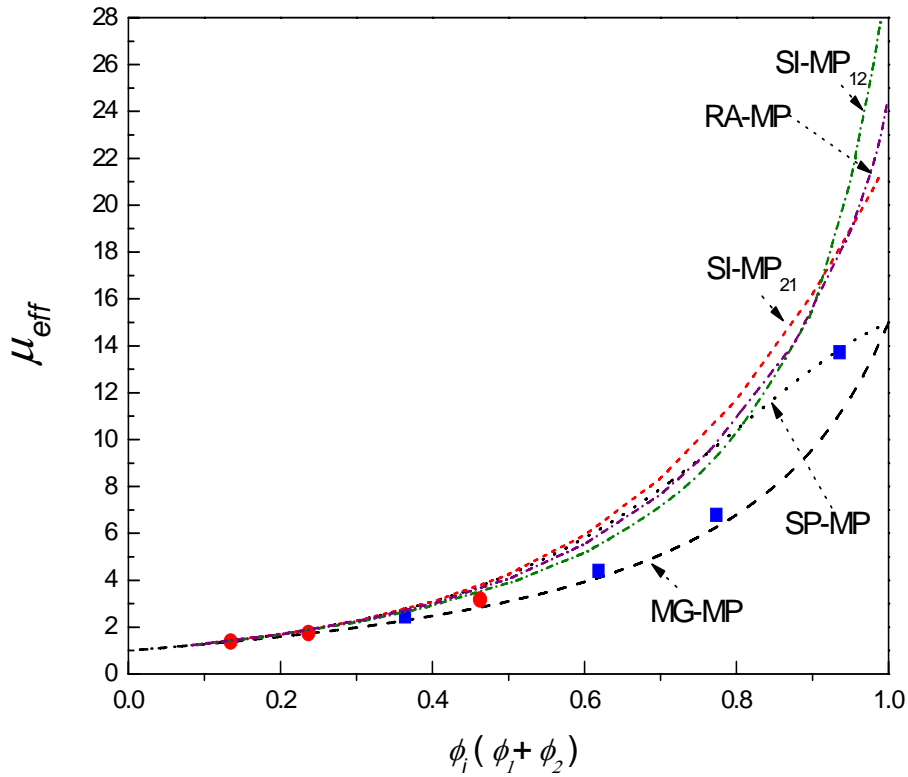


Fig. 3.12  $\phi_1$  dependence of  $\mu_{\text{eff}}$  obtained from PS-MP, MG-MP, SI-MP<sub>12</sub>, SI-MP<sub>21</sub> and RA-MP methods (dotted line) and FE simulations (“●”: spherical inclusions, “■”: cubic inclusions) for a model containing two types of inclusions arranged in a 6x6x6 array with  $\mu_1 = 100$  and  $\mu_2 = 10$ . The matrix has a  $\mu_m$  of 1.  $\phi_1:\phi_2 = 1:2$ , i.e. Scheme (ii) in Fig.3.6.

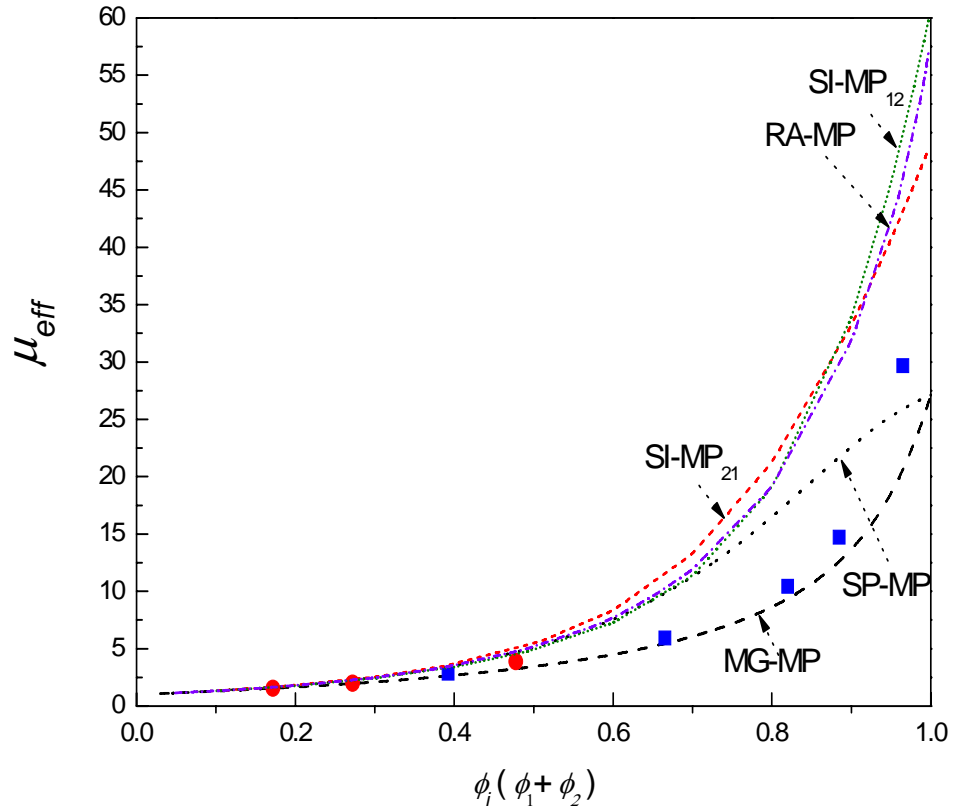


Fig. 3.13  $\phi_i$  dependence of  $\mu_{eff}$  obtained from PS-MP, MG-MP, SI-MP<sub>12</sub>, SI-MP<sub>21</sub> and RA-MP methods (dotted line) and FE simulations (“●”: spherical inclusions, “■”: cubic inclusions) for a model containing two types of inclusions arranged in a 6x6x6 array with  $\mu_1 = 100$  and  $\mu_2 = 10$ . The matrix has a  $\mu_m$  of 1.  $\phi_1:\phi_2 = 2:1$ , i.e. Scheme (iii) in Fig.3.6.



### 3.4.3 $\phi_I$ dependence of $\varepsilon_i$ and $\mu_{eff}$ obtained from different methods

In this section, we present the dependence of  $\mu_{eff}$  on  $\phi_I$ , with  $\phi_i = \phi_I + \phi_2$  kept as a constant. In other words,  $\phi_I$  is varied to scan across 0 to  $\phi_i$ , while  $\phi_2$  varies concurrently as  $\phi_i - \phi_I$ . We selected two values of  $\phi_i$ , namely 0.42 and 0.73 in this study, which lead to Scheme (iv) and (v) as depicted in Fig. 3.6.  $\mu_1$  and  $\mu_2$  are fixed at 10 and 2.

Results of the calculations are shown in Fig. 3.14 and 3.15. Some common features observed are summarized as follows.

- (i) The calculated value of  $\mu_{eff}$  increases with increasing  $\phi_I$ . This feature is expected, because the increase of magnetic inclusion volume fraction should raise the average permeability of the overall system.
- (ii) The PS-MP and MG-MP data still form the upper and lower bounds of all the data produced by the RA-MP processes and FE simulations. The separation between these two extremes is more pronounced with increasing  $\phi_I$ . For example, their difference varies from about 2% to 18% when  $\phi_I$  is increased from 0 to 0.4 for the case of  $\phi_i = 0.4$ .
- (iii) In the region of low  $\phi_I$ , for both  $\phi_i = 0.42$  and 0.73, the results of all approaches are similar. For higher a value of  $\phi_I$ , the results of  $\mu_{eff}$  obtained from a RA-MP process and FE simulation deviate from each other. The former becomes closer to the PS-MP result, while the latter approaches the MG-MP result.
- (iv) Assuming that the FE data are closer to the true  $\mu_{eff}$  values, one concludes that both the PS-MP and RA-MP methods overestimate the  $\mu_{eff}$  value possibly because of the introduction of excessive modification to the matrix. The



percentage error is larger when the volume fraction  $\phi_I$  increases; or inclusions of higher permeabilities are used.

At last, the results of MG-MP are always lower than the FE values, because the model considers the influence of one inclusion and does not introduce large enough modification to the properties of the matrix.

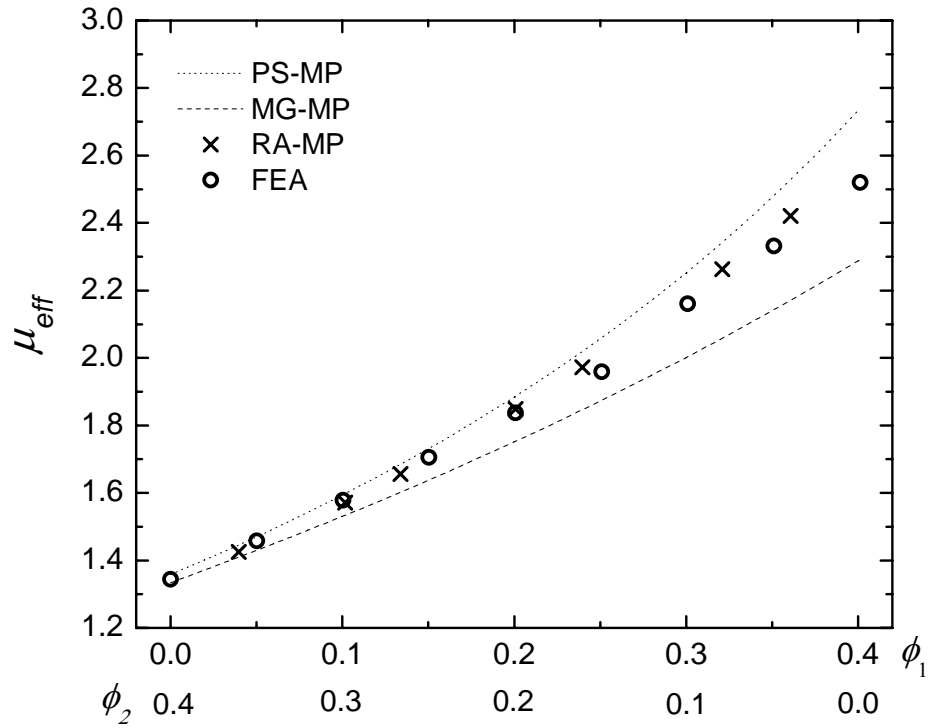


Fig. 3.14  $\phi_1$  dependence of  $\mu_{eff}$  under the condition of a fixed  $\phi_I = 0.42$ , i.e. Scheme (iv) in Fig.3.6.  $\mu_1 = 10$  and  $\mu_2 = 2$ . PS-MP method (dotted curve); MG-MP method (dashed curve); RA-MP processes “x”; FEA simulations “o” associated with a 4x4x4 spherical inclusion array.

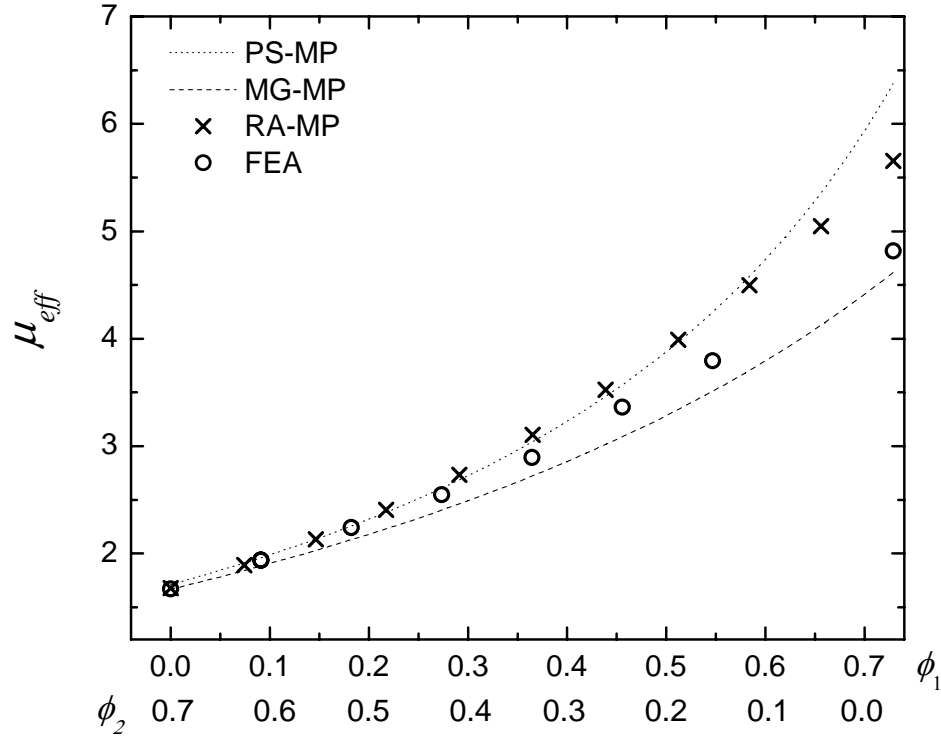


Fig. 3.15  $\phi_1$  dependence of  $\mu_{eff}$  under the condition of a fixed  $\phi_i = 0.73$ , i.e. Scheme (v)

in Fig.3.6.  $\mu_1 = 10$  and  $\mu_2 = 2$ .

Dotted curves : PS-MP method

Dashed curves : MG-MP method

$\times$  : RA-MP processes

$\circ$  : FEA simulation with spherical inclusions

We repeated the calculations of  $\mu_{eff}$  by setting  $\mu_1$  and  $\mu_2$  at higher values of 100 and 10.

With the total inclusion volume fraction  $\phi_i$  fixed at 0.42,  $\phi_l$  was varied from 0 to 0.42.

Concurrently,  $\phi_2$  varies according to  $\phi_i - \phi_l$  from 0.42 to 0. This is expressed as

Scheme (iv) in Fig. 3.6. As shown in Fig. 3.16, most of the FE data lie around the



midway between the PS-MP and MG-MP curves. If the FE results are closer to the real  $\mu_{eff}$  values, both the PS-MP and MG-MP results show some errors in estimating the permeability of the composite. Compared with the previous results obtained with the use of smaller  $\mu_1$  and  $\mu_2$  equal to 10 and 2, the discrepancy the estimates from the PS-MP and MG-MP methods is enlarged if higher values of  $\mu_1$  and  $\mu_2$  are used. It is further noticed that the RA-MP results are basically consistent with the FE results at low  $\phi_i$  values, but approach towards the PS-MP curve when  $\phi_i$  increases. Such a deviation is also more pronounced with the use of higher values of  $\mu_1$  and  $\mu_2$ .

Based on these results, we assert that the analytic approaches employed in this part of study, i.e. the PS-MP, MG-MP and RA-MP processes, still need further investigations in order to justify their correction and accuracy in predicting the overall permeability of a 3-phase composite.

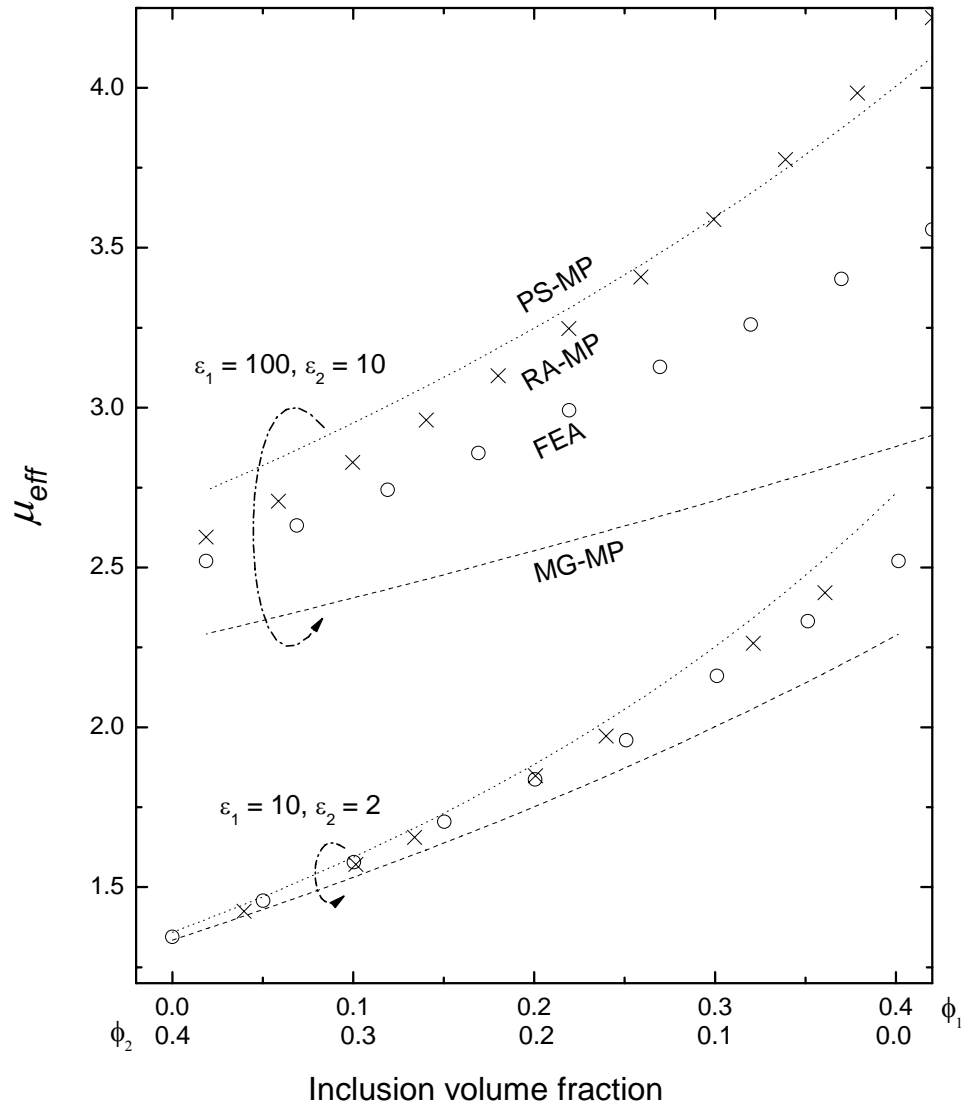


Fig. 3.16  $\phi_1$  dependence of  $\mu_{eff}$  for  $\mu_1$  and  $\mu_2$  equal to 100 and 10; and 10 and 2 respectively. The overall inclusion volume fraction  $\phi_t$  is fixed at 0.42.

Dotted curves: PS-MP method;

dashed curves: MG-MP method;

$\times$  : RA-MP process

$\circ$  : FE simulation with spherical inclusions.



### 3.4.4 Influence of the order of distribution of inclusions

In order to investigate how the pattern of the distribution of the inclusions affects the  $\mu_{eff}$  value of a composite, we performed simulations with the use of FE method by setting the inclusions to locate in three different patterns as depicted in Fig. 3.17. For all these models, the volume fractions of the two types of inclusion are in the same ratio of  $\phi_1 : \phi_2 = 1:1$ . In these models, the inclusions are (i) randomly assigned to the sites of a 4x4x4 cubic array, referred to as the random pattern; (ii) arranged to form two layers of different inclusion types aligned in parallel to the applied  $H$ -field, referred to as the parallel pattern; and (iii) arranged to form two layers of different inclusion types aligned perpendicular to the applied  $H$ -field, referred to as the perpendicular pattern.

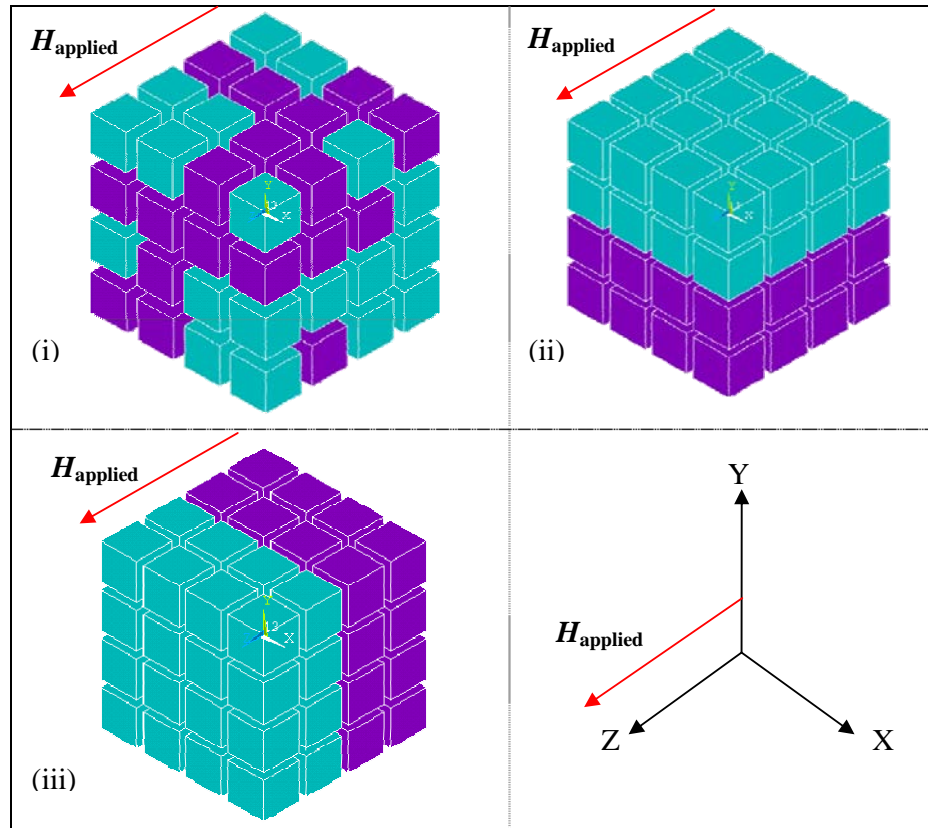


Fig. 3.17 Three FE models with inclusions located (i) randomly (random pattern); (ii) in two layers aligned in parallel to the applied field (parallel pattern) and (iii) in two layers perpendicular to the applied field (perpendicular pattern). In all cases,  $\phi_1:\phi_2 = 1:1$ .

Fig. 3.18 shows that for a certain combination of  $\mu_1$  and  $\mu_2$  equal to 10 and 2, and 100 and 10; and the total inclusion volume fractions  $\phi_i = 0.125$  and 0.6, the estimated value of  $\mu_{eff}$  for the perpendicular pattern is always the lowest, and that of the parallel pattern is the highest. This is because the demagnetization effect in the inclusions of the



former cases is the strongest, while that of latter case is the weakest. In addition, the result of the random pattern always lies between the above values. As a typical example, for  $\mu_1$  and  $\mu_2 = 10$  and 2,  $\mu_{eff}$  obtained from the parallel pattern is 3% higher than that of the random pattern. The result of the random pattern is 7% higher than that of the perpendicular pattern. In another example, when  $\mu_1$  and  $\mu_2$  are set to be 100 and 10, the result of  $\mu_{eff}$  of the parallel pattern is 2% above the random one. The result of the random in this case is 2% higher than that of the perpendicular pattern. All these features are explained based on the demagnetization effect in the inclusions.

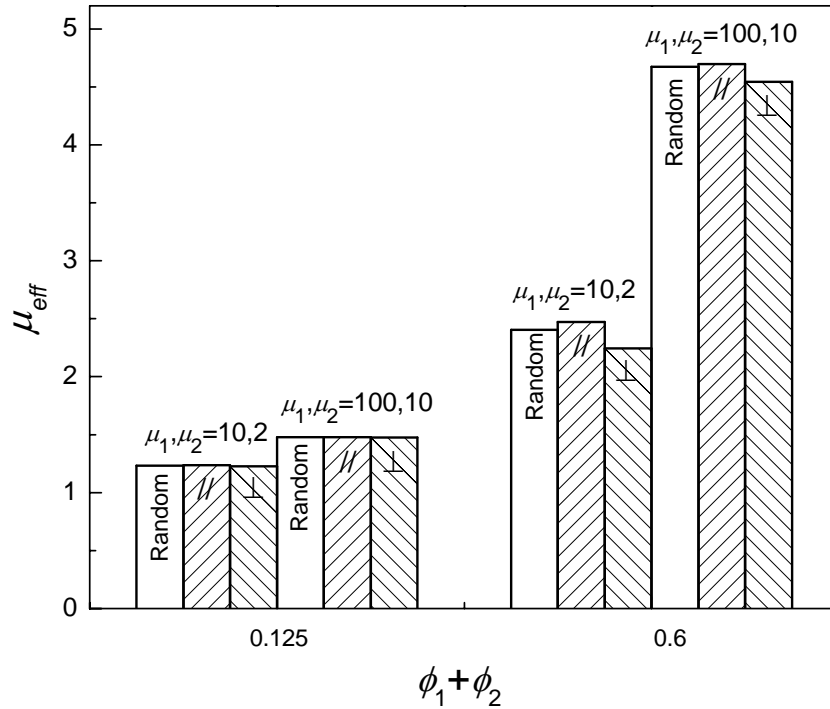


Fig. 3.18 Estimated values of  $\mu_{eff}$  obtained from distribution patterns of inclusions, with  $\mu_1$  and  $\mu_2$  set at 10 and 2, or 100 and 10; and  $\phi_1$  set at 0.125 and 0.6. In all the calculations,  $\phi_1:\phi_2$  is fixed at 1:1.



## **Chapter 4    A method for determining the permeability of a material $\mu_{real}$ by combining vibrating sample magnetometer and FE method**

This chapter describes a method to determine the permeability  $\mu$  of a material by combining the experimental measurement by using vibrating sample magnetometer (VSM) and FE method. This approach is proposed to eliminate the demagnetization effect without requiring the sample to be made in a standard form for a conventional test.

### **4.1 Conventional method and VSM for the determination of $\mu$**

Determination of a permeability  $\mu$  is practically important in selecting a magnetic material for a specific application. A common method for measuring  $\mu$ , named after Rowland's ring, is to wind a magnetization coil and sampling coil over a toroidal



sample as shown in Fig. 4.1 [Greenslade]. By passing a current to the magnetization coil, a magnetic field ( $\vec{H}$ ) is generated inside the sample which is being magnetized. The magnetic induction ( $\vec{B}$ ) inside the sample can be calculated from the voltage induced in the sampling coil. Finally, the relationship between magnetic induction and magnetic field ( $B$ - $H$  loop) can be determined.



*Fig. 4.1 Configuration of a Rowland's ring.*

In principle, one can derive all the parameters related to the magnetic properties of the substance from the  $B$ - $H$  loop. For example,  $\mu$  can be determined from the ratio between  $B$  and  $H$ . However, the requirement of making a ring-shaped sample is usually not easily realized, such as the cases of film, plate, wire and powder samples.



On the other hand, a VSM instrument recording the apparent relationship between  $B$  and  $H$ . VSM has the advantage of being easily operated, and is a mature commercial product widely available in the market [Burgei, et al., 2003; Hoon, 1983; Samwel, et al., 1998]. It also allows samples of different shapes to be used in measurements.

In general, the relationship between  $B$  and  $H$  recorded with a VSM is not the same as the true  $B$ - $H$  loop of the material. Unless the sample is a long and thin wire aligned in parallel with the applied  $H$ -field ( $\vec{H}_{applied}$ ), otherwise demagnetization would occur to make the internal  $H$ -field to be lower than  $\vec{H}_{applied}$ . Denoting the  $B$ -field and  $H$ -field inside the specimen as  $\vec{B}_{internal}$  and  $\vec{H}_{internal}$  respectively, their magnitudes are correlated with an expression:

$$\vec{B}_{internal} = \mu_0 \mu_{real} \vec{H}_{internal} . \quad (4-1)$$

However, a VSM measurement cannot detect  $\vec{H}_{internal}$  directly but only the applied field,  $\vec{H}_{applied}$ , at a point outside the sample is monitored. Hence, if  $\vec{H}_{applied}$  is wrongly used as if it is  $\vec{H}_{internal}$ , an apparent relative permeability  $\mu_{apparent}$  would be derived according to the relationship [Foner, 1956; Foner, 1959]:

$$\vec{B}_{internal} = \mu_0 \mu_{apparent} \vec{H}_{applied} . \quad (4-2)$$



Now the ratio between  $\mu_{real}$  and  $\mu_{apparent}$  is:

$$\frac{\mu_{apparent}}{\mu_{real}} = \frac{H_{internal}}{H_{apparent}} \quad (4-3)$$

The ratio  $|\vec{H}_{applied}| / |\vec{H}_{real}|$  is solved according to the following two expressions:

$$\mu_o \mu_{real} \vec{H}_{internal} = \mu_o \vec{H}_{internal} + \mu_o \vec{M} \quad (= \vec{B}_{internal}) \quad \text{and} \quad (4-4)$$

$$\vec{H}_{internal} = \vec{H}_{applied} - D \vec{M} \quad , \quad (4-5)$$

where  $D$  is defined as the demagnetization factor. It is in general smaller than 1, and is particularly equal to 1/3 for a sphere [Chen and Goldfarb, 1991; Osborn, 1945; Paterson and Cooke, 1998; Tang, et al., 2005]. Solving Eqs. (4-4) and (4-5), one obtains:

$$\frac{H_{internal}}{H_{applied}} = \frac{1}{1 + D(\mu_{real} - 1)} \quad (4-6)$$

For strong magnetic materials like iron (Fe) or nickel (Ni),  $\mu_{real} \gg 1$ , such that:

$$\frac{H_{internal}}{H_{applied}} \approx \frac{1}{1 + D\mu_{real}} \quad (4-7)$$

One obtains:

$$\frac{\mu_{apparent}}{\mu_{real}} \approx \frac{1}{1 + D\mu_{real}} \quad (4-8)$$

In case that  $\mu_{real} \gg 1$  and the factor  $D$  has a moderate value in the order of 1, the value of  $\mu_{apparent}$  thus derived would be much smaller than  $\mu_{real}$ . Though one can correct the result according to the sample geometry and by making use of the tabulated values of



$D$  [Aharoni, 1998; Clarke, 1999; Graef and Beleggia, 2006; Matyuk and Osipov, 2000], the error could be large because the result would be extremely sensitive to the variation in  $D$ .

Another method is to perform VSM measurements on a very long and thin wire sample aligned along the applied magnetic field. If the specimen has a very large length-to-width ratio (referred to as aspect ratio afterwards), such that  $D$  is small enough to satisfy the condition  $D\mu_{real} \ll 1$ , the measured  $\mu_m$  value would become close to  $\mu_{real}$ . As a rough estimate, an aspect ratio in the order of 1000 is required to give a good result if  $\mu_{real}$  of the material is around 3000. For some materials, it may be difficult to prepare a thin wire specimen to satisfy this requirement. With these constraints, VSM is not a useful machine for determining the permeability of a substance.



## 4.2 Our method for the estimation of $\mu$

### 4.2.1 VSM measurement

VSM measurements are first performed on samples with different aspect ratios in a broad range. The samples are not necessary to be made to have a very large aspect ratio to suppress the demagnetization effect to a negligible level. In fact, in most cases, fabrication of such a specimen is quite impractical.

We first define the true  $\mu_{real}$  of a substance and the  $\mu_{apparent}$  value from the  $B$ - $H_{internal}$  relationship recorded in a VSM measurement. Fig. 4.2a represents schematically the true  $M$ - $H_{internal}$  loop of a substance, where the slope at low field strength around zero is defined as the  $\mu_{real}$ , which is to be estimated in this study. Fig. 4.2b shows the apparent  $M$ - $H_{applied}$  loop recorded with VSM, which is more inclined and the slope at the low field region is defined as the  $\mu_{apparent}$ .

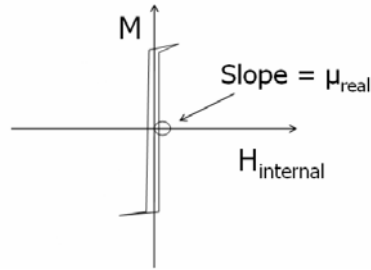


Fig. 4.2a

*Schematic illustration of  $\mu_{real} = B_{internal} / (H_{internal} \mu_0)$ , i.e. the slope of the true  $M$ - $H_{internal}$  loop near  $M = 0$ .*

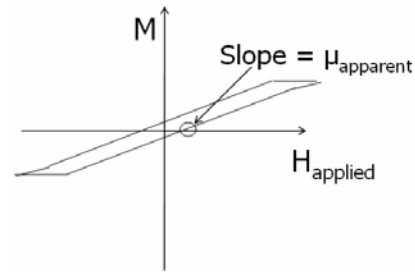


Fig. 4.2b

*Schematic illustration of  $\mu_{apparent} = B_{internal} / (H_{applied} \mu_0)$ , i.e. the slope of the  $M$ - $H_{applied}$  loop near  $M = 0$ .*

### 4.2.2 FEM simulations

FE analyses are performed to simulate VSM processes to establish theoretical relationships of  $\mu_{apparent}$  verse the aspect ratio of samples. Calculations are performed with  $\mu_{real}$  as a parameter varying in the range from 10 to  $10^4$ .

The model for the FE simulations is depicted in Fig. 4.3. A specimen was placed at the midway between two current coils. The first type of specimen was set to have a square cross-sectional area with a length  $z$  and an edge length of  $x (= y)$ . The second type of sample was in a rod shape with a length  $z$  and a diameter  $d$ . A sample was aligned with



its length along the applied  $H$ -field. The length of all the specimens ( $z$ ) was set to be equal to 6 mm. The aspect ratio  $z/x$  (for rectangular prisms) or  $z/d$  (for rods) was varied from 1 to 1000. Four true permeability values  $\mu_{real}$ , denoted as  $\mu_{real-1} = 10$ ,  $\mu_{real-2} = 500$ ,  $\mu_{real-3} = 3000$  and  $\mu_{real-4} = 10000$ , were assigned to the sample successively. A medium, presumed to be air with a relative permeability of 1, was created to embrace all the components.

Furthermore, plate samples having a length of  $z$ , a rectangular cross-sectional area with edges denoted as  $x$  and  $y$  (width), were investigated to see the influence of the change in width. Simulation for a sphere sample was performed for reference. It is noticed that the correctness of the calculations performed in this part of study is supported by the attainment of a  $D$  value =  $1/3$ , consistent with the prediction from basic electromagnetic theory.

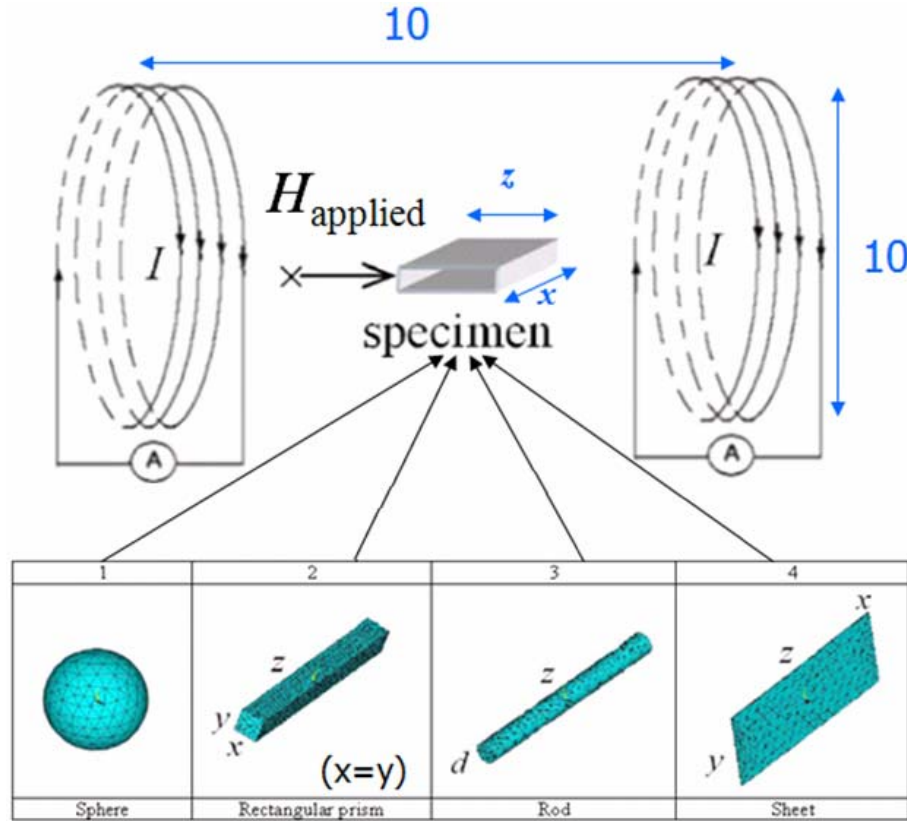


Fig. 4.3 FEA model for the simulations of VSM processes. Samples are assigned to have square ( $x = y$ ), rectangular ( $x \neq y$ ), and circular (diameter =  $d$ ) cross-sectional areas. Calculation for a spherical sample is preformed for reference.

For a particular  $\mu_{real-i}$  and  $z/x$  or  $z/d$ , a current was set to pass through the coils to set up an externally applied magnetic field  $\vec{H}_{applied}$  in the gap. The current was successively increased such that the magnitude of the  $\vec{H}_{applied}$  field was scanned over a broad range. Meanwhile, the magnitude of  $\vec{H}_{internal}$  and the corresponding magnetic induction  $\vec{B}_{internal}$  were calculated. The average values of the magnetic field and magnetic induction, denoted as  $\langle \vec{H}_{internal} \rangle_i$  and  $\langle \vec{B}_{internal} \rangle_i$ , over the whole volume of the



specimen were deduced. The apparent relative permeability  $\mu_{apparent}$  defined in Eq. (4-2)

can thus be derived according to the equation:

$$\langle \bar{B}_{internal} \rangle_i = \mu_o \mu_{apparent} \langle \bar{H}_{applied} \rangle \quad (4-9)$$

Relationships between the predicted  $\mu_{apparent}$  and aspect ratio  $z/x$  or  $z/d$  for various  $\mu_{real-i}$

values = 10, 500, 3000 and 10000 for  $i=1, 2, 3$  and 4 were thus obtained and shown in

Fig. 4.4.

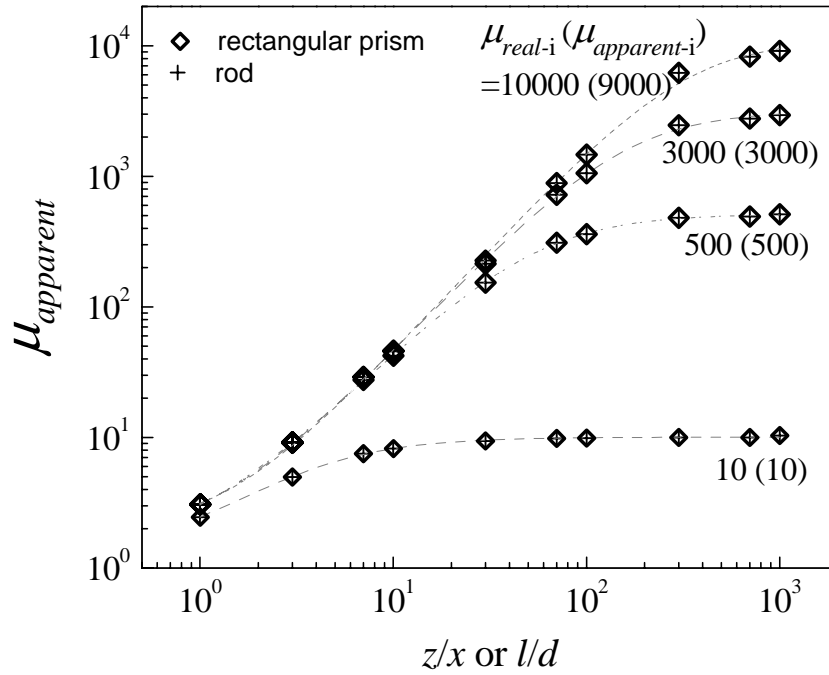


Fig.4.4 Predicted results of  $\mu_{apparent}$  with VSM measurements versus aspect ratio  $z/x$  or  $z/d$  varying from 1 to 1000, for four  $\mu_{real-i} = 10, 500, 3000$  and 10000 respectively.

“ $\diamond$ ”: rectangular prism samples; “+”: rod samples.



One first notices that for all the  $\mu_{real}$  values investigated, demagnetization effect is more pronounced in the region of small  $z/x$  and  $z/d$ . Second,  $\mu_{apparent}$  of a material with a relatively low  $\mu_{real}$  value starts to reach the  $\mu_{real}$  value at a lower aspect ratio  $z/x$  (or  $z/d$ ). For example, for  $\mu_{real-1} = 10$ , the  $\mu_{apparent}$  value starts to increase to around  $\mu_{apparent}$  at  $z/x \approx 10$ . For a curve of a higher relative permeability, e.g.  $\mu_{real-2} = 500$ , the demagnetization effect is more significant. The  $\mu_{apparent}$  value becomes close to the true value only when  $z/x$  is increased to around 300.

At last, we note that for a specific  $\mu_{real}$ , the  $\mu_{apparent}$  versus aspect ratio relationships of a rectangular prism and a rod with the same length-to-thickness ratio ( $z/x = z/d$ ) are basically consistent. This implies that the results of these two sample geometries have no observable difference.

The next step was to find out explicit functional relationships correlating  $\mu_{apparent}$  and  $z/x$  (or  $z/d$ ) for a specific  $\mu_{real}$  value. We applied sigmoid functions to fit the four groups of predicted  $\mu_{apparent-i}$  data obtained from FE analyses, with  $\mu_{real-1} = 10$ ,  $\mu_{real-2} = 500$ ,  $\mu_{real-3} = 3000$  and  $\mu_{real-4} = 10000$ , respectively. The general form of a sigmoid function is:



$$\mu_{apparent-i} = B_i + \frac{A_i - B_i}{1 + (1/r_{0i})^{p_i} (z/x)^{p_i}}, \quad (4-10)$$

where  $A_i$ ,  $B_i$ ,  $r_{0i}$  and  $p_i$  are the fitting parameters,  $z/x$  is the aspect ratio. The index  $i = 1, 2, 3$  and  $4$  corresponds to the four  $\mu_{real-i}$  values. The function form is also applicable to a rod sample if the free parameter  $z/x$  is replaced by  $z/d$ . The values of the parameters leading to the best fits to the curves in Fig. 4.4 are tabulated in Table 4.1.

Table 4.1 Optimized parameters in Eq. (4-10) to give the best fit to the curves shown in

Fig. 4.4.

$i$	1	2	3	4
$\mu_{real-i}$	10	500	3000	10 000
$A_i$	$1.07 \pm 0.86$	$1.46 \pm 0.25$	$1.76 \pm 0.2$	$1.94 \pm 0.19$
$B_i$	$10 \pm 0.24$	$513 \pm 16.2$	$3180 \pm 119$	$11150 \pm 536$
$r_{0i}$	$3.6 \pm 0.68$	$53.7 \pm 3.5$	$160 \pm 9.1$	$330 \pm 20$
$p_i$	$1.33 \pm 0.29$	$1.45 \pm 0.04$	$1.53 \pm 0.02$	$1.57 \pm 0.02$

From Table 4.1, it was found that the four data for each of the parameters,  $A_i$ ,  $B_i$ ,  $r_{0i}$  and  $p_i$ , exhibit some systematic dependence on  $\mu_{real-i}$  ( $i = 1, \dots, 4$ ). We were thus inspired to create a function for each of them with  $\mu_{real}$  as a free parameter. Through direct inspection, sigmoid functions were selected for establishing the functions for  $A_i$ ,  $r_{0i}$  and  $p_i$ ; and a second-order polynomial was selected for  $B_i$ . Using symbols  $A$ ,  $B$ ,  $r_o$  and  $p$  to



express these four functions, one can write:

$$A = b_{12} + (b_{11} - b_{12})/[1 + (\mu_{real} / b_{13})^{b_{14}}], \quad (4-11)$$

$$B = b_{21} + b_{22} \mu_r + b_{23} \mu_{real}^2, \quad (4-12)$$

$$r_o = b_{32} + (b_{31} - b_{32})/[1 + (\mu_{real} / b_{33})^{b_{34}}], \text{ and} \quad (4-13)$$

$$p = b_{42} + (b_{41} - b_{42})/[1 + (\mu_{real} / b_{43})^{b_{44}}]. \quad (4-14)$$

Using the data listed in Table 4.1, the values of the coefficients  $b_{j,k}$  ( $j, k = 1, 2, 3, \text{ and } 4$ )

are deduced by curve fitting. Substituting these values to Eqs. (4-11) to (4-14), one obtains:

$$A = 2.281 + (0.9786 - 2.281)/[1 + (\mu_{real} / 1385)^{0.524}], \quad (4-15)$$

$$B = -3.632 + 1.037 \mu_{real} + 7.78 \times 10^{-6} \mu_{real}^2, \quad (4-16)$$

$$r_o = 998.4 + (3.668 - 998.4)/[1 + (\mu_{real} / 25402)^{0.774}], \text{ and} \quad (4-17)$$

$$p = 1.626 + (1.305 - 1.626)/[1 + (\mu_{real} / 698.2)^{0.584}]. \quad (4-18)$$

Eqs. (4-15) to (4-18) were then utilized to reform Eq. (4-10), from which a predicted apparent permeability  $\mu_{apparent}$  obtained from a VSM measurement can be directly calculated once a  $\mu_{real}$  and a  $z/x$  (or  $z/d$ ) value were given. Implicitly:

$$\mu_{apparent} = \mu_{apparent}(\mu_{real}, z/x). \quad (4-19)$$



With this formula, one can generate as many curves as wish. Fig. 4.5 shows many plots created with Eq. (4-19) by substituting various  $\mu_{real}$  values in the range from 100 to 700, and  $z/x$  values in the range from 0 to 200.

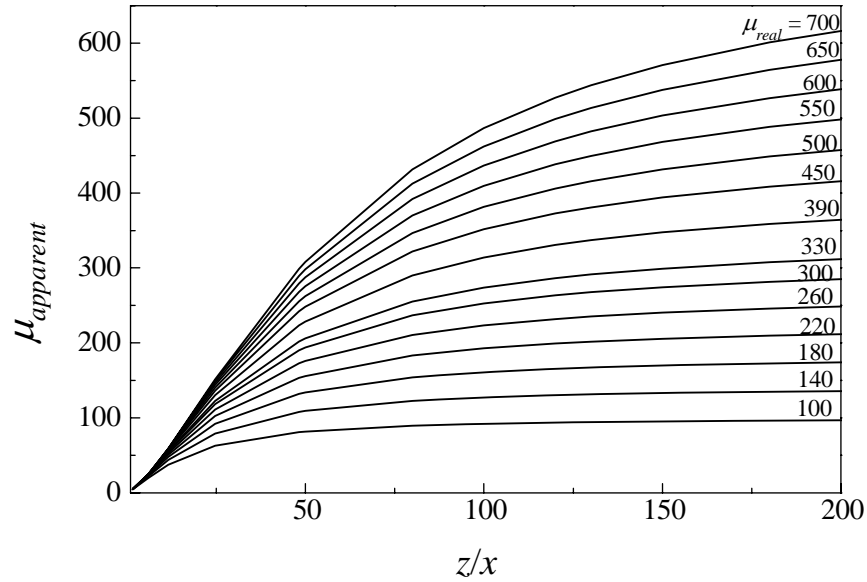


Fig. 4.5 Plots of  $\mu_{apparent}$  versus aspect ratio ( $z/x$ ) with  $\mu_{real}$  varying from 100 to 700.

#### 4.2.3 Estimate $\mu_{real}$ by correlating the results of FE analyses and VSM

##### measurements

VSM measurements were then performed on a series of samples of different aspect ratio, such that a set of experimental relative permeability denoted as  $\mu_{measurement}$  is obtained. These data are then plotted in Fig. 4.5. Normally, these data would distribute



in the figure in a narrow band bounded by a set of curves corresponding to a narrow range of  $\mu_{real}$  covering the real value.

We particularly point out that this method is advantageous for having no need to prepare a sample with a very large aspect ratio to completely eliminate demagnetization effect. The method does not rely on the measurement of one sample and then correct the result according to tabulated demagnetization factor  $D$ . Instead, the method utilizes the measurements on a group of samples with various aspect ratios, so that the error would be much smaller.



### 4.3 Results and discussions of two application examples: Fe

#### and Ni

We tried to verify the applicability of the above method by applying it to pure Fe and Ni rods/wires samples, we made to have different aspect ratios ( $z/d$ ). For Fe specimens, the  $z/d$  values used are 1.6, 6, 12, 25, 48, 90 and 122. For Ni specimens, the  $z/d$  values are 1.7, 6, 12, 35, 82 and 143.

Fig. 4.6 shows the relationship between  $M$  and  $\vec{H}_{applied}$  of Fe and Ni obtained from VSM measurements. These curves, are in fact better described by the expression  $\mu_{apparent} = |\vec{B}_{internal}| / (|\vec{H}_{applied}| \mu_0)$ , and are not directly related to  $\mu_{real}$ . For a sample of a larger  $z/d$  ratio, the corresponding curve appears to be steeper, showing that demagnetization effect is less significant in this sample.

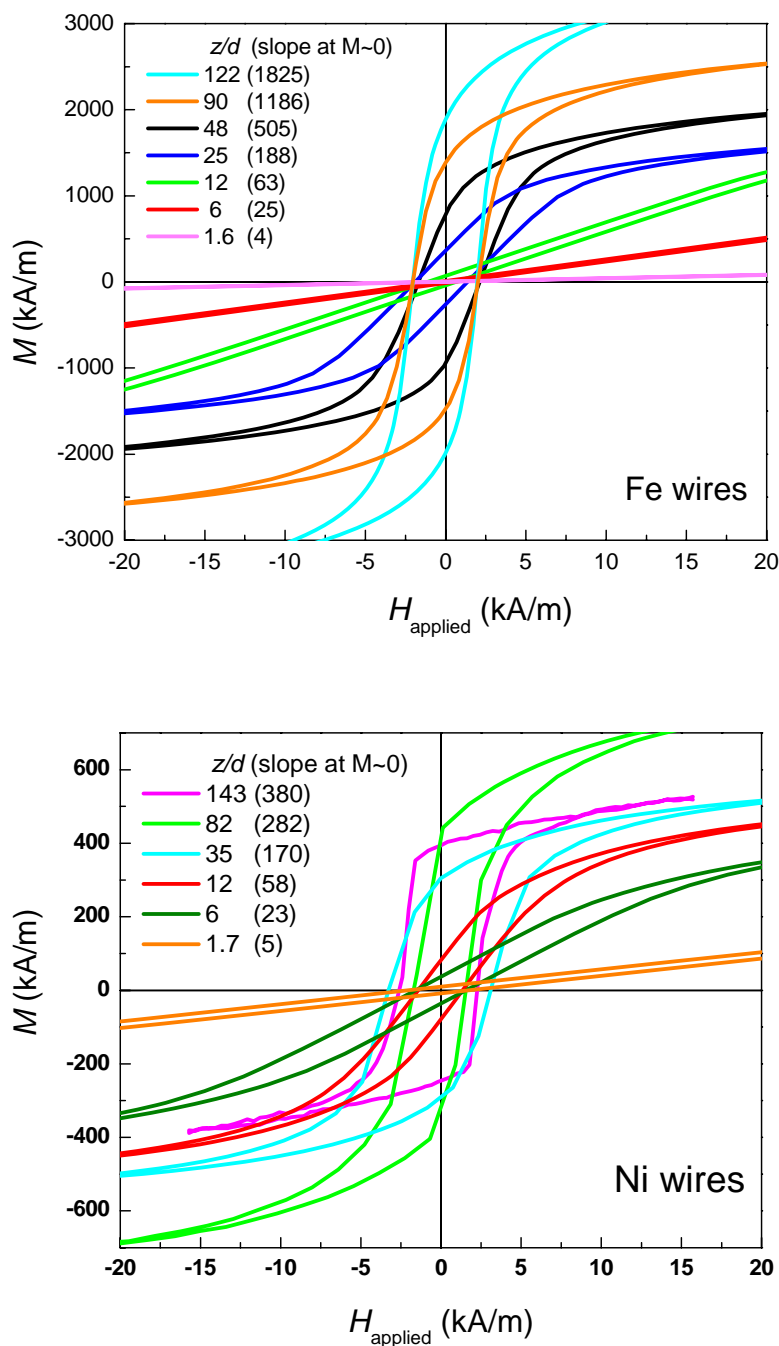


Fig. 4.6 Relationships of  $M$  versus  $H_{applied}$  of Fe and Ni wires with different aspect ratios recorded by using VSM. The slope of a curve at the low field region is labelled.



The slopes of these curves evaluated at low field region in Fig. 4.6 are derived and denoted as  $\mu_{apparent}$ . They are then plotted in Fig. 4.5. For Fe or Ni, the data points are bounded between two predicted  $\mu_{apparent}$  curves obtained from Eq. (4-19).

Fig. 4.7 shows more clearly the bounds of the data of each material. It is found that for Fe wires, the data points are bounded between two calculated curves of  $\mu_{real} = 8000$  and 10000. A reasonable estimate of  $\mu_{real}$  of Fe is 9000, which is basically consistent with the published value of bulk Fe.

For Ni wires, the data points fall between the calculated  $\mu_{real}$  curves of  $\mu_{real} = 360$  and 450. The most reasonable estimate of  $\mu_{real}$  of Ni is 400, which is also close to the published value of bulk Ni.

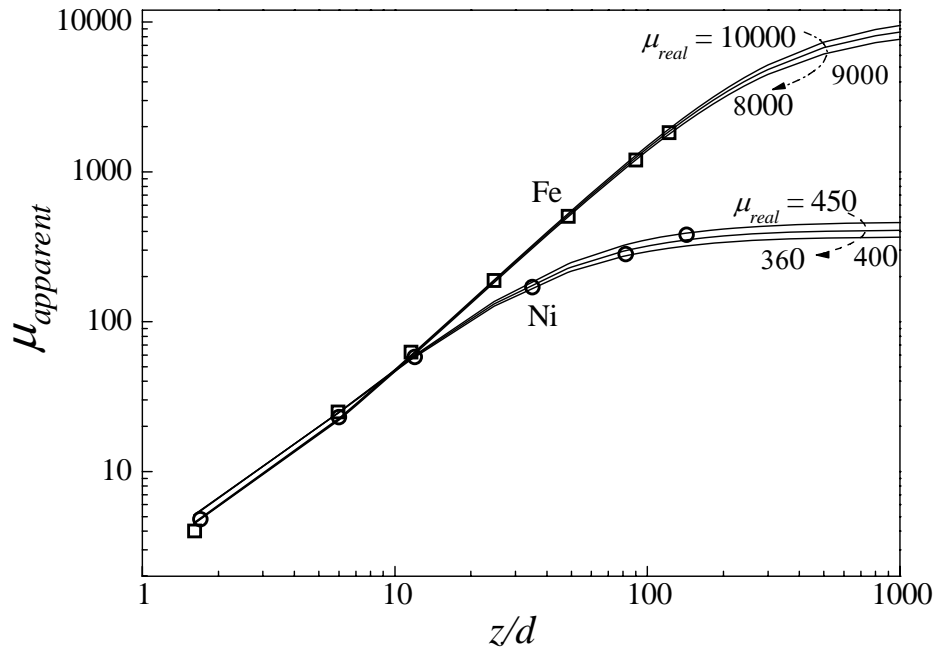


Fig.4.7 Experimental  $\mu_{measured}$  values of Fe and Ni wires bounded by corresponding curves of  $\mu_{apparent}$  versus  $z/x$  derived from Eq. (4-19) “□”: Fe wires; “○”: Ni wires.

Finally, we note that the width  $y$  of a rectangular prism can affect the value of  $\mu_{apparent}$  significantly as shown in Fig. 4.8. For a specimen with a fixed  $z/x = 100$ , when the ratio of  $y/z$  is increased from 0.01 to 1 (a sheet in the form as shown in Fig. 4.3), demagnetization becomes more pronounced. The  $\mu_{apparent}$  value drops by one order of magnitude from the true  $\mu_{real}$  value of 3000.

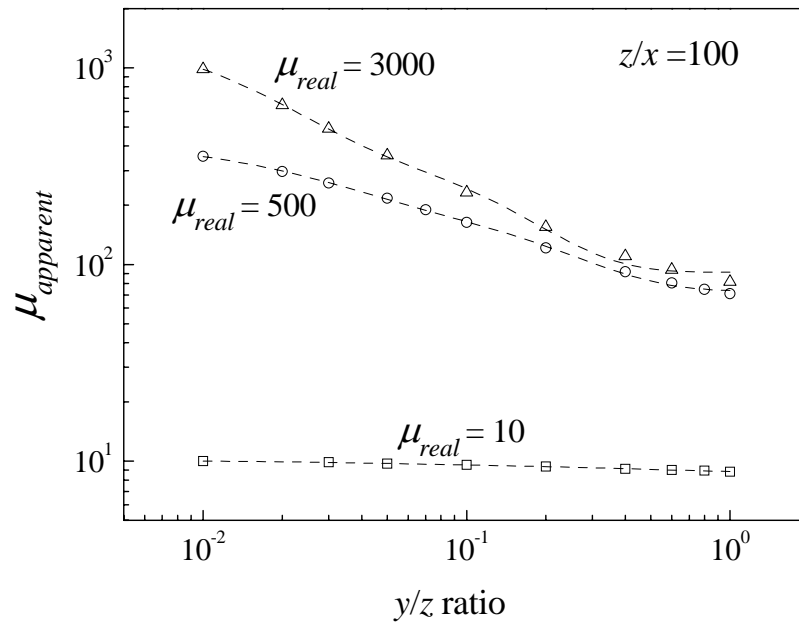


Fig. 4.8 Theoretically predicted apparent permeability  $\mu_{apparent}$  obtained by using VSM measurements for rectangular prisms with  $z/x = 100$  and  $y/z$  from 0.01 to 1, showing increasing demagnetization effect with increasing width of the sample.



## Chapter 5 Conclusions

### 5.1 Overall summary

We have completed three major studies in this project. The first study is to investigate the effective relative permittivity  $\epsilon_{eff}$  of 2-phase composites containing dielectric inclusions, and the effective relative permeability  $\mu_{eff}$  of 2-phase composites containing magnetic inclusions by applying several representative analytic models and FE simulations. Assuming that the FE results are closer to the real values, the results derived from the analytic models are compared with the FE results in order to examine the effectiveness of the analytic theories, which are based on some assumptions or simplifications, whereas the accuracy at higher inclusion volume fraction is supposed to be quite uncertainty.

The second study is to investigate the value of  $\epsilon_{eff}$  of a 3-phase composite containing two kinds of dielectric inclusions; or the effective relative permeability  $\mu_{eff}$  of 3-phase composites containing two kinds of magnetic inclusions by applying various analytic methods and FE simulations. Comparisons between the analytic and simulated results were performed to examine the effectiveness of the analytic models. In addition, the



flexibility of the FE method was utilized to investigate some parametric dependences of  $\varepsilon_{eff}$  (or  $\mu_{eff}$ ), such as the dependence on the inclusion shape, and the dependence on the distribution of the inclusions in a composite.

The third study is to develop a method to estimate the relative permeability  $\mu$  of a soft magnet by combining experimental results measured with a VSM and FE simulations. This method was designed to diminish the demagnetization effect in order to obtain the true  $\mu$  value of the material. The effectiveness of the method was demonstrated by applying it to Fe and Ni respectively.

According to the results obtained, we first conclude that the mathematical formulation used for analyzing  $\varepsilon_{eff}$  of a composite containing dielectric inclusions is the same as that for analyzing  $\mu_{eff}$  of a composite containing magnetic inclusions. Hence, the formulae developed for the former system, as those widely used in literature, can also be used in the latter system by replacing  $\vec{E}$  with  $\vec{H}$ ; and  $\vec{D}$  with  $\vec{B}$ . The expressions developed for  $\varepsilon_{eff}$  of a composite can also be converted and used for describing  $\mu_{eff}$  by replacing  $\varepsilon_{eff}$  with  $\mu_{eff}$  in the formula. This principle is applied throughout the thesis.



## 5.2 Conclusions on the study of 2-phase composites

Results obtained from the analyses on 2-phase composites show that in the region of low (dilute) inclusion volume fraction, say  $\phi_i \leq 0.1$ , the values of  $\varepsilon_{eff}$  (or  $\mu_{eff}$ ) estimated by using all the analytic methods employed, including the M-G, Bruggeman, P-S, Landauer and Rayleigh methods, are close and consistent with the FE results. In this region, the interaction between the inclusions is weak, such that the difference between these methods is negligible. In the region of higher inclusion volume fraction, the interaction between the inclusions becomes stronger, and the results deduced from them are more diversified. In particular, the M-G theory does not take account of the effect caused by the interaction between the inclusions, and hence the data of  $\varepsilon_{eff}$  deduced from this model are the lowest and form a lower bound of those derived from other methods.

The Bruggeman, P-S and Landauer methods consider the interaction between inclusions by modifying the matrix properties. The Rayleigh method is designed to give an exact solution with periodic boundary condition, and so the influence from the interaction between inclusions is also included. Results show that the values of  $\varepsilon_{eff}$  (or  $\mu_{eff}$ ) deduced from the M-G, Bruggeman, Rayleigh, P-S and Landauer theories are



in an ascending order. In particular, the data deduced from the Landauer method form the upper bound of the data points obtained by using other methods.

Compared with the results of FE analyses which are supposed to better estimate  $\varepsilon_{eff}$  (or  $\mu_{eff}$ ), we found that in the range of  $\phi_i$  below 0.2, all analytic methods give good results of  $\varepsilon_{eff}$  (or  $\mu_{eff}$ ). For  $\phi_i \leq 0.52$ , the FE results for spherical inclusion array agree with the results of the Rayleigh theory, and the error  $< 0.2\%$ . However, the results deduced from the M-G theory are too low, while that of the Landauer method are too high. Their discrepancy is enlarged with increasing  $\phi_i$ , suggesting that the methods may need further modifications. For high  $\phi_i$  exceeding 0.52, models of cubic inclusion arrays are used. FE results approach to those of the M-G theory, because the composite with such a high cubic inclusion fraction can be regarded as if it has parallel magnetic plates.

Furthermore, the estimated value of  $\varepsilon_{eff}$  (or  $\mu_{eff}$ ) of a composite obtained from the FE method containing wire inclusions was found to depend sensitively on the orientation of the inclusions. A higher value of  $\varepsilon_{eff}$  (or  $\mu_{eff}$ ) is obtained if the wires are aligned along the applied  $H$ -field. It is found to be two times higher than that of the case when the wires are aligned perpendicular to the applied  $H$ -field.



### 5.3 Conclusions on the study of 3-phase composites

For the studies on 3-phase (0-0-3) composites containing two types of inclusions with  $\varepsilon_1$  and  $\varepsilon_2$  (or  $\mu_1$  and  $\mu_2$ ), and volume fractions of  $\phi_1$  and  $\phi_2$ , various methods were employed to estimate the values of  $\varepsilon_{eff}$  (or  $\mu_{eff}$ ). These methods include:

1. Maxwell-Garnett multiphase (MG-MP) method which is generated by modifying the M-G theory for a 2-phase composite;
2. Poon-Shin multiphase (PS-MP) method which is generated by modifying the P-S method for a 2-phase composite;
3. Incremental-multiphase (I-MP) method, which is further subdivided into three methods depending on the sequence of adding the inclusions. A process proceeded by adding one type of inclusion in differential steps followed by the addition of the inclusions of the second types in the same way is called the sequential multiphase (SI-MP) method. A process proceeded by adding the two types of inclusions in differential steps with respective probabilities in a ratio equal to their volume fractions is called the randomly-accumulative multiphase (RA-MP) method.
4. FE method with a model containing spherical and cubic inclusions arranged in 4x4x4 or 6x6x6 periodic arrays. The results obtained by using these two inclusion geometries only have a difference less than 3%. Hence, the latter is used to give



data for composites of high inclusion volume fractions above 0.4 for comparing with the results deduced from the above analytic theories.

First, at any specific value of  $\phi_i$  in the range under investigations, the data derived from the I-MP theory roughly form the upper bound of those derived from other methods. Second, the three I-MP processes do not give the same result, though they are supposed to describe the same composite system. In a SI-MP process performed by adding inclusions of a lower relative permittivity (or permeability) first gives a high  $\varepsilon_{eff}$  (or  $\mu_{eff}$ ) value, and the reverse is detected if the inclusions of a higher relative permittivity are added first. The result produced by using a RA-MP process lies in between. This inconsistency suggests that the I-MP methods are not exact and need further improvement. The data produced by using the MG-MP method form the lower bound of the data deduced from other methods.

In the range of low inclusion volume fractions  $\phi_i \leq 0.3$ , all analytic methods give similar results which are close to those deduced from the FE method. Hence, in this region, the analytic methods are considered to be valid. For higher  $\phi_i$  in the range from 0.3 to 0.9, the results of the PS-MP and I-MP approaches are higher than the FE data,



implying that these analytic methods overestimate the  $\varepsilon_{eff}$  (or  $\mu_{eff}$ ) values, possibly due to the introduction of excessive modification to the matrix. Typically, in the case of  $\varepsilon_1 : \varepsilon_2$  (or  $\mu_1 : \mu_2$ ) = 5 : 1, the error between the results of the RA-MP and FE methods is about 5%. On the other hand, the results of MG-MP method show underestimation and are lower than the FE results.

FE simulations show that the arrangement of the inclusions in a composite affects the result. The estimated value of  $\varepsilon_{eff}$  (or  $\mu_{eff}$ ) is the largest if the two types of inclusions form two layers which are oriented in parallel to the applied field, and is the lowest if the two layers are oriented perpendicular to the applied field. The result of the case with the inclusions randomly distributed lies in between.



## 5.4 Conclusions on the method for determining $\mu$ by combining VSM and FE simulations

We developed a method to estimate the dynamic permeability of a soft magnet by combining vibrating sample magnetometer (VSM) analysis and FEA. It starts from measuring the apparent permeability ( $\mu_{\text{apparent}}$ ) with a series of specimens having different aspect ratios by using VSM, with the length of the sample aligned in parallel with the applied field. The measured value is smaller than real one,  $\mu$ , due to demagnetization effect. Numerical simulations are then performed to predict the measured  $\mu_{\text{apparent}}$  by emulating the VSM measurements. The calculated and measured values are compared through curve fitting to give an estimate of  $\mu$ . The result obtained is more accurate than that obtained by correcting the VSM measurement data with tabulated demagnetization factor based on one sample geometry. The method is proved to be valid according to the pilot tests on Fe and Ni. It is also advantageous of not requiring the sample to be made in a ring shape as that for a standard Rowland's ring measurement.



## References

**Aharoni A.**, 1998, *J. Appl. Phys.*, **83**, 3432.

**ANSYS**, 2007a, *Theoretical reference for ANSYS and ANSYS Workbench*, ANSYS, Inc., **ANSYS 11.0**, Ch.5 Electromagnetic field fundamental.

**ANSYS**, 2007b, *Release notes*, ANSYS, Inc., **ANSYS 11.0**.

**ANSYS**, 2007c, *Release 11.0 Documentation for ANSYS*, ANSYS, Inc., **ANSYS 11.0**, Element reference.

[http://www.kxcad.net/ansys/ANSYS/ansyshelp/Hlp\\_E\\_SOURC36.html](http://www.kxcad.net/ansys/ANSYS/ansyshelp/Hlp_E_SOURC36.html)

**ANSYS**, 2007d, *Release 11.0 Documentation for ANSYS*, ANSYS, Inc., **ANSYS 11.0**, Element reference.

[http://www.kxcad.net/ansys/ANSYS/ansyshelp/Hlp\\_E\\_SOLID96.html](http://www.kxcad.net/ansys/ANSYS/ansyshelp/Hlp_E_SOLID96.html)

**Bregar V. B.**, 2005, *Phys. Rev. B*, **71**, 174418.

**Bregar V. B. and Pavlin M.**, 2004, *J. Appl. Phys.*, **95**, 6289.

**Bruggeman D. A. G.**, 1935, *Ann. Phys-Berlin.*, **416**, 636.

**Burgei W., Pechan M. J. and Jaeger H.**, 2003, *Am. J. Phys.*, **71**, 825.

**Cedillo E., Ocampo J., Rivera V. and Valenzuela R.**, 1980, *J. phys. E: Sci. Instrum.*, **13**, 383.

**Chen D. X. B., Brug J. A. and Goldfarb R. B.**, 1991, *IEEE T. Magn.*, **27**, 3601.

**Chen L. F., Ong C. K., Tan B. T. G. and Deng C. R.**, 1998, *J. Mater. Sci.*, **33**, 5891.



- Chevalier A. and Floc'h M. L.**, 2001, *J. Appl. Phys.*, **90**, 3462.
- Chew K. H., Shin F. G., Ploss B., Chan H. L. W. and Choy C. L.**, 2003, *J. Appl. Phys.*, **94**, 1134.
- Clarke D. B.**, 1999, *IEEE T. Magn.*, **35**, 4440.
- Daniel L. and Corcolle R.**, 2007, *IEEE T. Magn.*, **43**, 3153.
- Darius T. R.**, 2008, *J. Young Investigators*, **18**,  
<http://www.jyi.org/research/re.php?id=1493>.
- Drnovsek B.**, 2008, *J. Appl. Phys.*, **103**, 07D924.
- Emets Y. P.**, 2005, *Tech. Phys.*, **50**, 207.
- Foner S.**, 1956, *Rev. Sci. Instrum.*, **27**, 548.
- Foner S.**, 1959, *Rev. Sci. Instrum.*, **30**, 548.
- Goncharenko A. V.**, 2003, *Phys. Rev. E*, **68**, 041108.
- Graef M. D. and Beleggia M.**, 2006, *J. Magn. Magn. Mater.*, **305**, 403.
- Greenslade B.**, *Instruments for natural philosophy, Rowland's ring* (Kenyon College),  
[http://physics.kenyon.edu/EarlyApparatus/Electricity/Rowlands\\_Ring/Rowlands\\_Ring.html](http://physics.kenyon.edu/EarlyApparatus/Electricity/Rowlands_Ring/Rowlands_Ring.html).
- Hallouet B. and Pelster R.**, 2007, *J. Nanomaterials*, **2007**, 80814.
- Hoon S. R.**, 1983, *Eur. J. Phys.*, **4**, 61.



**Jylhä L. and Sihvola A.**, 2007, *EMTS 2007, International URSL Commission B – Electromagnetic Theory Symposium*.

**Kärkkäinen K., Sihvola A. and Nikoskinen K.**, 2001, *IEEE T. Geosci. Remote*, **39**, 1013.

**Landauer R.**, 1952, *J. Appl. Phys.*, **23**, 179.

**Matyuk V. F. and Osipov A. A.**, 2000, *Russ. J. Nondestruct.*, **36**, 27.

**Maxwell Garnett J. C.**, 1904, *Philoso. T. R. Soc. A*, **203**, 385.

**Merrill W. M., Diaz R. E., LoRe M. M., Squires M. C. and Alexopoulos N. G.**, 1999, **47**, 142.

**Miles P. A., Westphal W. B. and Hippel A. V.**, 1957, *Rev. Mod. Phys.*, **29**, 279.

**Osborn J. A.**, 1945, *Phys. Rev.*, **67**, 351.

**Paterson J. H., Cooke S. J. and Phelps A. D. R.**, 1998, *J. Magn. Magn. Mater.*, **177**, 1472.

**Périn F.**, 2004, *Eur. J. Mech. A-Solid.*, **23**, 139.

**Poon Y. M. and Shin F. G.**, 2004, *J. Mater. Sci.*, **39**, 1277.

**Rayleigh R. S.**, 1892, *Phil. Mag. S.5*, **34**, 481.

**Reitz J. R., Milford F. J. and Christy R. W.**, 1962, *Foundations of electromagnetic theory* (Reading, Mass.: Addison-Wesley Pub. Co.), p. 294.

**Samwel E. O., Bolhuis T. and Lodder J. C.**, 1998, *Rev. Sci. Instrum.*, **69**, 3204.



**Sareni B., Kriihenbuhl L., Beroual A. and Nicolas A.,** 1997, *IEEE T. Magn.*, **33**, 1580.

**Shamonin M., Snarskii A. and Zhenirovskyy M.,** 2004, *NDT&E Int.*, **37**, 35.

**Shokrollahi H. and Jangorban K.,** 2007, *J. Mater. Process. Tech.*, **189**, 1.

**Sihvola A. H.,** 1999a, *Electromagnetic mixing formulas and applications* (London: Institution of Electrical Engineers), p. 40.

**Sihvola A. H.,** 1999b, *Electromagnetic mixing formulas and applications* (London: Institution of Electrical Engineers), p. 48.

**Sihvola A. H.,** 1999c, *Electromagnetic mixing formulas and applications* (London: Institution of Electrical Engineers), p. 61.

**Sihvola A. H.,** 1999d, *Electromagnetic mixing formulas and applications* (London: Institution of Electrical Engineers), p. 151.

**Sihvola A. H.,** 1999e, *Electromagnetic mixing formulas and applications* (London: Institution of Electrical Engineers), p. 161.

**Sihvola A. H.,** 1999f, *Electromagnetic mixing formulas and applications* (London: Institution of Electrical Engineers), p. 168.

**Stroud D.,** 1979, *Phys. Rev. B*, **19**, 1783.

**Tang K., Zhang H. W., Wen Q. Y. and Zhong Z. Y.,** 2005, *Physica B*, **363**, 96.

**Waki H., Igarashi H. and Honma T.,** 2005a, *IEEE T. Magn.*, **41**, 1520.

**Waki H., Igarashi H. and Honma T.,** 2005b, *Compel.*, **24**, 566.



**Waki H., Igarashi H. and Honma T.**, 2006, *Physica B*, **372**, 383.

**Whites K. W.**, 1999, *IEEE*, **3**, 1934.

**Wong C. K., Wong Y. W. and Shin F. G.**, 2002, *J. Appl. Phys.*, **92**, 3974.

**Xue Q.**, 2003, *Physica B*, **325**, 195.